2011

Anaplasma phagocytophilum remodels its host cell-derived vacuole into a protective niche by redecorating the vacuolar membrane with select Rab GTPases and bacterial proteins

Bernice Huang
Virginia Commonwealth University

ANAPLASMA PHAGOCYTOPHILUM REMODELS ITS HOST CELL-DERIVED VACUOLE INTO A PROTECTIVE NICHE BY REDECORATING THE VACUOLAR MEMBRANE WITH SELECT RAB GTPASES AND BACTERIAL PROTEINS

A dissertation submitted in partial fulfillment of the requirements for the degree of Doctor of Philosophy at Virginia Commonwealth University.

by

BERNICE HUANG
Bachelor of Science, University of Richmond, 2005

Director: Jason A. Carlyon, Ph.D.
Assistant Professor, Department of Microbiology and Immunology

Virginia Commonwealth University
Richmond, Virginia
December 2011

Acknowledgment

First and foremost, I would like to thank Dr. Jason Carlyon for his mentorship. His guidance, contagious passion for science, and consistent encouragement enabled my development as a scientist. I also extend thanks to my graduate committee: Drs. Richard Marconi, Todd Kitten, Dennis Ohman, and Ghislaine Mayer for their scientific input and expertise throughout this project. In addition, I want to thank Dr. Francine Marciano-Cabral for her valued advice and friendship.

I wish to thank past and present members of the Carlyon lab for their intellectual input, technical assistance and benchside banter. In particular, Dr. Nore Ojogun for her willingness to walk to lab through treacherous storms and Dr. Matt Troese for his understated humor. Current lab members I would also like to thank are Hilary Truchan, Dr. Amandeep Kahlon, Stephanie Ragland, Lauren VieBrock and Dr. Andrea Beyer.

I would like to thank my friends for their encouragement and fun times throughout my graduate career. Specifically, Erica Longenbach for her unwavering support and entertainment, Melissa Jamerson for her friendship throughout graduate school, and Aaron Wolen for always making me laugh and making sure my axes were labeled.

Last but not least, I would like to express my heartfelt gratitude to my parents for their unconditional love and support throughout my life, without which I would never be where I am today. Thank you for always encouraging me to pursue my interests and accepting 28 years of homemade gifts.

Table of Contents

List of figures vi

List of tables viii

List of abbreviations ix

Abstract xiv

1 Introduction 1

1.1 *Anaplasma phagocytophilum* 1

1.2 Ecology and epidemiology 2

1.3 Human granulocytic anaplasmosis 5

1.4 The *A. phagocytophilum* genome 6

1.5 *A. phagocytophilum* intracellular development 9

1.6 Subversion of host antimicrobial defenses 10

1.7 Pathogenesis and immune responses 13

1.8 Establishing an intracellular niche 15

1.9 Research objectives 16

2 Materials and Methods 18

3 The *A. phagocytophilum*-occupied vacuole (ApV) selectively recruits Rab-GTPases that are predominantly associated with recycling endosomes 37

3.1 Introduction . . . 37

3.2 Results . . . 41

3.2.1 Fluorescent protein-tagged Rab1, Rab4A, Rab10, Rab11A, Rab14, Rab22A and Rab35 localize to the ApV. . . . 41

3.2.2 The ApV recruits Rabs upon formation and continues to do so throughout infection. . . . 45

3.2.3 Endogenous Rab14 localizes to the ApV. . . . 46

3.2.4 GFP-Rab10 and GFP-Rab14 localization to the ApV is not dependent on an intact Golgi apparatus. . . . 49

3.2.5 GFP-Rab1, GFP-Rab4A, GFP-Rab11A, GFP-Rab14 and GFP-Rab35 associate with the ApV in a guanine nucleotide-dependent manner, but GFP-Rab10 localizes to the ApV in a guanine nucleotide-independent manner. . . . 49

3.2.6 Selective recruitment of GFP- or RFP-Rab GTPases to the ApV is dependent on *A. phagocytophilum* protein synthesis. . . . 55

3.3 Discussion . . . 58

4 *A. phagocytophilum* APH_1387 is expressed throughout bacterial intracellular development and localizes to the pathogen-occupied vacuolar membrane (PVM) 67

4.1 Introduction . . . 67

4.2 Results . . . 68

4.2.1 APH_1387 has limited homology to any previously described protein. 68

4.2.2 APH_1387 is more abundant in *A. phagocytophilum* RC organisms than in DC organisms. . . . 70

4.2.3 APH_1387 is induced following bacterial entry into host cells and localizes to the AVM. 72
4.2.4 APH_1387 localizes to the AVM during *A. phagocytophilum* infection of human myeloid and endothelial cell lines and tick embryonic cell lines. 75
4.2.5 APH_1387 is expressed and localizes to the AVM throughout *A. phagocytophilum* intracellular development in HL-60 cells. 75
4.2.6 APH_1387 is expressed and localizes to the AVM *in vivo.* 81
4.3 Discussion 81

5 *A. phagocytophilum* APH_0032 is expressed late during infection and localizes to the pathogen-occupied vacuolar membrane 85
5.1 Introduction 85
5.2 Results 86
5.2.1 APH_0032 displays limited similarity to other known proteins but exhibits predicted secondary structural characteristics that are suggestive of AVM localization. 86
5.2.2 APH_0032 is present in higher abundance in *A. phagocytophilum* RC organisms than in DC organisms. 88
5.2.3 APH_0032 is not detected until 24 h post infection and localizes to the AVM. 90
5.2.4 APH_0032 localizes to the AVM during *A. phagocytophilum* infection of human myeloid and endothelial cell lines and tick embryonic cell lines. 90
5.2.5 APH_0032 is not amply expressed by *A. phagocytophilum* and does not localize to the AVM until 24 h post infection of HL-60 cells. . . 93

5.2.6 APH_0032 is expressed and localizes to the AVM during *in vivo* *A. phagocytophilum* infection and *aph_0032* and *aph_1387* are transcribed during *A. phagocytophilum* residence in tick salivary glands. 97
5.3 Discussion 99

6 *A. phagocytophilum* proteins APH_1387 and APH_0032 are expressed on the cytoplasmic face of the AVM and are critical for ApV development. 102
6.1 Introduction 102
6.2 Results 103
6.2.1 GFP tagged APH_1387 and APH_0032 constructs used in this study. 103
6.2.2 *A. phagocytophilum* AnkA, but not APH_0032 or APH_1387 can be heterologously secreted by the *L. pneumophila* Dot/Icm T4SS secretion system. 106
6.2.3 The N-terminal non-repeat regions of APH_0032 and APH_1387 possess domains that facilitate association with host cell membranes. 108
6.2.4 APH_1387 and APH_0032 are exposed on the cytoplasmic face of the AVM. 111
6.2.5 Ectopic expression of GFP-tagged APH_1387 and APH_0032 interferes with *A. phagocytophilum* development in RF/6A cells. 117
6.3 Discussion 122

7 Monoubiquitinated proteins decorate the *A. phagocytophilum*-occupied vacuolar membrane (AVM) 127
7.1 Introduction 127
7.2 Results 129
7.2.1 Ubiquitinated proteins accumulate on the AVM. 129

7.2.2 The AVM accumulates ubiquitinated proteins over the course of *A. phagocytophilum* infection in HL-60 cells. 132
7.2.3 The AVM is monoubiquitinated. 137
7.2.4 *de novo* bacterial protein synthesis is important for continued association of ubiquitinated proteins at the AVM. 137
7.3 Discussion 138

8 Conclusions 142

Bibliography 147

Copyrighted license material 168

Vita 170

List of Figures

1 *A. phagocytophilum* infected cells. 3

2 Lifecycle of *Ixodes* spp. ticks. 4

3 Biphasic development of *A. phagocytophilum* in HL-60 cells. 11

4 Selective GFP- or RFP-Rab GTPase localization to the *A. phagocytophilum*-occupied vacuole (ApV). 42

5 Percentages of ApVs exhibiting GFP- or RFP-Rab GTPase localization. . . 44

6 Time-course analyses of GFP- or RFP-Rab GTPase recruitment to the ApV. 47

7 Endogenous Rab14 localizes to the ApV. 48

8 GFP-Rab10 and GFP-Rab14 localization to the ApV is insensitive to BFA. . 50

9 Localization of GFP-Rab1, GFP-Rab4A, GFP-Rab11A, GFP-Rab14 and GFP-Rab35 to the ApV is guanine nucleotide-dependent, while GFP-Rab10 association with the ApV is guanine nucleotide-independent. 53

10 Selective recruitment of GFP- or RFP-Rab GTPases to the ApV is dependent on bacterial protein synthesis. 56

11 Model indicating the Rab GTPases and host cell membrane traffic pathways that are hijacked by the ApV. 59

12 Schematic diagram of *A. phagocytophilum* APH_1387 and its secondary structure. 69

13 Screening of *A. phagocytophilum*-infected HL-60 cells and host cell-free bacterial populations with anti-APH_1387. 71

14 *A. phagocytophilum* APH_1387 is detectable on the surfaces of intravacuolar bacteria and localizes to the AVM in infected host cells. 73

15 Kinetics of APH_1387 expression and AVM localization in *A. phagocytophilum*-infected cells. 76

16 Assessment of *A. phagocytophilum* APH_1387 expression and localization to the AVM by immunoelectron microscopy. 79

17 *A. phagocytophilum* APH_1387 is expressed and associates with the AVM during *in vivo* infection. 82

18 Schematic representation of *A. phagocytophilum* APH_0032, sequence, and secondary structure analyses. 87

19 APH_0032 is present in greater abundance in lysates of *A. phagocytophilum* RC organisms compared to DC organisms. 89

20 *A. phagocytophilum* APH_0032 is detectable on the surfaces of intravacuolar bacteria and localizes to the AVM in infected host cells. 91

21 Kinetics of APH_0032 expression and AVM localization in *A. phagocytophilum*-infected HL-60 cells. 94

22 Assessment of *A. phagocytophilum* APH_0032 expression and localization to the AVM by immunoelectron microscopy. 95

23 *A. phagocytophilum* APH_0032 is expressed and modifies the AVM during *in vivo* infection. 98

24 Schematic representation of APH_0032 gene constructs used in this study. . 104

25 Schematic representation of APH_1387 gene constructs used in this study. . 105

26 *A. phagocytophilum* AnkA, but not APH_0032 or APH_1387 can be secreted by the *Legionella pneumophila* Dot/Icm secretion system. 107

27 Deletion analysis of APH_0032 reveals a N-terminal domain necessary for host cell membrane association. 109

28 Deletion analysis of APH_1387 identifies a N-terminal domain, residues 101-112, necessary for host cell membrane association. 112

29 APH_1387 and APH_0032 contain portions exposed on the cytoplasmic face of the AVM. 115

30 Ectopically expressed GFP-1387 interferes with ApV development at 24 h post infection. 118

31 Ectopically expressed GFP-APH_1387 and GFP-APH_0032 competitively inhibit ApV development at 48 h post infection. 120

32 Monoubiquitinated proteins decorate the AVM in HL-60 cells. 130

33 Ubiquitinated proteins localize to the AVM in infected host cells. 131

34 Ubiquitinated proteins are detectable on the AVM following *A. phagocytophilum* entry into nascent vacuoles and continue to accumulate on the AVM throughout infection. 133

35 Percentages of AVMs exhibiting ubiquitinated protein association over the course of *A. phagocytophilum* infection of HL-60 cells. 136

36 Ubiquitin association with the AVM is dependent on bacterial protein synthesis. 139

37 The *A. phagocytophilum*-occupied vacuole interacts with a broad repertoire of host pathways to facilitate its intracellular survival strategy in host cells. . 143

List of Tables

1 Oligonucleotides used to amplify select Rab GTPases. 20

2 Oligonucleotides used to generate GFP-APH_1387 and -APH_0032 fusion constructs. 22

3 Oligonucleotides used to generate CyaA fusion constructs 25

4 Rab GTPases examined in this study 39

List of Abbreviations

°C	degrees Celsius
A. phagocytophilum	*Anaplasma phagocytophilum*
g	relative centrifugal force (RCF), or g-force
μg	microgram
μl	microliter
Ab	antibody
ApV	*A. phagocytophilum*-occupied vacuole
AVM	*A. phagocytophilum*-occupied vacuolar membrane
BFA	Brefeldin A
BLAST	basic local alignment search tool
BME	β-mercaptoethanol
BMMC	Bone marrow derived mast cell
BSA	bovine serum albumin
cAMP	adenosine 3',5'-monophosphate
CDC	Centers for Disease Control
CO_2	carbon dioxide
CyaA	adenylate cyclase
CYE	charcoal yeast extract
DAPI	4'-6-diamidino-2-phenylindole
DC	dense-cored cell form of *A. phagocytophilum*
DMEM	Dulbecco's Modified Eagle's Medium

DNA	deoxyribonucleic acid
DTT	dithiothreitol
EDTA	ethylenediaminetetraacetic acid
EE	early endosome
ER	endoplasmic reticulum
ERC	endocytic recycling center
FBS	fetal bovine serum
GAP	GTPase-activating protein
GDF	GDI displacement factor
GDI	guanine nucleotide dissociation inhibitor
GEF	guanine nucleotide exchange factor
GFP	green fluorescent protein
GTP	guanosine triphosphate
h	hour
HCl	hydrochloric acid
HGA	human granulocytic anaplasmosis
HGE	human granulocytic ehrlichiosis
HRP	horseradish peroxidase
IC	pre-Golgi intermediate compartment
IFA	indirect immunofluorescence analysis
IFN-γ	interferon-γ (gamma)
IL	interleukin
IMDM	Iscove's Modified Dulbecco's Medium
Inc	chlamydial inclusion membrane protein
IPTG	isopropyl-β-D-thiogalactopyranoside

kDa	kilodalton
KOH	potassium hydroxide
LAMP-1	Lysosomal-associated membrane protein-1
LB	Luria-Bertani
LCV	*Legionella*-containing vacuole
LCVM	*Legionella*-containing vacuolar membrane
LE	late endosome
LPS	lipopolysaccharide
mAb	monoclonal antibody
Mb	megabases
MBP	maltose binding protein
MEM	Minimum Essential Medium
$Mg(CH_3COO)_2$	magnesium hydroxide
$MgCl_2$	magnesium chloride
MHC	major histocompatibility complex
min	minute
ml	milliliter
mM	millimolar
MPR	mannose-6-phosphate receptor
MPV	*Mycobacteria*-pathogen vacuole
Msp2 (P44)	major surface protein 2 (44-kDa protein)
$NaC_2H_3O_2$	sodium acetate
NaCl	sodium chloride
NADPH	nicotinamide adenine dinucleotide phosphate-oxidase
$NaHCO_3$	sodium bicarbonate

NaOH	sodium hydroxide
ng	nanogram
nM	nanometer
O_2^-	superoxide
PAGE	polyacrylamide gel electrophoresis
PAMPs	pathogen-associated molecular patterns
PBS	phosphate buffered saline
PCR	Polymerase chain reaction
PFA	paraformaldehyde
PM	plasma membrane
PMA	phorbol 12-myristate 13-acetate
PSGL-1	Platelet selectin glycoprotein ligand-1
PV	pathogen-occupied vacuole
PVM	pathogen-occupied vacuolar membrane
RC	reticulate cell form of *A. phagocytophilum*
RE	recycling endosome
RFP	red fluorescent protein
ROS	reactive oxygen species
rpm	revolutions per minute
RPMI	Rosewell Park Memorial Institute
RT-PCR	reverse transcriptase polymerase chain reaction
s	second
SCID	severe combined immunodeficiency
SCV	*Salmonella*-containing vacuole
SDS	sodium dodecyl sulfate

SG	secretory granule
sLe^x	siayl Lewis x
SV	synaptic vesicle
T1SS	type I secretion system
T4SS	type IV secretion system
TBS-t (0.5)	tris-buffered saline with 5% tween-20
TFR	transferrin receptor
TGN	*trans*-Golgi network
TIGR	the institute for genomic research
TMD	transmembrane domain
TNF-α	tumor necrosis factor-α
TRP	tandem repeat protein

Abstract

ANAPLASMA PHAGOCYTOPHILUM REMODELS ITS HOST CELL-DERIVED VACUOLE INTO A PROTECTIVE NICHE BY REDECORATING THE VACUOLAR MEMBRANE WITH SELECT RAB GTPASES AND BACTERIAL PROTEINS

By Bernice Huang, Ph.D.

A dissertation submitted in partial fulfillment of the requirements for the degree of Doctor of Philosophy at Virginia Commonwealth University.

Virginia Commonwealth University, 2011

Major Director: Jason A. Carlyon, Ph.D.
Assistant Professor, Department of Microbiology and Immunology

Anaplasma phagocytophilum is an obligate intracellular bacterium that infects neutrophils to cause the emerging tick-transmitted disease, human granulocytic anaplasmosis (HGA). Following entry, the pathogen replicates within a host cell-derived vacuole that fails to mature along the endocytic pathway, does not acidify, and does not fuse with lysosomes. Selective fusogenicity is prototypical of many vacuole-adapted pathogens and has been attributed, at least in part, to pathogen modification of the vacuolar inclusion membrane and/or to selective recruitment or exclusion of host trafficking regulators. As a result, the *A. phagocytophilum*-occupied vacuolar membrane (AVM) provides a unique interface to study the host-pathogen interactions critical to *A. phagocytophilum* intracellular survival.

Diverse vacuole-adapted pathogens – including *Chlamydia*, *Legionella*, and *Salmonella* spp. – selectively recruit host Rab GTPases to their vacuolar membranes to establish replicative permissive niches within their host cells. Rab GTPases coordinate many aspects

of endocytic and exocytic cargo delivery. We determined that the *A. phagocytophilum*-occupied vacuole (ApV) selectively recruits a subset of fluorescently-tagged Rabs that are predominantly associated with recycling endosomes. Another emerging theme among vacuole-adapted pathogens is the ability to hijack ubiquitin machinery to modulate host cellular processes. Mono- and polyubiquitination differentially dictate the subcellular localization, activity, and fate of protein substrates. Monoubiquitination directs membrane traffic from the plasma membrane to the endosome and has been shown to promote autophagy. We show that monoubiquitinated proteins decorate the AVM during infection of promyelocytic HL-60 cells, endothelial RF/6A cells, and to a lesser extent, embryonic tick ISE6 cells. Importantly, tetracycline treatment concomitantly promotes loss of the recycling endosome-associated GFP-Rabs and ubiquitinated proteins and acquisition of the late endosomal marker, Rab7, and lysosomal marker, LAMP-1, implicating bacterial-derived proteins in the ApV's altered fusogenicity. Therefore, we rationalized that *A. phagocytophilum*-encoded proteins that associate with the AVM may establish interactions with the host cell that are important for intracellular survival. By focusing on *A. phagocytophilum* proteins that are induced during host infection, we identified the first two bacterial-encoded proteins – APH_1387 and APH_0032 – that modify the AVM. Although functional studies are hindered by the lack of a system to genetically manipulate *Anaplasma*, the pathobiological roles of APH_1387 and APH_0032 are likely unique, as both proteins exhibit very little or no homology with any previously described protein. APH_1387 and APH_0032 are present at the cytoplasmic face of the AVM, therefore they likely interact with host proteins. We demonstrate that ectopic expression of APH_1387 and APH_0032 inhibits the ApV development in *A. phagocytophilum* infected cells. The results presented in this dissertation contribute to our understanding of how *A. phagocytophilum* modifies the vacuolar membrane in which it resides to establish a safe haven and evade lysosomal degradation.

Introduction

1.1 *Anaplasma phagocytophilum*

Anaplasma phagocytophilum is a Gram-negative bacterium in the family Anaplasmataceae, in the order Rickettsiales and the class α-Proteobacteria (53). All members of this family are obligate intracellular bacteria that replicate exclusively in membrane-bound compartments within their respective host cells and are the causative agents of animal and human diseases (162). To date, five species are known to infect humans, *A. phagocytophilum*, *Ehrlichia chaffeensis*, *Ehrlichia ewingii*, *Ehrlichia canis* and *Neorickettsia sennetsu*. Collectively, infections caused by members of this family are referred to as ehrlichioses. *A. phagocytophilum* was first identified as a veterinary pathogen in 1932 and was originally classified as two separate *Ehrlichia* species. The first human infection was documented in 1994 and was referred to as human granulocytic ehrlichiosis (HGE) (35). In 2001, taxonomic reclassification based on improved genetic analyses of 16S rRNA gene and *groESL* operon sequence results and surface protein genes grouped the three former species, *Ehrlichia equi*, *Ehrlichia phagocytophila* and the HGE agent into the single species, *A. phagocytophilum* (53). Following the revised nomenclature, *A. phagocytophilum* infection is now referred to as human granulocytic anaplasmosis (HGA) (53).

A. phagocytophilum is a small (0.2-2 μm diameter) pleomorphic coccobacillary bacterium that replicates within a host cell derived vacuole to form microcolonies (35). Microcolonies are typically 2-7 μm in diameter and can be visualized by Giemsa staining (**Figure**

1) (13, 35). The hallmark feature of *A. phagocytophilum* is its unique tropism for replicating inside neutrophils. The human promyelocytic leukaemia cell line, HL-60, is used for standard *in vitro* cultivation studies (72). In addition, *A. phagocytophilum* infects endothelial cells *in vivo* and *in vitro* and mast cells and megakaryocytes *in vitro* (75, 82, 133, 143).

1.2 Ecology and epidemiology

In its natural environment, *A. phagocytophilum* cycles between its *Ixodes* tick vector and small mammalian hosts, the primary of which is the white-footed mouse, *Peromyscus leucopus* (**Figure 2**). Humans are accidental hosts. In the United States, the vector includes *Ixodes scapularis* in the northeast and upper midwest, and *I. pacificus* and *I. spinipalis* in the Pacific coast and mountain regions, respectively (195). It is estimated that 10-50% of *I. scapularis* ticks in the United States are infected with *A. phagocytophilum* (121, 147). Within Europe and Asia, the vectors are *I. ricinus* and *I. persulcatus*, respectively (26, 146). In addition to *A. phagocytophilum*, *Ixodes* spp. are the vectors for *Borrelia burgdorferi* (25) and *Babesia microti* (185), the causative agents of Lyme disease and babesiosis, respectively. Coinfection of *Ixodes* spp. ticks with one or more of the aforementioned pathogens has been confirmed (194, 200). The lifecycle of *Ixodes* spp. ticks span 2 to 3 years and includes three developmental stages, larva, nymph, and adult (**Figure 2**). Each developmental stage feeds only once (9, 12, 194). Tick acquisition of *A. phagocytophilum* occurs during a blood meal of an infected mammalian host, but since there is no transovarial transmission, once an adult tick has laid eggs, the *A. phagocytophilum* infection cycle is interrupted. Within the tick, *A. phagocytophilum* replicates inside cells of the midgut and salivary glands.

Geography is an important factor in the epidemiology of anaplasmosis. The areas with high incidence rates of *A. phagocytophilum* infection correspond to the distribution of *Ixodes* spp. HGA was first identified in 1994 in patients from Wisconsin and Minnesota and it

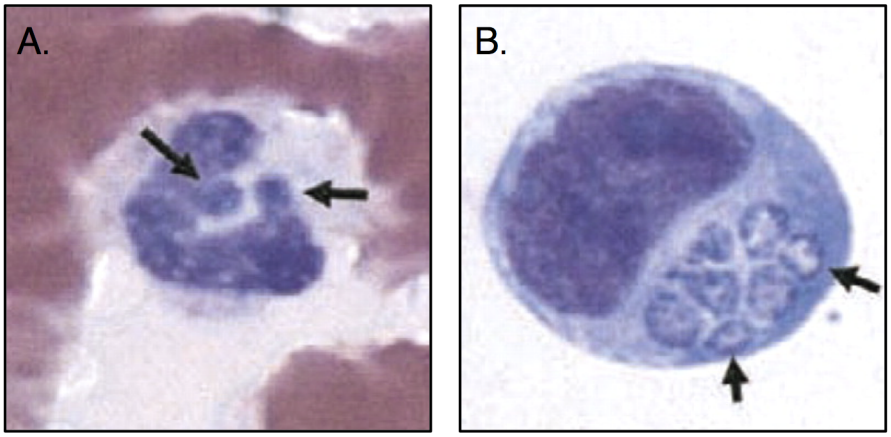

Figure 1. *A. phagocytophilum* infected cells.
Giemsa stained *A. phagocytophilum* infected (**A**) peripheral blood neutrophils and (**B**) human HL-60 promyelocytic cells in tissue culture. Microcolonies appear as circular blue inclusions in the cytoplasm of the host cells, denoted by the arrows. Image from: Dumler JS, Madigan JE, Pusterla N, Bakken JS. Ehrlichioses in humans: epidemiology, clinical presentation, diagnosis, and treatment. Clin Infect Dis 2007;45 Suppl 1:S45-51.

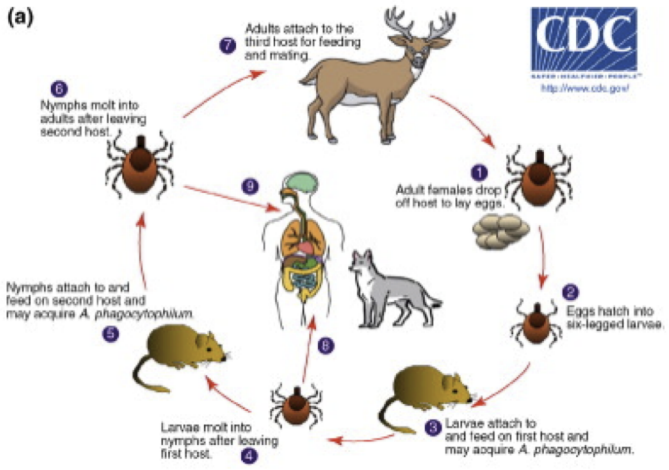

Figure 2. Lifecycle of *Ixodes* spp. ticks.
Ticks acquire *A. phagocytophilum* from infected mammals through a blood meal. The bacterium is transmitted to a susceptible mammal during the ticks next blood meal. Since there is no transovarial transmission, once an adult tick has laid eggs, the *A. phagocytophilum* infection cycle is disrupted. Humans are accidental hosts and are not part of the normal tick life cycle. Image from: Nicholson, W.L, K.E. Allen, J.H. McQuiston, E.B. Breitschwerdt and S.E. Little. 2010. The increasing recognition of rickettsial pathogens in dogs and people. Trends in Parasitology 26(4):205-212.

became a nationally notifiable disease in 1999 (11, 35). Since 1999, the number of reported cases has steadily increased, with 1,761 cases of *A. phagocytophilum* infection documented in 2010 (33). However, the numbers likely underrepresent the true incidence and prevalence as many cases of HGA follow a mild course or go unrecognized. Seroepidemiological data estimate that in regions where the disease is endemic 15-36% of the populations have been infected (2, 13).

1.3 Human granulocytic anaplasmosis

Clinical manifestations and treatment. The onset of HGA typically occurs 5-21 days after a bite from an infected tick (195). Clinical presentations of the disease range in severity from asymptomatic to severe febrile illness and in rare cases death. Commonly associated symptoms include headache, malaise, fever, chills and myalgia (55). Laboratory findings can include leukopenia, thrombocytopenia, and elevated levels of serum hepatic enzymes (43, 55). While the disease is often self-limiting, severe infections and poor outcomes have been linked to patients with underlying medical conditions, preexisting immune dysfunction, or when antibiotic therapy was not provided in a timely manner (55, 164). Up to 17% of patients with severe HGA require intensive care hospitalization (12). In the United States, the case fatality rate is 0.7% and is largely associated with opportunistic infections. Most patients respond to doxycycline, which is the preferred treatment (195). Currently there is no vaccine available.

Diagnosis. The most rapid approach for diagnosis is examination of a Giemsa-stained peripheral blood smear for intravacuolar bacterial colonies within the cytosol of granulocytes, which appear dark blue (**Figure 1A**). This test is most useful during the first week of infection because sensitivity of the assay is 25-75% for *A. phagocytophilum* infection. Polymerase chain reaction (PCR) amplification of *A. phagocytophilum*-specific DNA can

also confirm diagnosis during acute infection with assay sensitivity reported to range between 67-90% (55). However, the most frequently used method for diagnostic confirmation is the serological detection of antibodies in patient serum by indirect immunofluorescence analysis (IFA). This method is most sensitive 2-4 weeks following disease onset because it requires that the patient has had sufficient time to develop an antibody response. Once a patient is seropositive, antibodies may persist for years in the absence of clinical infection (12). Therefore, a serologic reaction in the absence of clinical presentation should not definitively be interpreted as an active, persistent or even chronic infection (55).

1.4 The *A. phagocytophilum* genome

The genome of *A. phagocytophilum* strain HZ was annotated in 2006 and consists of a single circular chromosome of 1,471,282 base pairs with 41.6% G-C content (57). It is about one quarter the size of the *Escherichia coli* genome (57). The notably small genome size is common among obligate intracellular pathogens such as *Chlamydia trachomatis* (genome 1.04 Mb), *Rickettsia prowazekii* (genome 1.11 Mb) and *Coxiella burnetii* (genome 2 Mb) (10, 178, 189). It is thought to be a pathoadaptive evolutionary process where the bacteria compensate their gene loss with a greater ability to acquire nutrients from the host cell. Analysis of the genome has revealed unique and important insights into the obligate intracellular lifestyle of *A. phagocytophilum*. Among these is the notable absence of genes involved in lipopolysaccharide (LPS) and peptidoglycan biosynthesis (112). This is supported by electron micrographs of *A. phagocytophilum* that show an unusual morphology characterized by a pleomorphic and thin outer membrane that is atypical of Gram-negative bacteria (57, 112). These observations are consistent with the role of LPS and peptidoglycan in the maintenance of outer membrane integrity. The loss of these genes allow the bacteria to be tightly packed while replicating in the limited intravacuolar space within their host cell

(112). To compensate for the fragility of their cell wall, *A. phagocytophilum* incorporates cholesterol into its membrane (112). Further analysis revealed the genome encodes genes for the biosynthesis of most cofactors and vitamins and all necessary nucleotides (57). This suggests the bacterium does not need to compete with the host cell for these essential metabolites. Furthermore, it implicates the enzymes in these biosynthetic pathways are important for intracellular survival. However, *A. phagocytophilum* has a reduced capacity for amino acid biosynthesis, and can only make glycine, glutamine, glutamate, and aspartate; therefore it must acquire the remaining amino acids from the host (57).

Major surface protein 2 (Msp2 [P44]). The *A. phagocytophilum* genome has numerous repeats (12.7% of the genome), exemplified by over 100 copies of the *msp2 (p44)* genes encoding outer membrane Msp2 (P44) proteins (57). The *msp2 (p44)* genes are defined by a central hypervariable region of about 280 bp that is flanked by conserved sequences (57). Diverse *msp2 (p44)* paralogs are expressed in each developmental stage of *I. scapularis* ticks, in patients, and in animal models of infection (16, 59, 114, 208, 216, 217). Expansion of the Msp2 (P44) family is thought to provide a diverse antigenic population to aid in the establishment of new infections. Msp2 (P44) is the immunodominant, constitutively expressed, major outer membrane protein of *A. phagocytophilum*. It is the most abundant and most studied surface protein. Through RecF-dependent gene conversion at a single *msp2 (p44)* expression locus, *A. phagocytophilum* can presumably evade immune recognition and adapt to changing host environments (113). Msp2 (P44) has been shown to have pore-forming activity and there is some evidence that suggests it is an adhesin (88).

Protein secretion systems. A virulence strategy used by many intracellular pathogens is the manipulation of host processes by secreted bacterial effectors. Bacteria use at least six distinct protein secretion systems, termed type I to type VI secretion systems (148). Homologs of type I secretion system (T1SS) and type IV secretion system (T4SS) components are encoded by the *A. phagocytophilum* genome (57). *A. phagocytophilum* lacks

genes for type II and type III secretion systems (57). Analysis based on conserved domains showed *A. phagocytophilum* encodes a T4SS homologous to the VirB/D system of *Agrobacterium tumefaciens* (140, 142). Exemplifying the repetitive nature of the genome, *A. phagocytophilum* carries up to eight nonidentical copies of these genes (57). T4SSs are broadly defined as macromolecular transporters with components ancestrally related to the conjugation system of Gram-negative bacteria. In pathogenic bacteria, many of these T4SSs are recognized as transporters of virulence proteins that manipulate eukaryotic cell processes. To date, only two *A. phagocytophilum* T4SS effectors have been identified, ankrin repeat protein A (AnkA) and *Anaplasma* translocated substrate 1 (Ats-1) (111, 139). AnkA was initially identified from a genomic DNA expression library screened with *A. phagocytophilum* infected dog sera (190) and Ats-1 was discovered by yeast two-hybrid using *A. phagocytophilum* VirD4 as bait against an *A. phagocytophilum* genomic prey library (139). Both AnkA and Ats-1 have basic C-terminal domains similar to T4SS effectors of *A. tumefaciens* (201). Binding of *A. phagocytophilum* to host cells promotes AnkA delivery into the host cytoplasm where it interacts with a host adaptor protein that recruits Abl-1 tyrosine kinase for AnkA phosphorylation (95, 111, 161). AnkA activation of the Abl-1 signalling pathway is crucial for bacterial infection. Subsequently, phosphorylated AnkA binds tyrosine phosphatase SHP1, conceivably to block host signaling pathways (95). Studies have shown that a large proportion of AnkA localizes to the nucleus (32, 66, 150). Within the nucleus, AnkA interacts with a range of targets, including ATC-rich sequences and transcriptional regulatory regions of the CYBB locus, to suppress innate immune activation (32, 66, 150). Ats-1 localizes to host cell mitochondria and delays apoptosis (139).

The overall genetic intractability of obligate intracellular bacteria has limited the use of molecular techniques in understanding the genetic basis of their pathogenesis. However, the *Himar1* transposase system has allowed for the random insertion of constructs encoding spectinomycin resistance and fluorescent proteins into the *A. phagocytophilum* chromosomes

(60). The resulting transgenic bacteria have been useful in host-pathogen interaction studies. This system has been successful for other obligate intracellular bacteria such as *C. burnetti* and *R. prowazekii* (18, 102, 118). The continued development of genetic tools should soon enable methods for site-specific gene inactivation and complementation and advance our understanding of virulence factors involved in the pathogenesis of these intracellular organisms. The most recent breakthrough has been the development of a medium that supports axenic growth of *C. burnetti* (144, 145). Significantly, this has allowed axenically grown organisms to be electroporated and plated for colony formation. As a result, it is easier to generate isogenic knock-out mutants for use in functional studies.

1.5 *A. phagocytophilum* intracellular development

Adhesion to sLe^x-modified PSGL-1. Siayl Lewis x (sLe^x)-modified platelet selectin glycoprotein ligand-1 (PSGL-1) is the only known receptor used by *A. phagocytophilum* to bind and invade human neutrophils, bone marrow derived progenitors, and myeloid cell lines (73). Specifically, *A. phagocytophilum* cooperatively recognizes α-2,3-sialic acid and α-1,3-fucose of sLe^x and amino acid determinants in the PSGL-1 N-terminus (73). PSGL-1 is present on granulocytes and monocytes and facilitates tethering to endothelial cells. Binding of *A. phagocytophilum* activates the PSGL-1 signaling pathway, which results in Syk mediated tyrosine phosphorylation of ROCK1 (161, 184, 196). ROCK1 mediates actin cytoskeleton reorganization and is important for bacterial invasion. Inhibiting either Syk or ROCK1 using siRNA significantly impairs *A. phagocytophilum* infection (196). The human promyelocytic cell line HL-60 expresses PSGL-1 and is used for standard *in vitro* cultivation of *A. phagocytophilum* (72). An enriched subpopulation of *A. phagocytophilum*, termed NCH-1A2, binds HL-60 cells in a sLe^x and PSGL-1 independent manner, suggesting the use of alternative receptor(s) for infection (160, 173). Support for this premise is the ability

of *A. phagocytophilum* to bind and infect endothelial cells *in vivo* and *in vitro*, which do not express PSGL-1 (133). Further support is *A. phagocytophilum* binding to murine neutrophils requires α-1,3-fucosylated ligands, but not PSGL-1 (29). The alternative host receptors as well as the *A. phagocytophilum* adhesin(s) that mediates attachment are unknown.

Developmental cycle. Within the host cell *A. phagocytophilum* undergoes a biphasic developmental cycle that consists of two distinct morphological forms, a larger pleomorphic reticulate cell (RC) form and a smaller dense-cored cell (DC) form (**Figure 3A**) (199). By electron microscopy, DCs are distinguished by a dense nucleoid and a ruffled outer membrane, whereas RCs have dispersed nucleoids and are pleomorphic in form (**Figure 3B and C**) (199). The DC binds to the cell surface and mediates entry into neutrophils or human myeloid cells, while the RC does not. Similar results have been observed for *A. phagocytophilum* binding to ISE6 tick embryonic cells (132). It takes approximately 4 h to detect individual DCs within nascent vacuoles (20, 28, 96, 199). At 12 h, most of the *A. phagocytophilum*-occupied vacuoles (ApV) contain a few RCs, indicating DC organisms have converted to metabolically active RCs and have initiated replication by binary fission (110, 199). By 24 h, multiple RCs are observed within each ApV (**Figure 3A**). The loss of LPS and peptidoglycan from the cell wall presumably affords the bacteria structural flexibility so they can be tightly packed within the inclusion (112). Also by 24 h, some RCs begin to condense into DCs and are subsequently released from the cell to initiate new infections. Reinfection occurs between 24 and 32 h (199).

1.6 Subversion of host antimicrobial defenses

Neutrophils are the first line of defense against invading pathogens. Therefore to establish a safe haven in such an inhospitable host, *A. phagocytophilum* has evolved mechanisms to subvert an array of powerful antimicrobial defenses. The strategies used are complex and

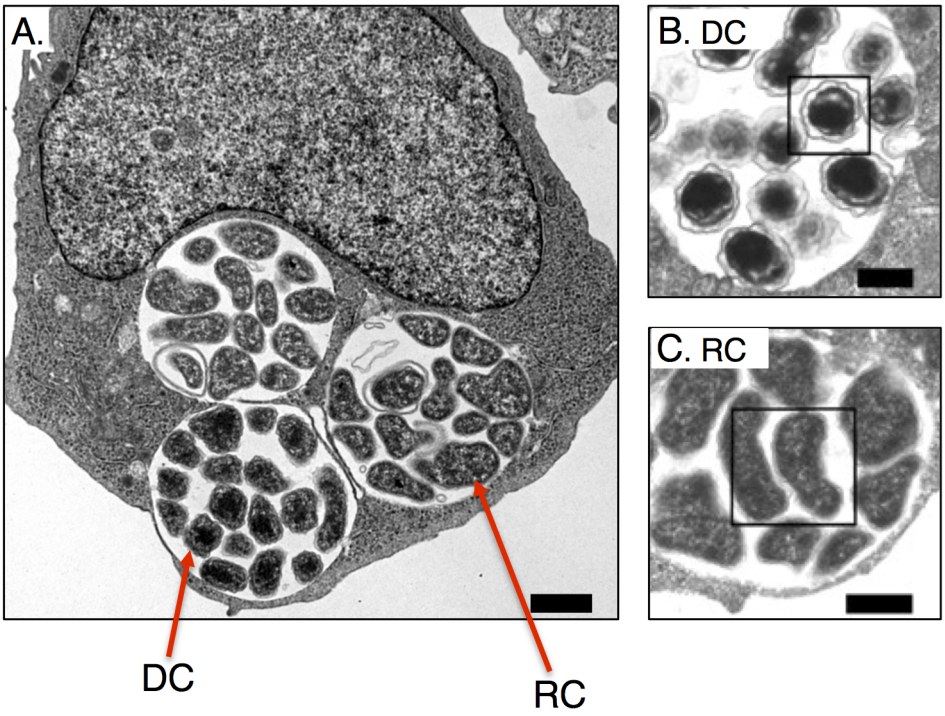

Figure 3. Biphasic development of *A. phagocytophilum* in HL-60 cells.
(**A**) Transmission electron micrograph of an *A. phagocytophilum* infected HL-60 cell at 24 h post infection. *A. phagocytophilum* undergoes a biphasic developmental cycle that consists of two morphologically distinct forms – (**B**) a dense-cored cell (DC) and a (**C**) pleomorphic reticulate cell (RC). The insets demarcated by solid boxes in **B** and **C**, are representative images of a DC and a RC, respectively. The DC binds to host cells and induces its internalization into a nascent vacuole where it converts to the RC form. The RC begins to replicate and by 24 h post infection multiple bacteria can be seen in an inclusion. In addition, at 24 h the RC begin to revert back to the DC form to prepare for reinfection. Scale bar equals 1 μm. Image from: Troese MJ, Carlyon JA. *Anaplasma phagocytophilum* dense-cored organisms mediate cellular adherence through recognition of human P-selectin glycoprotein ligand 1. Infect Immun 2009;77(9):4018-4027.

multifactorial.

Inhibition of O_2^- production. Upon exposure to pathogens, a primary means used by neutrophils to destroy bacteria is the generation of toxic oxygen intermediates derived from superoxide (O_2^-). Collectively, the influx of O_2^- into the phagosome that is reduced to H_2O_2 and HOCl, and the potassium-dependent release of proteases destroys engulfed bacteria (158, 169). In activated neutrophils, the nicotinamide adenine dinucleotide phosphate-oxidase (NADPH) complex is rapidly assembled at the phagosome and/or plasma membrane. In resting neutrophils, the components are dispersed and segregated into membranes of secretory vesicles and specific granules. To combat oxygen-dependent killing, *A. phagocytophilum* blocks the assembly of a functional NADPH oxidase in the ApV membrane and inhibits transcription of components necessary for generating O_2^- (28, 31, 96, 130). In addition, *A. phagocytophilum* detoxifies O_2^- triggered by exogenous stimuli, such as LPS, or *E. coli* (28). These inhibitory effects are consistent with *in vivo* observations of reduced NADPH oxidase activity in neutrophils from *A. phagocytophilum* infected mice (29, 207).

Inhibition of neutrophil apoptosis. Although abundant, neutrophils have a very short half-life in circulation (8-20 h) (3). Peripheral blood neutrophils are naturally programmed for spontaneous apoptosis. However, in response to infection induced apoptosis is readily and rapidly initiated (39). As a survival strategy, *A. phagocytophilum* prolongs the life span of their naturally short-lived host cell by delaying neutrophil apoptosis (67, 68, 214). This affords the bacterium sufficient time to replicate. *In vitro*, *A. phagocytophilum* infected neutrophils remain non-apoptotic for up to 96 h, with similar results observed in *A. phagocytophilum* infected ovine neutrophils *ex vivo* (68, 214). Reactive oxygen species (ROS) initiate neutrophil apoptosis by activating the death receptor pathway. Furthermore, there is a reduced rate of apoptosis observed in NADPH oxidase deficient neutrophils (89, 174). Therefore the ability of *A. phagocytophilum* to delay apoptosis is coupled to its active interference of ROS production. Spontaneous apoptosis can also be initiated by Fas receptor

clustering on the cell surface. Studies have shown *A. phagocytophilum* prevents clustering of Fas and consequently blocks apoptosis (67). Neutrophil apoptosis is also initiated by the translocation and insertion of the proapoptotic protein Bax into the mitochondrial membrane. The *A. phagocytophilum* T4SS effector Ats-1 contains a cleavable N-terminal targeting sequence that localizes it to the mitochondrial matrix and prevents Bax translocation (139). As a result, apoptosis is blocked. Microarray studies have reported increased transcription of the antiapoptotic *bcl-2* family during *A. phagocytophilum* infection of neutrophils (20, 109). Collectively, *A. phagocytophilum* has evolved multiple mechanisms to target and delay host apoptosis.

1.7 Pathogenesis and immune responses

Neutrophils express receptors that recognize pathogen-associated molecular patterns (PAMPs) on the surface of microorganisms, such as LPS and peptidoglycan. Such recognition triggers a robust innate immune response. Efficient clearance of microbial infections depend upon a productive cytokine response but may also contribute to disease severity and tissue damage. Evidence from murine models and human studies of *A. phagocytophilum* infection highlight a discrepancy between bacterial burden and histopathology, suggesting the innate immune response contributes more to disease pathology than pathogen load (13, 54, 56). In human *A. phagocytophilum* infection, the most prominent cytokine, gamma interferon (IFN-γ), is thought to be the critical contributor to histopathologic severity (23, 52, 123, 124). Support for this is IFN-γ deficient mice infected with *A. phagocytophilum* show a prominent increase in pathogen load yet exhibit complete loss of histopathologic lesions (4). However, when IL-10 (a cytokine that suppresses IFN-γ) is depleted, mice develop severe tissue lesions with no change in pathogen load (124). Together these studies establish a link between immune response and histopathologic injury that is independent of bacterial load. A recent

study extends these findings to a horse model, showing disease severity is dampened with attenuated immune response to *A. phagocytophilum* infection (45). The advantage of the horse model is that horses develop a very similar disease with the underlying histopathology to that observed in human disease.

The proinflammatory cytokines tumor necrosis factor α (TNF-α), IL-1β, IL-4, and IL-6 are not elevated in sera from HGA patients or infected mice (4, 56). In contrast, another study reported elevated transcription of IL-1β, TNF-α, and IL-6 in peripheral blood leukocytes and monocytes in response to *A. phagocytophilum* (100), suggesting a role for monocytes in the production of proinflammatory cytokines. The involvement of monocytes is supported by the activation of p38 MAPK and NF-κB in human monocytes, but not in human neutrophils, in response to *A. phagocytophilum*. It is unclear whether the lack of neutrophil activation is a result of active suppression by *A. phagocytophilum*. In addition, *A. phagocytophilum* inhibits mast cell activation, demonstrated by the failure of *A. phagocytophilum*-infected bone marrow derived mast cells (BMMCs) to secrete TNF-α, IL-6, and IL-13 upon IgE stimulation. Electron micrographs corroborate this by showing BMMCs containing *A. phagocytophilum* organisms do not degranulate (143).

A. phagocytophilum infection induces several chemokines, including IL-8, monocyte chemotactic protein 1, and macrophage inflammatory proteins 1α and 1β (5, 103). IL-8 is a chemokine that recruits neutrophils to sites of infection as a host defense against invading microbes. It has been demonstrated that *A. phagocytophilum* infected neutrophils secrete increased levels of IL-8 and upregulate expression of the IL-8 receptor (CXCR2) (5, 191). Thus, *A. phagocytophilum* may exploit host IL-8 response to effectively recruit naive neutrophils and promote bacterial dissemination (5). Overall, evidence indicates *A. phagocytophilum* manipulates signaling pathways involved in host phagocyte activation but the exact mechanisms are yet to be fully understood.

1.8 Establishing an intracellular niche

Bacteria that adapt to an intracellular lifestyle are protected from cytosolic immune surveillance and the subsequent signaling cascades they activate. However, within an infected cell, the pathogen must overcome powerful host antimicrobial defenses that can trigger fusion with lysosomes, autophagy, and/or apoptosis. In addition the integrity and stability of the pathogen-occupied vacuole (PV) must be carefully maintained to evade detection by host immune surveillance. Although some intracellular pathogens escape from the PV and reside in the cytoplasm, many remain exclusively in membrane-bound compartments. Initially upon entry, the PV shares molecular features of early endosomes. But soon thereafter, pathogen-derived proteins and lipids modify the PVs and consequently their fusogenicity with host vesicular pathways is altered. As a result, PVs become unique compartments with features tailored to the survival strategy of the specific pathogen.

The *A. phagocytophilum*-occupied vacuole. *A. phagocytophilum* resides and replicates exclusively within a host-cell derived vacuole that exhibits an altered fusogenicity. It does not resemble early endosomes as it lacks transferrin receptor (TFR), early endosomal antigen I, Rab5, and annexins I, II, IV and VI (129, 209). It lacks endosomal markers α-adaptin and clathrin heavy chain. It does not acidify, does not acquire the late endosomal/lysosomal markers myeloperoxidase, CD63, Lysosomal-associated membrane protein 1 (LAMP-1) and vacuolar-type H^+ ATPase and avoids lysosomal fusion. The ApV excludes fusion with secretory vesicles and specific granules harboring NADPH oxidase and proteolytic enzymes (28, 96, 130). Furthermore, it fails to acquire Golgi vesicular markers β-coat protein (COP) or C6-NBD-ceramide, and bacterial growth is unhindered by the Golgi apparatus destabilizing agent, Brefeldin A (BFA) (129).

While the ApV stains negative for most endosomal, lysosomal and Golgi markers, it is not an inert compartment that is completely sequestered from membrane traffic. The

ApV acquires endocytosed bovine serum albumin (BSA)-gold (209), which indicates that it intercepts some arm of endocytic traffic. Moreover, mannose-6-phosphate receptor (MPR), which is found on late endosomes, pre-lysosomes and trans-Golgi vesicles (69), and major histocompatibility complex (MHC) class I and class II molecules, which traffic from the Golgi to recycling endosomes and the plasma membrane (8, 136), are found on the ApV (129). Also, the AVM has been shown to accumulate early autophagosomal markers, caveolae markers, and cholesterol, each of which is important for bacterial survival, as well as multiple signaling molecules (112, 141). How the ApV interfaces with desired vesicular trafficking pathways while excluding those that facilitate microbial killing is poorly understood.

1.9 Research objectives

Vacuole-adapted pathogens have evolved complex functional interfaces involving specific bacterial-encoded proteins to modulate host cellular functions and establish a replicative permissive niche. Therefore, the pathogen-occupied vacuolar membrane (PVM) is a crucial interface to study host-pathogen interactions and elucidate the pathways the bacteria exploit. *A. phagocytophilum* modifies the vacuole in which it resides to evade lysosomal degradation and subvert antimicrobial defenses. However, the mechanism by which this occurs is poorly understood. We reasoned that because bacterial protein synthesis is required for successful establishment of a protective niche, *A. phagocytophilum* encoded proteins that modify the ApV are likely candidates for manipulating host cellular processes (70). The work presented here focuses on the intracellular trafficking of the ApV and describes the contribution of bacterial encoded proteins. This work is divided into two research goals; the first is to assess whether the altered fusogenicity of the ApV is attributable to the selective acquisition of host membrane traffic regulators, specifically Rab GTPases, and the second is to identify

and characterize *A. phagocytophilum*-encoded proteins that modify the ApV. These analyses provide insight into *A. phagocytophilum's* ability to target conserved host pathways and contribute to our understanding of how bacterial pathogens control their intracellular fate.

Materials and Methods

Cell lines and *in vitro* cultivation of *A. phagocytophilum*.

The human promyelocytic cell lines HL-60 (American Type Culture Collection [ATCC] CCL-240; Manassas, VA) and THP-1 (ATCC TIB-202) and *A. phagocytophilum* strain NCH-1-infected HL-60 and THP-1 cells were cultivated in Iscove's Modified Dulbecco's Medium (IMDM-10; Invitrogen, Carlsbad, CA) supplemented with 10% fetal bovine serum (FBS; Gemini Bio-Products, Sacramento, CA). The human microvascular endothelial cell line HMEC-1 (1) was obtained from the Centers for Disease Control (CDC) and Prevention (Atlanta, GA). Uninfected and *A. phagocytophilum*-infected HMEC-1 cells were propagated in MCDB 131 (Mediatech, Herndon, VA) supplemented with 10 ng ml^{-1} epidermal growth factor (Becton Dickinson, Franklin Lakes, NJ), 1.0 μg ml^{-1} hydrocortisone (Sigma, St. Louis, MO), and 10% FBS. RF/6A monkey choroidal endothelial cells (ATCC CRL-1780) were cultured in Dulbecco's Modified Eagle's Medium (DMEM; Invitrogen) supplemented with 10% FBS (Gemini Bio-Products), 2 mM L-glutamine, 1x Minimum Essential Medium (MEM) non-essential amino acids (Invitrogen), and 15 mM HEPES. HeLa 229 epithelial cells (ATCC CCL-1.2) were grown in Roswell Park Memorial Institute 1640 medium (RPMI; Invitrogen) supplemented with 10% FBS. All cell lines described above were maintained at 37°C in 5% CO_2. ISE6 cells, which were derived from *I. scapularis* embryos (132), were a kind gift from Dr. Ulrike Munderloh and Curt Nelson (University of Minnesota, Minneapolis, MN). Uninfected and *A. phagocytophilum* infected ISE6 cells were maintained

in L15B300 medium supplemented with 5% FBS, 0.1% bovine lipoprotein concentrate, pH 7.2 at 34°C in closed flasks (132). L15B300 medium for *A. phagocytophilum* infected cultures was buffered with 25 mM HEPES and 0.25% $NaHCO_3$ and the pH was adjusted to 7.5-7.7 with NaOH.

Generation of fluorescent protein-tagged Rab GTPases.

Constructs encoding green fluorescent protein (GFP)-tagged Rab5 and GFP-Rab7 were kindly provided by Anthony Nicola (Virginia Commonwealth University). Constructs encoding human GFP-Rab1, GFP-Rab4A, GFP-Rab6A, GFP-Rab10, and GFP-Rab11A have been previously described (171). pEGFP-Rab2A, pEGFP-Rab3A, pEGFP-Rab8A, pEGFP-Rab14 and pEGFP-Rab18 were constructed by cloning the coding regions of the respective human gene contained on *Bam*HI/*Xho*I fragments (Missouri S&T cDNA Resource Center) into the *Bgl*II and *Sal*I sites of pEGFPC1 (Clontech, Palo Alto, CA). pEGFP-Rab33A was constructed by cloning the coding region of human Rab33A contained within an *Eco*RI/*Xho*I fragment on pCDNA3.1-Rab33A (Missouri S&T cDNA Resource Center) into the *Eco*RI and *Sal*I sites of pEGFPC2. pEGFP-Rab35 was constructed by PCR amplification using a gene-specific primer designed with a 5′ *Eco*RI site and a 3′ gene-specific primer with a *Xho*I site (**Table 1**). The PCR product was digested with *Eco*RI and *Xho*I and cloned into the *Eco*RI and *Sal*I sites of pEGFPC2. PCR amplifications were performed using HiFidelity Platinum *Taq* polymerase (Invitrogen), and the fusion construct was confirmed by DNA sequencing (BioResource Center, Cornell University, Ithaca, NY). Human Rab13, Rab20, Rab22A, Rab23, and Rab27A coding sequences were PCR amplified from cDNA templates purchased from Open Biosystems (Thermo Scientific, Huntsville, AL). Mouse Rab9A coding sequence was PCR amplified from a construct encoding GST-tagged Rab9A. Primers used for amplifying the Rab9A, Rab13, Rab20, Rab22A, Rab23, and Rab27 coding sequences are listed in **Table 1**. PCR products

Table 1. Oligonucleotides used to amplify select Rab GTPases.

Rab GTPase	N-terminal Primer ($5' - 3'$)	C-terminal Primer ($5' - 3'$)
Rab9A	GTGGATCC[a]ATGGCAGGAAAATCGTCTCT	AGGGATCCTCAACAGCAAGATGGAGTTTG
Rab10(S22N)	CCGGAGTGGGGAAGAACTGCGTCCTTTTTC	CGAAAAAGGACGCAGTTCTTCCCCACTCCGG
Rab10(Q68L)	GGATACAGCAGGCCTGGAGCGATTTCAC	GTGAAATCGCTCCAGGCCTGCTGTATCC
Rab10N(N122I)	GAAAGAATGTTACTAGGAATCAAGTGTGATATGGAC	GTCCATATCACACTTGATTCCTAGTAACATTCTTTC
Rab11A(S25N)	GGTGTTGGAAAGAATAATCTCCTGTCTCG	CGAGACAGGAGATTATTCTTTCCAACACC
Rab13	GTGGATCCATGGCCAAAGCCTACGACCA	AGGGATCCTCAGCCCAGGGAGCACTTGT
Rab20	GTGGATCCATGAGGAAGCCCGACAGCAA	AGGGATCCTCAGGCACAACACCCAGATC
Rab22A	GTGGATCCATGGCGCTGAGGGAGCTCAA	AGGGATCCTCAGCAGCAGCTCCGCTTTG
Rab23	TCCCCCGGG[b]AATGTTGGAGGAAGATATGGA	TCCCCCGGGTTAGGGTATGCTACAGCTGC
Rab27A	GTGGATCCATGTCTGATGGAGATTATGA	AGGGATCCTCAACAGCCACATGCCCCCTT
Rab35	GAATTC[c]ATGGCCCGGGACTACGACC	CTCGAG[d]TTAGCAGCAGCGTTT

Underlined nucleotides correspond to restriction sites. **a.** *Bam*HI site. **b.** *Sma*I site. **c.** *Eco*RI site. **d.** *Xho*I site.

were first TA cloned into pGEM-T (Promega, Madison, WI) before digestion with either *Bam*HI or *Sma*I. *Bam*HI- or *Sma*I-digested Rab DNA fragments were ligated in-frame into *Bgl*II- or *Sma*I-linearized vector pTagRFP-TC (a gift from Bret Lindenbach, Yale University, New Haven, CT), which was created by replacing EGFP in the Clontech vector EGFPC3 with a photostable TagRFP-TC (179). The construction of pEGFP-Rab4A(S22N) and pEGFP-Rab4A(Q67L) has been described (170). pEGFP-Rab10(T23N), pEGFP-Rab10(Q68L), pEGFP-Rab10(N122I), pEGFP-Rab11A(S25N), pEGFP-Rab1A(S25N) and pEGFP-Rab1(AQ70L) were constructed using QuikChange (Stratagene, La Jolla, CA) using each respective wild-type fusion as template with the mutagenic oligonucleotides listed in **Table 1**. pEGFP-Rab11A(Q70L) was constructed by PCR amplification using a 5′ gene-specific primer designed with a 5′ *Eco*RI site and a 3′ gene-specific primer with a *Xho*I site (**Table 1**). The PCR product was digested with *Eco*RI and *Xho*I and cloned into the *Eco*RI and *Sal*I sites of pEGFPC2.

Generation of maltose-binding protein (MBP)-APH_1387 and MBP-APH_0032.

The pMal-c2x vector (New England Biolabs, Ipswich, MA) was made into a Gateway destination vector using the Gateway vector conversion system (Invitrogen) by following the manufacturer's protocol; this yielded pMal-c2x/DEST, which was transformed into One Shot *ccd*B Survival competent *E. coli* cells (Invitrogen). pMal-c2x/DEST was isolated from overnight cultures of transformants using a Qiaprep Spin miniprep kit (Qiagen, Valencia, CA). The *aph_1387* and *aph_0032* genes were amplified using Platinum Pfx DNA polymerase (Invitrogen) and the primer sets listed in **Table 2** for pENTR-*aph_1387* and pENTR-*aph_0032*, respectively. The underlined nucleotides correspond to nucleotides in a Gateway-compatible sequence. After we confirmed that the amplicons were the expected size by agarose gel electrophoresis, the amplicons were purified using a QIAquick PCR purification column (Qiagen) and cloned without ligation into pENTR/D-Topo (Invitrogen)

Table 2. Oligonucleotides used to generate GFP-APH_1387 and -APH_0032 fusion constructs.

Designation	N-terminal Primer ($5' - 3'$)	C-terminal Primer ($5' - 3'$)
pENTR-*aph_1387*	CACCATGTATGGTATAGATATAGAGCTAAG	CTAATAACTTAGAACATCTTCATCG
pENTR-*aph_1387*$_{\Delta 181\text{-}579}$	CACCTATGGTATAGATATAGAGCTAAGTGATTACAGAATTCC	CTAGTCTCAACTTCTTCAATTGCTGGTGCTTC
pENTR-*aph_1387*$_{\Delta 122\text{-}579}$	CACCTATGGTATAGATATAGAGCTAAGTGATTACAGAATTCC	CTAGTACATACCTGTACCCTCTTCCTCTTGC
pENTR-*aph_1387*$_{\Delta 101\text{-}579}$	CACCTATGGTATAGATATAGAGCTAAGTGATTACAGAATTCC	CTAACCACCTTCAGCAGTAGCAGC
pENTR-*aph_1387*$_{\Delta 1\text{-}91}$	CACCGGCAGAGCTGCTACTGCTGAAGGTGG	CTAGTCTCAACTTCTTCAATTGCTGGTGCTTC
pENTR-*aph_1387*$_{\Delta 1\text{-}111}$	CACCGTGCAAGAGGAAGAGGGTACAGG	CTAATAACTTAGAACATCTTCATCGTCAGGATCCTTTAACG
pENTR-*aph_1387*$_{\Delta 1\text{-}157}$	CACCTCGGGTGTAGATACGCAAGAAGAACAAG	CTAATAACTTAGAACATCTTCATCGTCAGGATCCTTTAACG
pENTR-*aph_0032*	CACCATGTTTGAACACAATATTCCTGATAC	TCACAACGCGAGCACGTC
pENTR-*aph_0032*$_{\Delta 313\text{-}620}$	CACCTTTGAACACAATATTCCTGATACATACACAGG	CTATAAAGGCAATGTACCTAGTTCCTGAACATTGTC
pENTR-*aph_0032*$_{\Delta 175\text{-}620}$	CACCTTTGAACACAATATTCCTGATACATACACAGG	CTAAGTATCGCTACTATTACACTTGCTGTCTTCAGC
pENTR-*aph_0032*$_{\Delta 143\text{-}620}$	CACCTTTGAACACAATATTCCTGATACATACACAGG	CCTACGGTTGAGGAGCTACTTCCTCG
pENTR-*aph_0032*$_{\Delta 1\text{-}134}$	CACCGGCCGAGGAAGTAGCTCCTCAACC	TCACAACGCGAGCACGTCATC
pENTR-*aph_0032*$_{\Delta 1\text{-}162}$	CACCGACACTGCTGAAGACAGCAAGTGTAATAGTAG	CTCACAACGCGAGCACGTCATC
pENTR-*aph_0032*$_{\Delta 1\text{-}301}$	CACCGACAATGTTCAGGAACTAGGTACATTGCC	TCACAACGCGAGCACGTCATC

Underlined nucleotides correspond to a Gateway entry vector-compatible sequence.

by following the manufacturer's instructions, which yielded the entry plasmids pENTR-*aph_1387* and pENTR-*aph_0032*. The entry plasmids were transformed into chemically competent *E. coli* One Shot cells (Invitrogen) and subsequently isolated from overnight cultures. The insert sequence and cloning junctions were verified.

One hundred fifty nanograms of pENTR-*aph_1387* and pENTR-*aph_0032* were incubated with 150 ng of pMal-c2x/DEST and LR Clonase II (Invitrogen) at 25°C for 1 h to facilitate recombination of the *aph_1387* and *aph_0032* inserts downstream of the gene encoding MBP of pMal-c2x/DEST, which yielded pMal-c2x-*aph_1387* and pMal-c2x-*aph_0032*. Proteinase K was added to a final concentration of 0.18 μg μl^{-1}, and then the preparations were incubated at 37°C for 10 min, after which the LR recombination reaction mixtures were transformed into *E. coli* DH5α cells (Novagen, Madison, WI). Cultures of the transformants were grown in Luria-Bertani (LB) medium containing 100 μg ml^{-1} ampicillin at 37°C with shaking at 250 revolutions per minute (rpm). When the cultures were in the mid-logarithmic phase of growth (optical density at 600 nm [OD_{600}], 0.4), expression of MBP-APH_1387 and MBP-APH_0032 were induced at 37°C by adding isopropyl-β-D-thiogalactopyranoside (IPTG) to a final concentration of 0.5 mM, and the cultures were grown for another 3 h. Portions (80 ml) of the induced bacterial suspensions were harvested by centrifugation at 4000 *g* for 10 min at 4°C. Each pellet was resuspended in 5 ml column buffer (20 mM Tris-HCl [pH 7.4], 200 mM NaCl, 1 mM EDTA) and frozen overnight at -20°C. Frozen pellets were thawed in cold water and placed in an ice-water bath, in which they were sonicated. Soluble crude extracts were recovered by centrifugation at 9000 *g* for 20 min at 4°C. The crude extracts were loaded onto columns containing amylose resin (New England Biolabs) at a flow rate of 1 ml per min. The columns were washed with 12 column volumes of column buffer. MBP-APH_1387 and MBP-APH_0032 were eluted in column buffer containing 10 mM maltose, and 3 ml MBP-APH_1387 and MBP-APH_0032 fractions were collected and were visualized by Coomassie brilliant blue

staining following resolution by sodium dodecyl sulfate-polyacrylamide gel electrophoresis (SDS-PAGE). Desired fractions were pooled and concentrated by centrifugation through an Amicon Ultra-4 centrifugal filter with a 50 kDa cutoff (Millipore, Bedford, MA) to minimize the content of undesired breakdown products. Concentrated protein preparations were quantified using the Bradford assay (96).

Generation of GFP tagged-APH_1387 and -APH_0032 constructs.

The full-length and truncated *aph_1387* and *aph_0032* genes were amplified using Platinum Pfx DNA polymerase (Invitrogen) and the primers listed in **Table 2**. The underlined nucleotides correspond to nucleotides in a Gateway-compatible sequence. The amplicons were confirmed by agarose gel electrophoresis, purified using a QIAquick PCR purification column (Qiagen) and cloned without ligation into pENTR/D-Topo (Invitrogen) using the manufacturer's instructions. The entry plasmids were transformed into chemically competent *E. coli* One Shot cells (Invitrogen) and subsequently isolated from overnight cultures. The insert sequence and cloning junctions were verified. One hundred fifty ng of each entry plasmid was incubated with 150 ng of pDest53 and LR Clonase II (Invitrogen) at 25°C for 1 h to facilitate recombination of the inserts downstream of the gene encoding GFP (N-terminal fusion vector). Proteinase K was added to each reaction to a final concentration of 0.18 μg μl^{-1} and incubated at 37°C for 10 min, after which the LR recombination mixtures were transformed into *E. coli* One Shot *ccd*B Survival T1 Phage-Resistant Cells (Invitrogen). Plasmid DNA was isolated from overnight cultures of the transformants grown in LB medium containing 100 μg ml^{-1} ampicillin at 37°C with shaking at 250 rpm.

Generation of CyaA plasmid construction and clone verification.

The *aph_0032* gene was amplified from *A. phagocytophilum* DNA using AccuPrime Pfx polymerase (Invitrogen) and the primer set listed in **Table 3** for pJB2581-*aph_0032*. Dif-

Table 3. Oligonucleotides used to generate CyaA fusion constructs

Designation	N-terminal Primer ($5' - 3'$)	C-terminal Primer ($5' - 3'$)
pJB2581-*aph_0032*	TTCCGGCTATGGATCCATGTTTGAACACAATATTCCTGATAC	ACAAGCTTGCATGCCTGCAGTCACAACGCGAGCACGTCA
pJB2581-*aph_0740*	TTCCGGCTATGGATCCGGAACTAGTAGCTCTTTTGCAGCT	ACAAGCTTGCATGCCTGCAGCTACCTACCGCGACCTCCTT
pJB2581-*aph_1387*	TTCCGGCTATGGATCCGTGGTAGTTGCTCCAGAAGCGC	ACAAGCTTGCATGCCTGCAGCTAATAACTTAGAACATCTTCA

Underlined nucleotides correspond to pJB2581 compatible sequence

ficulty in cloning and expressing the entire open reading frames of *aph_0740* (*ankA*) and *aph_1387* necessitated cloning the C-terminal 100 residues of these proteins using the primer sets listed in **Table 3** for pJB2581-*aph_0740* and pJB2581-*aph_1387*, respectively. It is important to note that the translocation signal of T4SS substrates is located in the C-terminus and the final 100 aa of T4SS substrates are sufficient for translocation (201). To allow high-efficiency recombinational cloning, the $5'$ ends of forward and reverse primers contain 15 bases (denoted by the underline) that are homologous with the sequence at the ends of the CyaA fusion vector pJB2581 linearized with *Bam*HI and *Pst*I. PCR products were cloned into pJB2581 (170) linearized with *Bam*HI/*Pst*I using the In-fusion Advantage PCR Cloning Kit (Clontech) to generate gene fusions encoding *A. phagocytophilum* proteins N-terminally fused to the C-terminus of CyaA. *L. pneumophila* was transformed with plasmid constructs by electroporation as previously described (203). Plasmids were isolated from colonies, and *Bam*HI/*Pst*I restriction enzyme digests were performed to confirm the presence of the expected restriction fragment. Expression of CyaA fusion proteins by wild type and DotA$^-$ *L. pneumophila* was verified by immunoblotting (203).

Transfections.

HL-60 Nucleofection. Uninfected or *A. phagocytophilum* infected HL-60 cells (2×10^6) were transiently transfected with 2 μg of endofree purified DNA (Qiagen) using the Nucleofector II device (Lonza, Cologne, Germany), Nucleofector solution V, and T-19 program, according to the manufacturer's protocol. Following nucleofection, the cells were transferred into 12-well plates containing 1.5 mL IMDM Media (Invitrogen) supplemented with 10% FBS and incubated at 37°C.

HeLa Transfection. HeLa cells were seeded onto coverslips and transfected with 0.4 μg of plasmid using Lipofectamine 2000 (Invitrogen) according to the manufacturer's protocol.

Twenty four hours post transfection cells were fixed in 4% paraformaldehyde (PFA) in phosphate buffered saline (PBS) for 1 h and permeabilized with ice-cold methanol for 30 s.

RF/6A electroporation. RF/6A cells were electroporated using the Gene Pulser Xcell System (Bio-Rad). RF/6A cells were resuspended in OPTI-MEM (Invitrogen) at a final density of 10^6 cells ml^{-1} and mixed with 3 μg plasmid DNA. The cells were subjected to a pulse in a 0.4 cm cuvette. The setting was 250 V, 1000 μF, with a 20 ms pulse time. Following electroporation, cells were immediately transferred into pre-warmed media, seeded onto coverslips and incubated at 37°C.

Immunofluorescence microscopy.

HL-60 and THP-1 cells. Asynchronous *A. phagocytophilum*-infected and uninfected control HL-60 or THP-1 cells were washed twice with PBS, cytocentrifuged onto glass slides using a 200 μl volume of 3×10^4 cells at 1000 *g* for 3 min in a Cytospin 4 centrifuge (Thermo Electron), followed by fixation and permeabilization in methanol for 4 min. In some cases, a synchronous *A. phagocytophilum* infection of HL-60 cells was established as described (87), after which aliquots were removed at multiple time points over a 72 h period. The nucleofected cells were incubated for 5 h at 37°C in 5% CO_2 in a humidified incubator. Cells were then washed twice with PBS, cytocentrifuged onto glass slides, fixed in 2% PFA for 20 min and permeabilized in ice-cold methanol for 30 s.

To assess for fluorescently tagged-Rab GTPase recruitment to the ApV at 4, 6, 8, and 12 h post infection, uninfected HL-60 cells were first nucleofected with plasmids encoding GFP- or red fluorescent protein (RFP)-tagged Rab GTPases. Five hours post-nucleofection, the cells were incubated with host cell-free *A. phagocytophilum* organisms then washed twice with PBS after 40 min and centrifuged at 300 *g* for 5 min to remove unbound bacteria. At the appropriate time points, the cells were fixed and labeled with antibodies as described above. Because we observed that GFP signal begins to fade in nucleofected cells between

18 and 24 h, it was necessary to infect HL-60 cells for an appropriate time period prior to nucleofection in order to more accurately assess GFP- or RFP-Rab recruitment to the ApV at time points beyond 12 h. Accordingly, HL-60 cells were incubated first with host cell-free *A. phagocytophilum* organisms then washed twice with PBS after 40 min to remove unbound bacteria. Seven h post infection, the cells were nucleofected with GFP- or RFP-Rab DNA, and then assessed at 5, 11, and 17 h post-nucleofection, which corresponded to 12, 18, and 24 h post infection, respectively. Cells that were nucleofected prior to infection and cells that were infected prior to nucleofection exhibited nearly identical numbers of bound *A. phagocytophilum* organisms at the beginning of each time course (data not shown), which confirmed that the infection rates for each set proceeded comparably. Likewise, examination of cells that were nucleofected prior to infection and cells that were infected prior to nucleofection at 12 h post infection revealed highly similar rates of GFP- or RFP-Rab GTPase recruitment to the ApV for all GFP- and RFP-Rabs examined.

HMEC-1, RF/6A and HeLa cells. HMEC-1, RF/6A or HeLa cells were grown on glass coverslips in 24-well tissue culture plates. HMEC-1 or RF/6A cells were incubated with host cell-free *A. phagocytophilum* organisms, centrifuged at 300 *g* for 5 min to facilitate bacterial attachment, followed by a 1 h incubation at 37°C in 5% CO_2. Next, the cells were washed twice with PBS to remove unbound bacteria. At appropriate time points cells were fixed in 4% PFA for 1 h followed by permeabilization in ice-cold methanol for 30 s.

C3H/H2N severe combined immunodeficiency (scid) mice. C3H/HeN scid mice were infected with NCH-1 exactly as previously described (28). On day 8 post infection, whole blood was collected by cardiocentesis in EDTA and centrifuged, and the leukocyte-rich buffy coat was removed and cytospun onto glass slides at 113 *g* for 5 min. The slides were fixed in ice-cold methanol and stored at -20°C until they were used.

ISE6 cells. To facilitate *A. phagocytophilum* infection of ISE6 cells, the tick cells were grown to confluence in 25 cm^2 flasks, after which they were incubated with 1×10^7 *A.*

phagocytophilum infected (≥90%) HL-60 cells in L15B300 medium at 34°C. After 3 days, the culture medium was replaced to replenish nutrients and remove any unlysed HL-60 cells. Infected ISE6 cells were cytocentrifuged, followed by fixation and permeabilization in methanol for 4 min. In some cases Ulrike Munderloh (University of Minnesota) kindly provided slides of PFA-fixed *A. phagocytophilum*-infected ISE6 cells.

All slides were blocked with 5% BSA in PBS for 1 h. Primary antibodies were: mAb FK2 (BIOMOL, UK), mAb FK1 (BIOMOL), rabbit polyclonal anti-APH_1387, rabbit polyclonal anti-APH_0032, mouse mAb anti-Msp2 (P44) 20B4 (kindly provided by J. Stephen Dumler of John Hopkins University, Baltimore, MD, USA), Rab14 (Aviva Systems Biology LLB, San Diego, CA, USA), LAMP-1 specific mAb (clone H4A3; University of Iowa Developmental Studies Hybridoma Bank, Iowa City), mouse GM130 (BD Transduction), mouse calnexin (BD Transduction). AlexaFluor fluorescent conjugated secondary antibodies (Invitrogen) were used at 1:1000 dilutions and incubated for 30 min. Coverslips were mounted with ProLong Gold Antifade with 4'-6'-diamidino-2-phenylindole (DAPI; Invitrogen) and examined by confocal microscopy.

Slides were examined by confocal microscopy using a TCS-SP2 AOBS inverted confocal microscope (Leica Microsystems, Bannockburn, IL). Some images were acquired by spinning disc confocal microscopy using a BX51 microscope (Olympus, Center Valley, PA) affixed with an Olympus disk spinning unit and an Orca-R2 CCD camera (Hammamatsu, Japan). Images were processed using the Slidebook software package (Intelligent Imaging Innovations, Denver, CO). In experiments where the ApV was measured, analyses were performed using ImageJ (National Institutes of Health, USA; rsb.info.nih.gov/ij).

BFA or tetracycline treatment of *A. phagocytophilum* infected HL-60 cells.

To determine whether continued association of GFP-Rab10 or GFP-Rab14 to the ApV is dependent on an intact Golgi apparatus, *A. phagocytophilum* infected HL-60 cells were

nucleofected to express GFP-Rab10 or GFP-Rab14. Two h post-nucleofection, BFA (EMD Biosciences, San Diego, CA) in methanol was added to a final concentration of 1 μg ml^{-1} for 3 h. Methanol alone served as a vehicle control. To determine whether an intact Golgi apparatus is required for initial GFP-Rab10 or GFP-Rab14 recruitment to the ApV, BFA was added to uninfected HL-60 cells immediately following nucleofection. After 3 h, host cell-free *A. phagocytophilum* organisms were added. After 2 h (5 h post nucleofection), the cells were washed to remove unbound bacteria followed by 4 h continued incubation in the presence of BFA. To determine whether selective Rab recruitment to the ApV is bacterial protein synthesis-dependent, *A. phagocytophilum* infected HL-60 cells were nucleofected to express GFP-Rab5, GFP-Rab7, GFP-Rab10, GFP-Rab11A, GFP-Rab14, RFP-Rab22A, or GFP-Rab35. Five h post-nucleofection, tetracycline (Sigma) solubilized in 70% ethanol was added to a final concentration of 10 μg ml^{-1} for 30 min. Ethanol alone served as a vehicle control. In some experiments, to determine whether the localization of ubiquitinated proteins to the AVM is bacterial protein synthesis-dependent, tetracycline was added to *A. phagocytophilum*-infected HL-60 cells for 1 h. After the appropriate incubation periods in the presence of BFA, tetracycline, or vehicle control, aliquots were removed, processed, and examined by confocal microscopy. To determine if tetracycline treatment promotes ApV-lysosomal fusion, *A. phagocytophilum* infected HL-60 cells expressing GFP-or RFP-Rabs of interest were screened with a LAMP-1-specific mAb (clone H4A3; University of Iowa Developmental Studies Hybridoma Bank) followed by anti-mouse IgG conjugated to Alexa Fluor 594 and examined by confocal microscopy.

In silico sequence analyses of APH_1387 and APH_0032.

The entire APH_1387 and APH_0032 sequences were analyzed using several algorithms in order to obtain clues that would help predict their secondary structure and their ability to associate with the AVM. TMPred (www.ch.embnet.org/software/TMPRED_form.html)

was used to determine if APH_1387 and/or APH_0032 has a transmembrane domain. Protean, which is part of the Lasergene software package (version 8.02; DNASTAR, Madison, WI), was used to assess whether APH_1387 and/or APH_0032 has regions of alpha helices and beta strands, alpha amphipathic sequences, and hydrophobicity, using the Garnier-Osguthorpe-Robson, Eisenberg, and Kyte-Doolittle algorithms, respectively (190, 199, 204). BLASTP (blast.ncbi.nlm.nih.gov/Blast.cgi) was used to identify protein sequences to which APH_1387 or APH_0032 exhibits homology. The SWISS-MODEL (swissmodel.expasy.org), 3Djigsaw (bmm.cancerresearchuk.org/3djigsaw), ESyPred3D (www.fundp.ac.be/sciences/biologie/urbm/bioinfo/esypred), and Geno3d (geno3dpbil.ibcp.fr/cgibin/geno3d_automat.pl?page=/GENO3D/geno3d_home.html) algorithms were used in attempts to predict a tertiary structure for APH_1387 or APH_0032.

Generation of anti-APH_1387 and anti-APH_0032 polyclonal antiserum.

MBP-APH_1387 and MBP-APH_0032 were submitted to Animal Pharm Services (Healdsburg, CA) for production of rabbit polyclonal antiserum. Immunoreactivity against MBP-APH_1387 and native *A. phagocytophilum* APH_1387 was confirmed by Western blotting, as was the lack of recognition of APH_1387 by preimmune serum. This was repeated to confirm immunoreactivity against MBP-APH_0032. Anti-MBP-APH_1387 and anti-MBP-APH_0032 are referred to as anti-APH_1387 and anti-APH_0032, respectively.

Preparation of host cell-free *A. phagocytophilum* populations containing DC and RC organisms or only DC organisms.

To isolate host cell-free *A. phagocytophilum* DC and RC organisms, infected (90%) HL-60 cells were mechanically disrupted by repeated passage through a 27-gauge needle. To isolate DC organisms, infected HL-60 cells were subjected to eight 8-s bursts on ice interspersed with 8-s rest periods using a Misonix S4000 ultrasonic processor (Farmingdale, NY) with

an amplitude setting of 30, which destroyed host cells and fragile RC organisms but not hardy DC organisms, as confirmed by transmission electron microscopy (data not shown). Bacteria were separated from unbroken host cells and debris by differential centrifugation as described previously (63).

Western blotting.

Whole-cell lysates were fractionated by SDS-PAGE, transferred to nitrocellulose, and screened using primary antibodies followed by horseradish peroxidase (HRP)-conjugated goat anti-rabbit IgG, as described previously (30). Actin was detected using anti-human actin mAb (Sigma). Some blots were screened using HGA patient antiserum or normal human serum (generously provided by Erol Fikrig of Yale University). Other primary antibodies were anti-GFP (Clontech), anti-APH_1387, anti-APH_0032. Densitometric analyses were performed using ImageJ (NIH) to quantitatively assess the relative amounts of APH_0032 in whole cell lysates of DC organisms versus DC and RC organisms. Densitometric analyses were also used to assess the increase in APH_1387 and APH_0032 band signal intensity over the course of infection of HL-60 cells. The ratios of the densitometric values for APH_1387 or APH_0032 and actin at different time points were plotted.

Immunoelectron microscopy.

HL-60 cells were incubated with host cell-free *A. phagocytophilum* for 40 min at 37°C . The cells were washed three times with PBS and centrifuged at 300 *g* for 5 min to remove unbound bacteria. At appropriate time points 1×10^6 cells were washed with cacodylate buffer and fixed in 1 ml of 3% PFA-0.05% glutaraldehyde in 0.1 M cacodylate buffer for 45 min at 4°C. The cells were washed four times by resuspending them in 1 ml cacodylate buffer and incubating them at room temperature for 15 min. Next, the Virginia Commonwealth University Department of Neurobiology and Anatomy Microscopy Core Facility transferred

washed cells onto 200-mesh Formvar-coated nickel grids. The grids were washed twice with PBS and blocked with 0.1% BSA/PBS for 1 h. Primary and secondary antibodies were stained sequentially for 1 h. Primary antibodies were anti-APH_1387 (1:200) and anti-APH_0032 (1:200). The secondary antibody was goat anti-rabbit IgG (1:10) conjugated to 6-nm gold particles (Electron Microscopy Sciences). Grids were viewed and images were recorded using a JEM-1230 transmission electron microscope (JOEL, Tokyo, Japan) equipped with a Gatan Ultra Scan 4000SP 4K x 4K charge-coupled device camera.

RT-PCR.

Sukanya Narasimhan (Yale University) kindly provided total RNA isolated from *A. phagocytophilum*-infected *I. scapularis* nymph salivary glands. Total RNA isolated from neutrophils (Gr-1-positive splenocytes) recovered from *A. phagocytophilum*-infected C3H/HeN mice on day 8 post infection has been described previously (31). cDNA stocks and PCR amplicons were generated as described (31) using primer 5′-ATGTTTGAACACAATATTCCTGATAC-3′ and 5′-TCACAACGCGAGCACGTC-3′ to target *aph_0032* transcript and primers 5′-ATGTATGGTATAGATATAGAGCTAAG-3′ and 5′-CCGTTGTGGAGGCATTATCGC-3′ to target *aph_1387* transcript.

***Legionella pneumophila*.**

L. pneumophila JR32 (wild type) and LELA3118 (DotA$^-$) strains were generously provided by Howard Shuman (Columbia University) and were cultured on charcoal yeast extract (CYE) agar plates containing streptomycin (50 μg ml^{-1}) and kanamycin (25 μg ml^{-1}), respectively. For plasmid selection, *L. pneumophila* transformants were additionally grown in the presence of chloramphenicol (10 μg ml^{-1}).

Adenylate cyclase (CyaA) translocation assay.

L. pneumophila transformants were incubated overnight in AYE broth containing chloramphenicol (10 μg ml^{-1}), diluted and then cultured until organisms displayed obvious motility by phase-contrast light microscopy. Prior to infection, THP-1 cells were treated with 200 nM phorbol 12-myristate 13-acetate (PMA; EMD Biosciences) to promote differentiation to an adherent, macrophage-like cell as previously described (204). Prior to infection, IPTG was added to *L. pneumophila* cultures at a final concentration of 1 mM for 2 h to induce expression of CyaA fusion proteins. PMA-differentiated THP-1 cells were plated in 24-well plates (1×10^6 cells/well) and infected with *L. pneumophila* expressing CyaA fusion proteins at a multiplicity of infection of approximately 20. Bacteria were added to wells and the plate centrifuged for 5 min at 180 *g* to initiate contact between organisms and THP-1 cells. After a 30 min incubation at 37°C in the presence of 1 mM IPTG, cells were washed three times in PBS and lysed in 500 μl of a solution containing 50 mM HCl and 0.1% Triton X-100. Samples were boiled for 5 min followed by the addition of 30 μl of 0.5 M NaOH to neutralize the acid. One ml of 95% ethanol was added to samples, which were incubated on ice for 5 min, dried under a vacuum, and resuspended in assay buffer [0.05 M sodium acetate (pH 5.8), 0.02% BSA]. The level of adenosine 3', 5'-monophosphate (cAMP) in dried samples was determined using the cAMP Enzyme immunoassay (GE Healthcare, Piscataway, NJ) according to the manufacturer's protocol. CyaA fusion proteins were considered positive for translocation when the increase in cAMP over CyaA alone (negative control) was at least 2.5-fold and this increase was abolished following expression of fusion proteins in the *L. pneumophila* DotA$^-$ mutant (LELA3118). A CyaA fusion to RalF, a well-characterized *L. pneumophila* Dot/Icm effector (135) was used as a positive control. cAMP levels resulting from translocation of CyaA-RalF were similar to those reported by Bardill et al (17).

Fluorescence-based assay to identify protein regions required for host membrane association.

To identify the region of APH_1387 that facilitates membrane association, HeLa cells were grown on 12 mm glass coverslips and transfected with 0.4 μg of Endofree purified DNA (Qiagen) using Lipofectamine 2000 (Invitrogen) according to the manufacturer's directions. Twenty four h following transfection, cells were washed three times with PBS which does not permeabilize the cells, and fixed in 4% PFA in PBS for 1 h. Duplicate cells were washed with digitonin buffer (125 mM $NaC_2H_3O_2$, 2.5 mM $Mg(CH_3COO)_2$, 25 mM HEPES-KOH, 1 mg ml^{-1} glucose, 1 mM DTT, pH 7.3), incubated with 30 μg ml^{-1} digitonin (Sigma) for 5 min to permeabilize the host cell plasma membrane, washed twice more with digitonin buffer, so that any GFP fusion protein not specifically associating with host-cell membranes was washed out, and fixed in 4% PFA for 1 h. Coverslips were mounted with ProLong Gold Antifade with DAPI (Invitrogen) and the slides were examined by immunofluorescence microscopy (28). Retention was calculated as the percentage of cells that remained GFP-positive after digitonin permeabilization.

Differential permeabilization with digitonin to determine protein topology in the AVM.

To determine whether APH_1387 or APH_0032 are exposed on the cytoplasmic face of the AVM, infected RF/6A cells were differentially permeabilized cells with digitonin or saponin which allows the delivery of antibodies to the cytoplasm or to all the intracellular compartments, respectively. Infected RF/6A cells were washed 2x with digitonin buffer and the plasma membrane was permeabilized by incubation with 30 μg ml^{-1} digitonin for 5 min at room temperature. Cells were then immediately washed with digitonin buffer and incubated with rabbit anti-APH_1387 or rabbit anti-APH_0032 at 37°C. After 20 min, the cells were washed with PBS and fixed with 4% PFA for 1 h. Antibodies bound after digitonin

permeabilization were detected with Alexa Fluor 594-conjugated anti-rabbit antibodies. To confirm that digitonin did not permeabilize the AVM, cells were also incubated with antibodies against Msp2 (P44), which is not expressed on the vacuolar membrane.

Statistical analysis.

The Student's t-test (paired) performed using the Prism 4.0 software package (Graphpad; San Diego, CA) was used to assess statistical significance. Statistical significance is indicated in figure legends (*P < 0.05; **P < 0.01; ***P < 0.001). In some cases, an Analysis of Variance (ANOVA) test was performed. If ANOVA indicated a group difference ($p < 0.05$) then Tukey's test was used to test for a significant difference among groups. Figures were generated using Prism 4.0 and the ggplot2 (210) package for R (193).

The *A. phagocytophilum*-occupied vacuole (ApV) selectively recruits Rab-GTPases that are predominantly associated with recycling endosomes

3.1 Introduction

The Rab family (>60 members) is the largest member of the Ras superfamily of small guanosine triphosphatases (GTPases) (24, 188). Rab GTPases localize to distinct organelles and dictate organelle identity. Specific Rabs cycle on and off endosomes in a dynamic process to control endosomal maturation, which ultimately results in lysosomal fusion. Each of the four steps in membrane trafficking that Rabs regulate – vesicle budding, vesicle delivery, vesicle tethering and fusion of the vesicle and target compartment membranes – are carried out by a diverse collection of effector molecules that bind to specific Rabs in their GTP-bound states. Rab GTPases are molecular switches that cycle between a cytoplasmic, GDP-bound, inactive state and a membrane-associated GTP-bound, active state.

The switch of a GDP-bound Rab to a GTP-bound-Rab is controlled by guanine nucleotide exchange factors (GEFs), which trigger the release of GDP, and GTPase-activating proteins (GAPs), which accelerate hydrolysis of the bound GTP to GDP (24, 188). In their GDP-bound state, Rabs are soluble and bound to guanine nucleotide dissociation inhibitor (GDI). At the acceptor membrane, Rab-GDI interacts with GDI displacement factor (GDF), which removes GDI to enable Rab membrane insertion. Next, a GEF catalyses the conversion of the

membrane bound Rab to its GTP-bound state, which induces a conformational change that allows it to interact with its effectors and initiate its downstream function. After inactivation by their specific GAPs, the GDP-bound Rabs are extracted from the membrane by GDI and returned to the cytosol.

Endosomal recycling pathways return much of the membrane proteins and lipids that are internalized during endocytosis to the plasma membrane (76). Endocytic mechanisms can be classified as either clathrin-dependent or clathrin-independent. TFR is an example of a clathrin-dependent endocytic cargo. In contrast to clathrin-dependent endocytosis, clathrin-independent endocytosis comes in many forms including macropinocytosis and phagocytosis. Unrelated forms of clathrin-independent endocytosis require free cholesterol. Proteins and lipids that reside in sphingolipid-rich lipid rafts are prominent clathrin-independent endocytosis cargo (76, 126, 172). Endogenous proteins that enter cells via clathrin-independent endocytosis include MHC class I proteins and proteins involved in amino acid uptake (22, 58, 157). Clathrin-independent endocytosis- and clathrin-dependent endocytosis-generated vesicles are delivered to the early endosome, which functions as a sorting station. From there, cargo can be routed for degradation to late endosomes and lysosomes or recycled along rapid or slow recycling endosome pathways. Clathrin-dependent endocytic cargo, such as TFR, can be returned to the plasma membrane via either rapid recycling endosomes or slow recycling endosomes, while clathrin-independent endocytic cargo is recycled exclusively by the slow recycling endosome pathway. In slow endocytic recycling, cargo is sorted from the early endosome to an endocytic recycling compartment from which recycling endosomes or tubular recycling endosomes emanate to return cargo to the plasma membrane (76). Several Rab GTPases regulate traffic and confer vesicle identities along recycling endosome pathways (**Table 4**). Rab5 is found on the early endosomes. Rab4 and Rab35 are on rapid recycling endosomes. Rab35 is also associated with tubular recycling endosomes that return cargo to the plasma membrane in both clathrin-dependent

Table 4. Rab GTPases examined in this study

Rab GTPase	Location(s)	Transport function(s)
Rab1	ER exit sites, IC	ER to Golgi, Golgi to ER, IC to PM
Rab2A	IC	ER to Golgi, Golgi to ER
Rab3A	SV, SG	Regulated exocytosis
Rab4A	Rapid RE	Endocytic recycling
Rab5	EE, PM, caveosomes	Endocytosis, EE formation
Rab6A	Golgi	Intra-Golgi, ER to Golgi, endosome to Golgi, Golgi to PM
Rab7	LE	EE to LE, lysosome biogenesis, phagosome maturation
Rab8A	ERC to tubular RE, TGN	ERC to tubular RE, TGN to PM
Rab9A	LE	LE to TGN
Rab10	EE to ERC, tubular RE, TGN	Endocytic recycling, TGN to PM
Rab11A	ERC, RE, tubular RE	Endocytic recycling
Rab13	Tight junctions, EE	Biogenesis of tight junctions
Rab14	EE, ERC, TGN	Endocytic recycling, TGN to EE
Rab18	ER, SG	ER to Golgi
Rab20	Dense apical tubules	Connexin-43 trafficking
Rab22A	EE to ERC, tubular RE	Endocytic recycling, EE to TGN
Rab23	PM, EE	Phagosome to lysosome fusion
Rab27A	SG, melanosomes, T-cell granules	Regulated secretion, Myosin Va recruitment
Rab33A	Medial Golgi	Golgi to ER, autophagy
Rab35	Tubular RE, rapid RE	Endocytic recycling

a. Data summarized from references by Grant and Donaldson (2009), Kelly et al. (2009) and Stenmark (2009).
b. ApV-associated Rab GTPases are denoted by bold text.
EE, early endosome; ER, endoplasmic reticulum; ERC, endocytic recycling center; IC, pre-Golgi intermediate compartment; LE, late endosome; PM, plasma membrane; RE, recycling endosome; SG, secretory granule; SV, synaptic vesicle; TGN, *trans*-Golgi network.

and -independent endocytosis (6). Rab10, Rab11, Rab14 and Rab22A are required for moving cargo from the early endosome to the endocytic recycling compartment (24, 99). The endocytic recycling compartment is defined by the presence of Rab11 and Rab14. Rab11 is also found on recycling endosomes, mediates delivery to the plasma membrane, is essential for MHC class I cargo recycling, and is needed to transport vesicles that bud off from tubular recycling endosomes to the plasma membrane (24). Rab14 is also found on early endosomes and the *trans*-Golgi network and mediates vesicular transport from the *trans*-Golgi network to the endocytic recycling compartment (99). Rab8 and Rab22A are required to transport cargo from the endocytic recycling compartment to Rab10-/Rab22A-/Rab35-positive tubular recycling endosomes (76, 188).

Selective retention of specific Rab proteins with the concomitant exclusion of others has been shown to regulate the construction of vacuolar organelles inhabited by several intracellular bacterial pathogens including *Mycobacterium tuberculosis* (98, 108, 202), *C. burnetii* (77, 78, 168), *Salmonella enterica* serovar Typhimurium (131, 182, 183, 187), *Chlamydia* species (42, 128, 170, 171) and *L. pneumophila* (49, 97, 120, 134). Here, we examined a panel of fluorescent protein-tagged Rab GTPases that function in a variety of membrane trafficking pathways and cellular processes (**Table 4**). We demonstrate that the ApV selectively recruits a subset of fluorescently tagged Rabs that predominantly associate with recycling endosomes in a tetracycline-sensitive manner. Endogenous Rab14 localizes to a comparable percentage of ApVs as its GFP-tagged counterpart. Recruitment of GFP-Rab1, GFP-Rab4A, GFP-Rab11A, GFP-Rab14 and GFP-Rab35 is guanine nucleotide-dependent, while recruitment of GFP-Rab10 is strikingly guanine nucleotide-independent. These data shed light on how *A. phagocytophilum* facilitates its intravacuolar survival and implicates the requirement of bacterial-derived proteins for this strategy.

3.2 Results

3.2.1 Fluorescent protein-tagged Rab1, Rab4A, Rab10, Rab11A, Rab14, Rab22A and Rab35 localize to the ApV.

We reasoned if Rab GTPases are important for the formation, development, and/or altered fusogenicity of the ApV, then specific Rab proteins would be recruited to the ApV while others would be excluded. To investigate this, we transiently nucleofected *A. phagocytophilum*-infected HL-60 cells with plasmids encoding a representative panel of 20 Rab GTPases N-terminally fused to GFP or RFP. The collection of Rabs examined, their organelle locales and functions are listed in **Table 4**. Fluorescently tagged Rabs used here have been confirmed to localize to subcellular compartments similar to those of their endogenous counter parts (171). At 5 h post nucleofection, we analyzed the association of GFP- or RFP-tagged Rabs, or GFP alone to the ApV by confocal microscopy. *A. phagocytophilum* inclusions were demarcated by labeling with a monoclonal antibody against the major surface protein Msp2 (P44), which is present on the *Anaplasma* surface, but not the AVM (91). A distinct subset of fluorescent protein tagged-Rab GTPases localizes to the ApV (**Figure 4** and **Figure 5**). GFP-Rab10, GFP-Rab11A, GFP-Rab14, RFP-Rab22A, GFP-Rab35, GFP-Rab1 and GFP-Rab4A localize to 51.3 $\pm$ 9.5, 42.5 $\pm$ 15.5, 27.5 $\pm$ 7.8, 55.9 $\pm$ 2.9, 46.2 $\pm$ 3.5, 5.5 $\pm$ 3.5 and 4.7 $\pm$ 3.2% of inclusions respectively. For most cells exhibiting Rab localization to the ApV, either all or none of the ApVs within a given HL-60 cell was fluorescent protein-tagged Rab-positive. As an example of a GFP-Rab that does not localize within a single infected cell, GFP-Rab11A associates with most but not all of the bacterial inclusions in the cell presented in **Figure 4D-F**. The accumulations of these fluorescent protein-Rabs at the ApV produce distinct aggregate signal that can be seen as either rim-like or punctate at the periphery of the inclusion membrane. Rim-like staining, which is typified by GFP-Rab10 (**Figure 4A-C**) and GFP-Rab35 (**Figure 4M-O**)

Figure 4. Selective GFP- or RFP-Rab GTPase localization to the *A. phagocytophilum*-occupied vacuole (ApV).

A. phagocytophilum-infected (**A-S**) or uninfected control (**T-V**) HL-60 cells were transiently nucleofected with DNA constructs to express the indicated GFP- or RFP-tagged Rab-GTPases or GFP alone. At 5 h post nucleofection, the cells were fixed and viewed by indirect immunofluorescence. **A-S.** Representative confocal micrograph images depicting localization of GFP-Rab10A (**A-C**), GFP-Rab11A (**D-F**), GFP-Rab14 (**G-I**), RFP-Rab22A (**J-L**), GFP-Rab35 (**M-O**) or GFP-Rab4A (**P**) or lack of recruitment of GFP-Rab18 (**Q**), GFP-Rab33A (**R**), or GFP alone (**S**) to the ApV are presented. Intravacuolar and HL-60 cell surface-associated *A. phagocytophilum* organisms were denoted by indirect immunofluorescence staining with mAb 20B4, which recognizes the *A. phagocytophilum* surface protein, Msp2 (P44), but not the AVM, followed by anti-mouse IgG conjugated to Alexa Fluor-594 (**B, E, H, N, P, Q, R, S**) or Alexa Fluor-488 (**K**). Panels **A, B, D, E, G, H, J, K, M** and **N** present single channel GFP (**A, D, G, M**), RFP (**J**) or Msp2 (P44) (**B, E, H, K, N**) fluorescence. Panels **C, F, I, L, O, P, Q, R** and **S** present merged fluorescent images. **T-V**. In the absence of infection, GFP-Rabs exhibit diffuse and/or organelle-like patterns of fluorescence. Asterisks demarcate HL-60 cell nuclei.

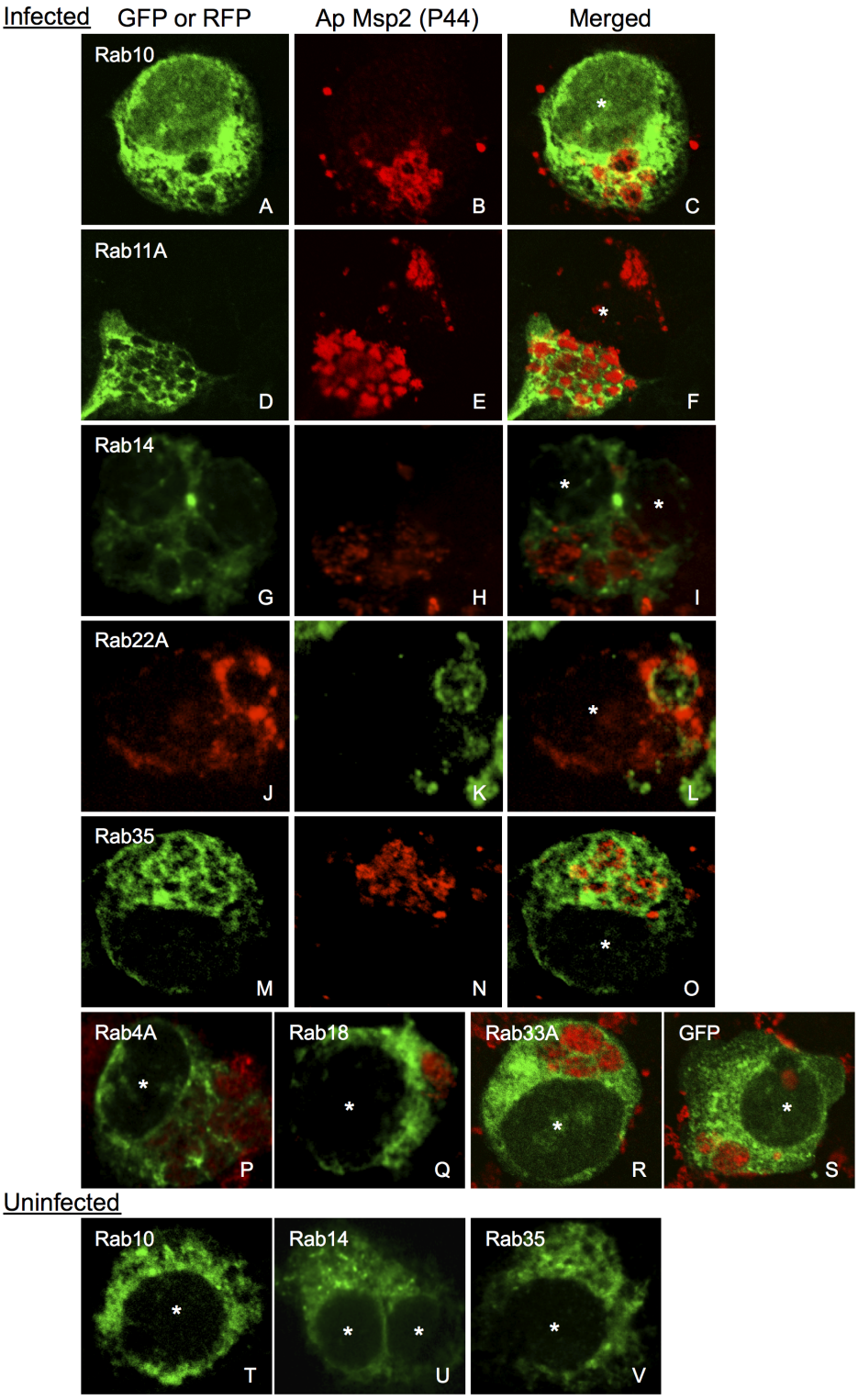
Infected
GFP or RFP
Ap Msp2 (P44)
Merged
Rab10
A
B
C
Rab11A
D
E
F
Rab14
G
H
I
Rab22A
J
K
L
Rab35
M
N
O
Rab4A
P
Rab18
Q
Rab33A
R
GFP
S
Uninfected
Rab10
T
Rab14
U
Rab35
V

Figure 4

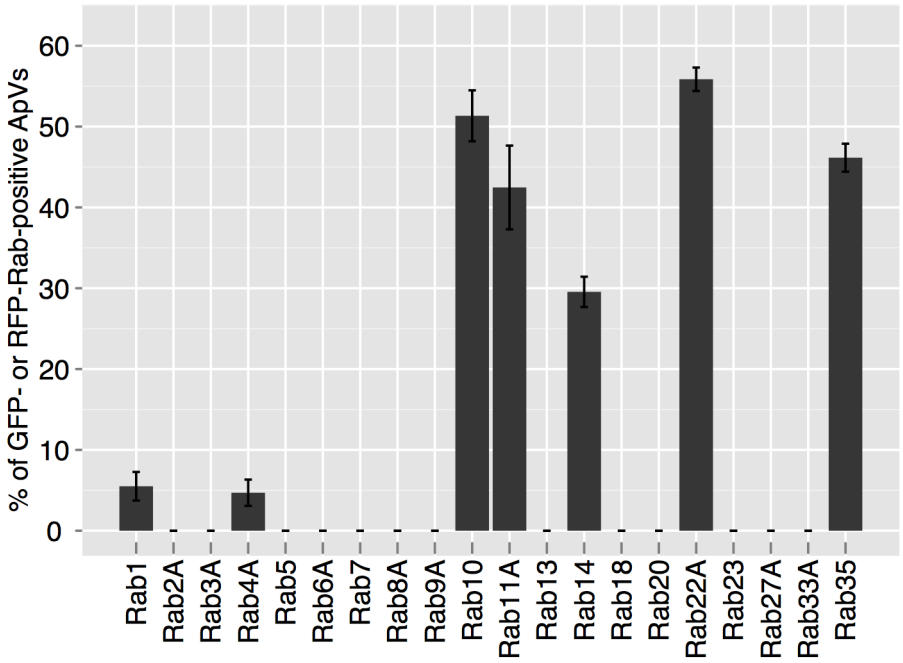

Figure 5. Percentages of ApVs exhibiting GFP- or RFP-Rab GTPase localization.
A. phagocytophilum inclusions as demarcated by anti-Msp2 (P44) staining of intravacuolar bacteria were scored for GFP- or RFP-Rab GTPase localization as in **Figure 4**. The number of GFP- or RFP-positive ApVs was divided by the total number of ApVs, which was multiplied by 100 to determine the percentage of ApVs to which each GFP- or RFP-Rab GTPase localized. Results are presented as the mean percentages (±SD) of ApVs exhibiting GFP- or RFP-Rab GTPase and are derived from two to four separate experiments. Up to 972 bacterial inclusions were examined for localization of each GFP- or RFP-Rab GTPase.

localization to the ApV, indicates that the GFP-Rab is uniformly distributed over the AVM's entirety. Punctate staining, as typified by GFP-Rab11A (**Figure 4D-F**), GFP-Rab14 (**Figure 4G-I**), RFP-Rab22A (**Figure 4J-L**) and GFP-Rab4A (**Figure 4P**), indicates recruitment to microdomains on the AVM. GFP alone and all other fluorescently tagged Rabs fail to associate specifically with the ApV and exhibit fluorescent signal that is diffuse throughout the cell or that is vesicle- and/or Golgi apparatus-associated (**Figure 4Q-S** and data not shown).

In the absence of infection, those fluorescent protein-tagged Rabs that otherwise localize to the ApV demonstrate organelle-like localization and/or diffuse staining patterns (**Figure 4T-V** and data not shown). Since not all fluorescently tagged Rab proteins associate with the ApV, GFP-Rab1, GFP-Rab4A, GFP-Rab10, GFP-Rab11A, GFP-Rab14, RFP-Rab22A and GFP-Rab35 localization to the ApV is likely specific and not due to non-specific association with GFP or RFP. The lack of detection of GFP-Rab5 recruitment to the ApV is consistent with the inability to detect endogenous Rab5 on the AVM (129). From these data, it can be concluded that the ApV primarily hijacks endocytic recycling traffic. The fluorescent protein-tagged Rabs that exhibit the highest degrees of association with the ApV – Rab10, Rab11A, Rab14, Rab22A and Rab35 – are specific to the endocytic recycling compartment, recycling endosomes and tubular recycling endosomes associated with the slow clathrin-independent endocytic recycling pathway (76). GFP-Rab4A, which is rapid recycling endosome-specific, is only found on 4.7% of ApVs (**Figure 5**). Thus, the ApV predominantly hijacks the slow clathrin-independent endocytic recycling pathway.

3.2.2 The ApV recruits Rabs upon formation and continues to do so throughout infection.

Previous work determined that the *A. phagocytophilum* developmental cycle, which consists of four distinct phases – (i) entry of a surface bound infectious DC organism into a

nascent ApV; (ii) conversion of the bacterium to a metabolically active RC organism; (iii) intravacuolar bacterial replication of RC organisms; and (iv) condensation of RC bacteria back to an inclusion full of DC organisms – takes approximately 24 h (199). Since the recruitment of Rab GTPases to the ApV may be temporally regulated with respect to the *A. phagocytophilum* developmental cycle and this, in turn, may influence the role that each Rab plays during *A. phagocytophilum* infection, we examined the association of several fluorescent protein-tagged Rabs to the ApV during the first 24 h of infection. At time 0, *Anaplasma* organisms were added to synchronously infect HL-60 cells. Consistent with previous reports by our and other laboratories (20, 28, 96), it took approximately 4 h for bound *A. phagocytophilum* bacteria to enter cells and form nascent vacuoles (data not shown). Beginning at 4 h, all fluorescent protein-tagged Rabs examined can be detected at the ApV (**Figure 6**). The percentages of ApVs positive for GFP-Rab4A, GFP-Rab10, GFP-Rab11A, RFP-Rab22A and GFP-Rab35, each of which is involved in endocytic recycling, continually increased throughout the course of infection. GFP-Rab14 localized to a considerably higher percentage of inclusions at 4 h than any other recycling endosome-associated GFP-Rab. By 24 h, however, the number of GFP-Rab14-positive ApVs had waned. The percentages of ApVs exhibiting association of endoplasmic reticulum/Golgi-specific GFP-Rab1 remained consistently low at all time points.

3.2.3 Endogenous Rab14 localizes to the ApV.

We next examined whether endogenous Rab14 associates with the ApV. *A. phagocytophilum*-infected HL-60 cells were screened with antibodies against Msp2 (P44) and human Rab14 and examined by confocal microscopy. As previously reported, Rab14 localized to vesicular structures that were ubiquitously distributed throughout the host cell cytoplasm (99). Examination of 1031 ApVs detected aggregate Rab14 staining on 37.9% of ApVs (**Figure 7**). Attempts at detecting endogenous Rab11 at the ApV were unsuccessful (data not shown).

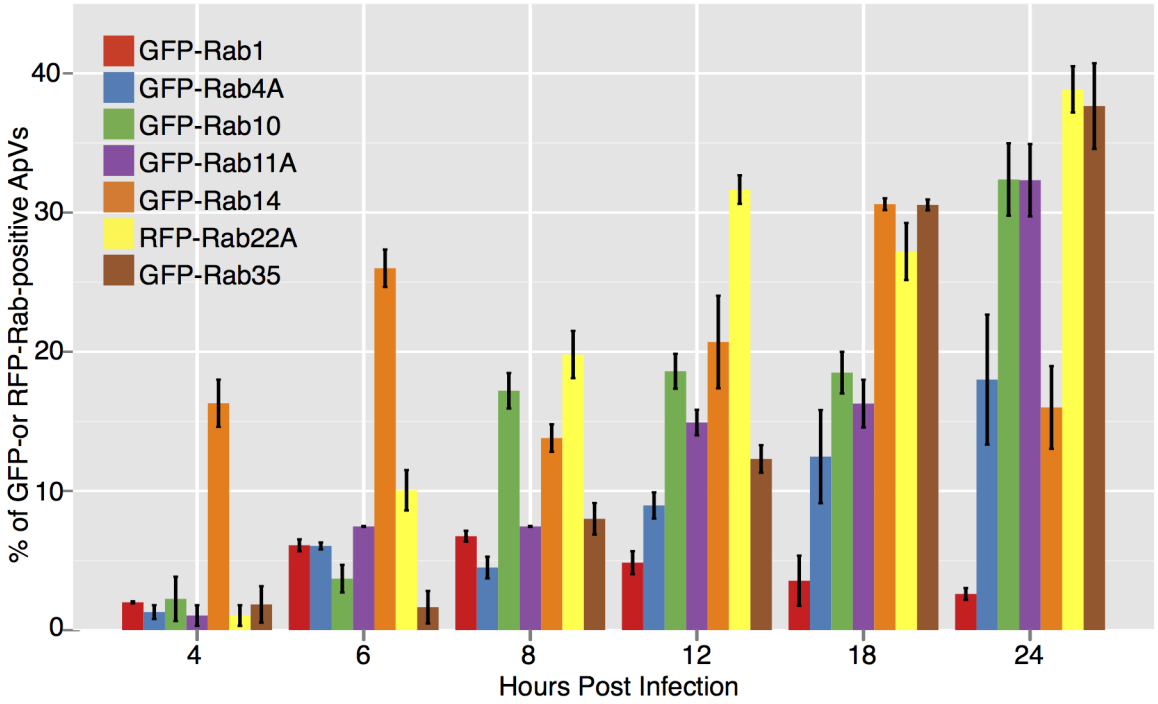

Figure 6. Time-course analyses of GFP- or RFP-Rab GTPase recruitment to the ApV. Percentages of ApVs to which GFP- or RFP-Rab GTPases associated are presented. Results are the mean (±SD) of two to five experiments. Up to 575 bacterial inclusions were examined for recruitment of each GFP- or RFP-Rab per time point. For assessment of GFP- or RFP-Rab GTPase association with the ApV at 4, 6, 8 and 12 h post infection, HL-60 cells were transiently nucleofected with DNA constructs encoding GFP- or RFP-Rab GTPases. At 12 h post nucleofection, the cells were synchronously infected with *A. phagocytophilum* for the time periods indicated and then fixed and examined by confocal microscopy. To assess GFP- or RFP-Rab GTPase recruitment to the ApV at 12, 18 and 24 h, HL-60 cells were synchronously infected with *A. phagocytophilum*. At 7 h post infection, the cells were nucleofected to express GFP- or RFP-Rab GTPases and fixed and examined at 12, 18 and 24 h post infection.

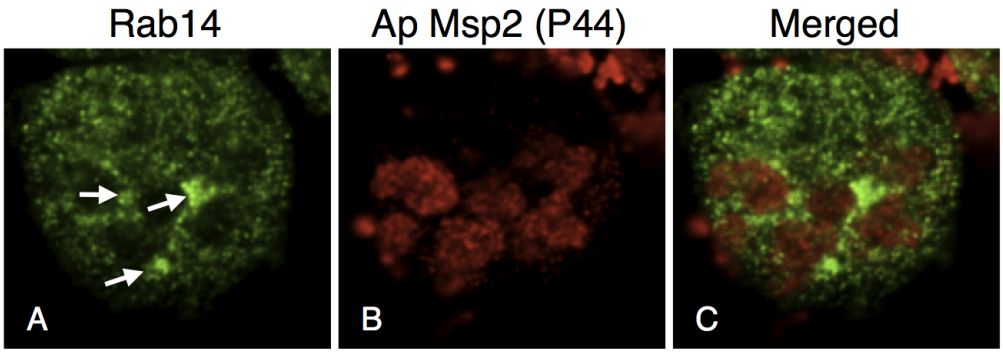

Figure 7. Endogenous Rab14 localizes to the ApV.
A. phagocytophilum-infected HL-60 cells were fixed and viewed by confocal microscopy. Rab14 was detected using rabbit polyclonal antisera against Rab14 followed by anti-rabbit IgG conjugated to Alexa Fluor-488. Intravacuolar and HL-60 cell surface-associated *A. phagocytophilum* organisms were denoted by indirect immunofluorescence staining with mAb 20B4, which recognizes the *A. phagocytophilum* surface protein, Msp2 (P44), but not the AVM, followed by anti-mouse IgG conjugated to Alexa Fluor-594. Panels **A, B** and **C** present single channel Rab14 detection, single channel Msp2 (P44) detection, and merged fluorescent images respectively. Arrows denote ApVs that exhibit pronounced Rab14 staining. Results are representative of a total of 1031 inclusions examined for two separate experiments.

3.2.4 GFP-Rab10 and GFP-Rab14 localization to the ApV is not dependent on an intact Golgi apparatus.

In addition to mediating cargo transfer from the early endosome to the endocytic recycling compartment, Rab10 is also found at the *trans*-Golgi network and directs transport of cargo from the *trans*-Golgi network to the plasma membrane (**Table 4**) (76). Likewise, Rab14 is not only found on early endosomes and the endocytic recycling compartment, but is also found on the *trans*-Golgi network and mediates traffic from the *trans*-Golgi network to the endocytic recycling compartment (**Table 4**) (94, 99). Therefore, Rab10 and/or Rab14 association with the ApV could be due to *A. phagocytophilum* hijacking endocytic recycling- and/or *trans*-Golgi network-derived traffic. To investigate the contribution of an intact Golgi network to GFP-Rab10 and GFP-Rab14 delivery to the ApV, infected HL-60 cells expressing GFP-Rab10 or GFP-Rab14 were treated with BFA. BFA treatment resulted in Golgi fragmentation, as detected by staining for the Golgi marker, GM130 (**Figure 8A-C**). Vehicle control treated cells exhibited intact Golgi apparatuses (**Figure 8D-F**) and GFP-Rab10 localization to the ApV (**Figure 8J-M**). GFP-Rab10 localization to the ApV in BFA-treated cells exhibited no difference from that observed for control cells whether BFA was added to cells with established *A. phagocytophilum* infections (**Figure 8G-I and M**) or prior to infection (data not shown). Highly similar results were observed for GFP-Rab14 recruitment to the ApV in BFA- treated cells (**Figure 8M**).

3.2.5 GFP-Rab1, GFP-Rab4A, GFP-Rab11A, GFP-Rab14 and GFP-Rab35 associate with the ApV in a guanine nucleotide-dependent manner, but GFP-Rab10 localizes to the ApV in a guanine nucleotide-independent manner.

Because Rab GTPases interact with their cognate effector proteins at target membranes in a guanine nucleotide-dependent manner (188), we were interested in whether GFP-

Figure 8. GFP-Rab10 and GFP-Rab14 localization to the ApV is insensitive to BFA. *A. phagocytophilum*-infected HL-60 cells expressing GFP-Rab10 or GFP-Rab14 were treated with BFA or vehicle control (methanol) for 3 h, after which the cells were fixed, processed for immunofluorescence microscopy and examined by confocal microscopy. **A–L**. Confocal micrograph images depicting GFP-Rab10 and immunofluorescent staining for the Golgi marker, GM130 or *A. phagocytophilum* Msp2 (P44). (**A–C** and **G–I**) BFA-treated cells. (**D–F** and **J–L**) Vehicle control-treated cells. (**A, D, G** and **J**) GFP-Rab10. (**B** and **E**) GM130. (**H** and **K**) Msp2 (P44). (**C, F, I** and **L**) merged images. **M**. Percentages of ApVs to which GFP-Rab10 or GFP-Rab14 associates in the absence or presence of BFA. Results are the mean ($\pm$SD) of two separate experiments. At least 361 ApVs inclusions were examined for GFP-Rab GTPase localization.

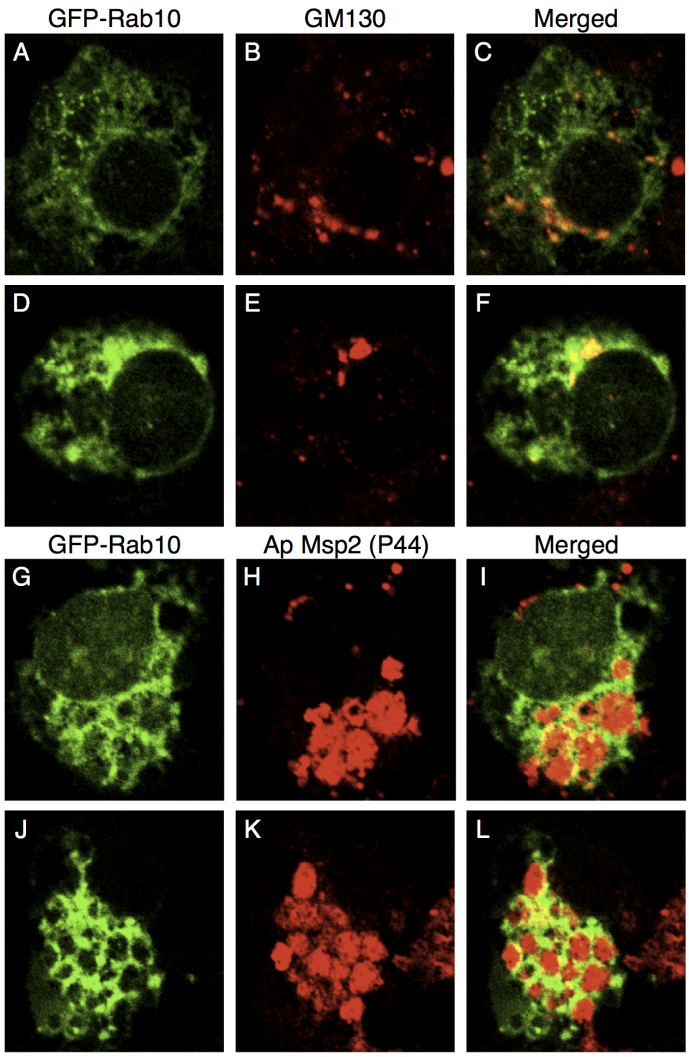
GFP-Rab10
GM130
Merged
A
B
C
D
E
F
GFP-Rab10
Ap Msp2 (P44)
Merged
G
H
I
J
K
L

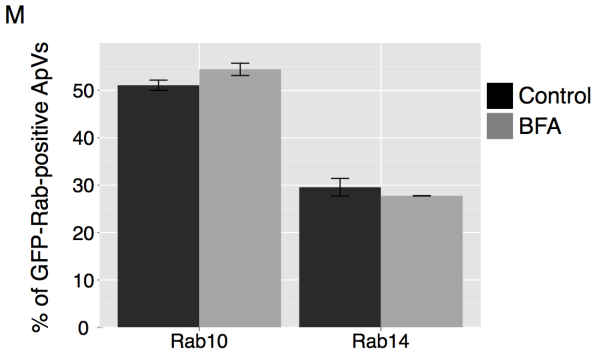
M
% of GFP-Rab-positive ApVs
0
10
20
30
40
50
Rab10
Rab14
Control
BFA

Figure 8

Rab1, GFP-Rab4A, GFP-Rab10, GFP-Rab11A, GFP-Rab14 or GFP-Rab35 interacts with the AVM in a similar manner. To investigate this, we assessed the intracellular locations of constitutively active GTPase-deficient GFP-Rab1A(Q70L), GFP-Rab4A(Q67L), GFP-Rab10(Q68L), GFP-Rab11A(Q70L), GFP-Rab14(Q76L) and GFP-Rab35(Q70L) and dominant negative GDP-restricted GFP-Rab1A(S25N), GFP-Rab4A(S22N), GFP-Rab10(T23N), GFP-Rab11A(S25N), GFP-Rab14(S25N) and GFP-Rab35(S22N) GFP-Rab proteins in infected cells. Dominant negative Rab mutants act by establishing stable interactions with GEFs, therefore they sequester available GEFs and prevent endogenous Rab GTPases from being activated (170). *A. phagocytophilum*-infected HL-60 cells were nucleofected to express each GFP-Rab. Five hours post nucleofection, the cells were fixed, screened with anti-Msp2 (P44) to denote *Anaplasma* inclusions, and examined for GFP-Rab recruitment to the ApV. As shown in **Figure 9A**, the wild-type and GTPase-deficient forms of GFP-Rab1, GFP-Rab4A, GFP-Rab11A, GFP-Rab14 and GFP-Rab35 localize to the ApV. Notably, considerably higher percentages of ApVs were positive for GFP-tagged, constitutively active forms of Rab1 and Rab4 than their wild-type counterparts. In contrast, the GDP-restricted forms of GFP-Rab1, GFP-Rab4A, GFP-Rab11A, GFP-Rab14 and GFP-Rab35 exhibited a significant decrease to or did not localize to the AVM. Overexpression of GDP-restricted Rab GTPases had no aberrant effects on the percentage of infected cells, numbers of ApVs per cell, or ApV gross morphology (data not shown). In contrast to the guanine nucleotide-dependent recruitment exhibited by GFP-Rab1, GFP-Rab4A, GFP-Rab11A, GFP-Rab14 and GFP-Rab35, GFP-Rab10 localization to the ApV is guanine nucleotide-independent. The wild-type, constitutively active GTPase-deficient and dominant negative GDP-restricted GFP-Rab10 fusions all localize to the ApV with comparable efficiencies (**Figure 9A**). Furthermore, the ability of GFP-Rab10(N122I), which is unable to bind guanine nucleotides, is only modestly reduced (**Figure 9B**).

Figure 9. Localization of GFP-Rab1, GFP-Rab4A, GFP-Rab11A, GFP-Rab14 and GFP-Rab35 to the ApV is guanine nucleotide-dependent, while GFP-Rab10 association with the ApV is guanine nucleotide-independent.
(**A**) *A. phagocytophilum*-infected HL-60 cells expressing GFP fusions of wild-type (WT), constitutively active GTPase-restricted (CA) and dominant negative GDP-restricted (DN) forms of Rab1, Rab4A, Rab10 and Rab11A were assessed for GFP-Rab recruitment to the ApV, which was demarcated by anti-Msp2 (P44) staining of intravacuolar bacteria. The number of GFP-positive ApVs was divided by the total number of ApVs, which was multiplied by 100 to determine the percentage of ApVs to which each GFP-Rab GTPase localized. Results are presented as the mean percentages ($\pm$SD) of ApVs exhibiting GFP-Rab GTPase recruitment and are derived from at least three experiments. A total of at least 642 bacterial inclusions were examined for recruitment of each GFP-Rab. (**B**) Comparison of the colocalization of GFP-Rab10 WT and GFP-Rab10N122I, which is a nucleotide-free mutant that is incapable of binding GTP or GDP (no-nucleotide, NN), to the ApV. Results are presented as the mean percentages ($\pm$SD) of ApVs exhibiting GFP-Rab GTPase recruitment and are derived from two experiments. Totals of 363 and 332 inclusions were examined for HL-60 cells expressing GFP-Rab10 and GFP-Rab10N122I respectively.

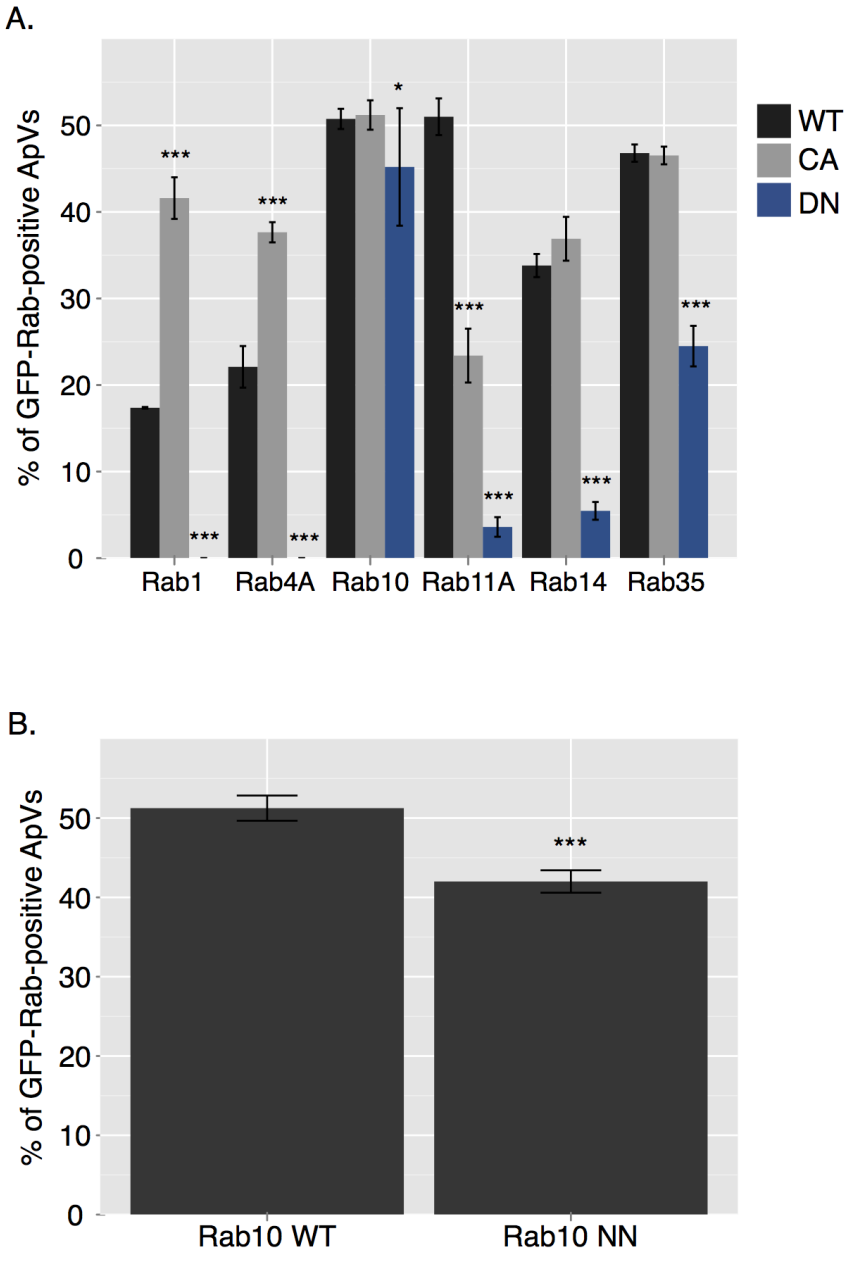
A.
% of GFP-Rab-positive ApVs
0
10
20
30
40
50
***
***
***
***
*
***
***
***
Rab1
Rab4A
Rab10
Rab11A
Rab14
Rab35
WT
CA
DN
B.
% of GFP-Rab-positive ApVs
0
10
20
30
40
50
***
Rab10 WT
Rab10 NN

Figure 9

3.2.6 Selective recruitment of GFP- or RFP-Rab GTPases to the ApV is dependent on *A. phagocytophilum* protein synthesis.

Because tetracycline treatment of *A. phagocytophilum*-infected host cells culminates in *A. phagocytophilum* delivery to lysosomes (70), we reasoned that bacterial protein synthesis is critical for the ApV to selectively recruit recycling endosome-associated Rabs and prevent maturation of the ApV along the endosomal-lysosomal pathway. Rab5 and Rab7 are found on endosomes and lysosomes, respectively (188), and do not normally associate with the ApV (**Table 4**). To test our hypothesis, we treated *A. phagocytophilum*-infected HL-60 cells expressing GFP-Rab5, GFP-Rab7, GFP-Rab10, GFP-Rab11A, GFP-Rab14, RFP-Rab22A and GFP-Rab35 with tetracycline or vehicle control for 30 min. The cells were fixed, screened with anti-Msp2 (P44) to denote bacterial inclusions, and examined for GFP-Rab localization to the ApV. With the exception of GFP-Rab5 and GFP-Rab7, all GFP-Rabs examined associated with the ApV in control cells (**Figure 10A**). GFP-Rab10, GFP-Rab11A, GFP-Rab14, RFP-Rab22A and GFP-Rab35 localization to the ApV was significantly reduced in tetracycline-treated cells. Concomitant with this phenomenon, the ApV became positive for GFP-Rab5 and GFP-Rab7 following the addition of tetracycline, which suggests that *de novo* bacterial protein synthesis is necessary for the ApV to intercept recycling endosome traffic and to block recruitment of Rab GTPases that promote endosomal maturation and lysosomal fusion. Indeed, $57.4 \pm 3.8\%$ of GFP-Rab7-positive ApVs were also positive for the lysosomal marker, LAMP-1 (**Figure 10B**). As expected, LAMP-1 localizes only to Rab7-positive vacuoles (188). Even though the lumens of GFP-Rab7-positive vacuoles were positive for Msp2 (P44) signal, intact organisms were rarely discernible (data not shown).

Figure 10. Selective recruitment of GFP- or RFP-Rab GTPases to the ApV is dependent on bacterial protein synthesis.

A. phagocytophilum-infected HL-60 cells were transiently nucleofected with DNA constructs encoding the indicated GFP- or RFP-Rab GTPase. At 5 h post nucleofection, tetracycline or vehicle control (70% ethanol) was added and incubation was continued. At 30 min, the cells were fixed and examined for GFP- or RFP-Rab GTPase association with the ApV. Intravacuolar *A. phagocytophilum* organisms were denoted by indirect immunofluorescence staining of Msp2 (P44). (**A**) GFP- or RFP-Rab localization to the ApV in the absence (–Tet) or 30 min post-addition of tetracycline (+Tet). Up to 817 bacterial inclusions were examined for GFP-Rab GTPase association per condition. Results are the mean (±SD) of at least three experiments. (**B**) GFP-Rab GTPase-positive *A. phagocytophilum* inclusions were examined for lysosomal fusion 30 min following the addition of tetracycline or vehicle control using a mAb directed against the lysosomal marker, LAMP-1. Up to 406 bacterial inclusions were examined for the localization of each GFP-Rab GTPase. Results are the mean (±SD) of at least three experiments. Statistically significant (*$P < 0.05$; **$P < 0.01$; ***$P < 0.001$) values are indicated.

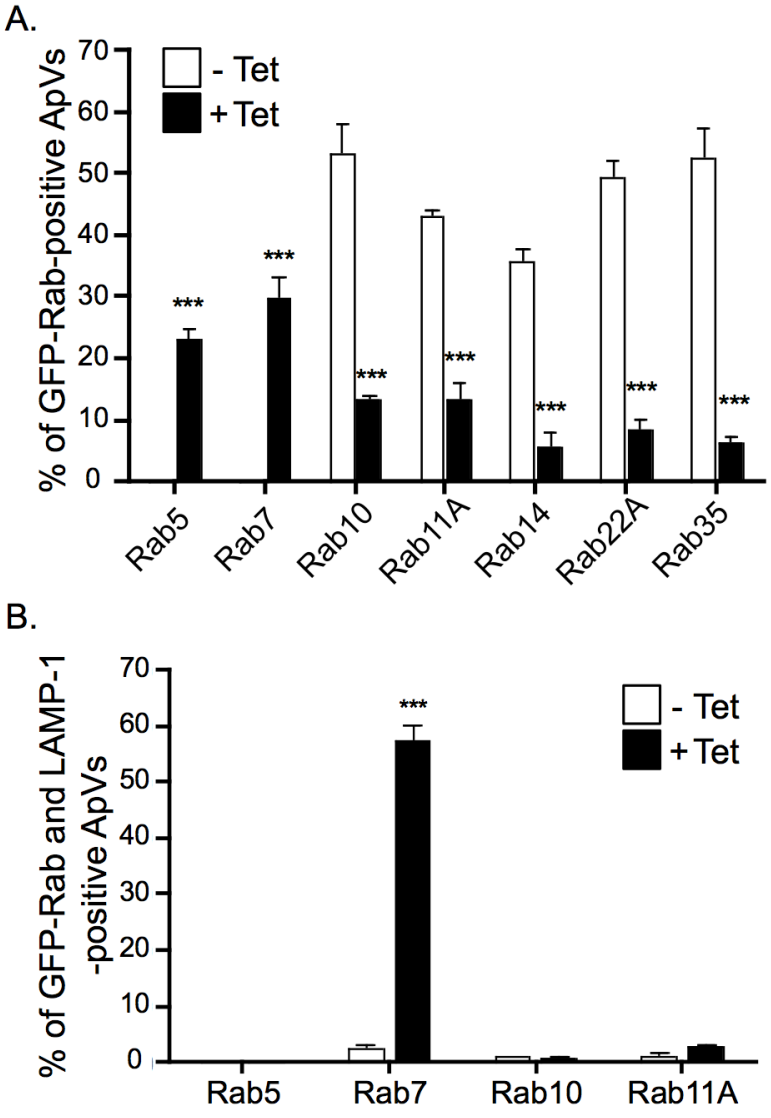
A.
% of GFP-Rab-positive ApVs
70
60
50
40
30
20
10
0
- Tet
+ Tet
***
Rab5
Rab7
Rab10
Rab11A
Rab14
Rab22A
Rab35
B.
% of GFP-Rab and LAMP-1 -positive ApVs
70
60
50
40
30
20
10
0
- Tet
+ Tet
***
Rab5
Rab7
Rab10
Rab11A

Figure 10

3.3 Discussion

Our data demonstrate that the ApV predominantly hijacks Rab-GTPases that regulate the slow clathrin-independent endocytic recycling pathway (summarized in **Figure 11**). The high degrees of colocalization with the ApV exhibited by GFP-Rab10, GFP-Rab11A, GFP-Rab14, RFP-Rab22A and GFP-Rab35 and the absence of GFP-Rab8 association with the ApV strongly suggest that the ApV hijacks the endocytic recycling compartment and tubular recycling endosomes. Doing so conceivably provides *A. phagocytophilum* with several intracellular survival advantages. *A. phagocytophilum* lacks genes necessary for synthesizing 16 amino acids (57). Since endogenous host proteins that are critical for amino acid uptake are brought into host cells via the slow clathrin-independent endocytic pathway (58), intercepting this pathway is a possible means by which the bacterium acquires amino acids. *A. phagocytophilum* incorporates cholesterol into its cell wall (112, 213), presumably to compensate for its lack of peptidoglycan (57). Since cholesterol is highly abundant in clathrin-independent endocytic recycling endosomes (126, 172), the bacterium may hijack tubular recycling endosomes as a means for obtaining cholesterol. Continual delivery of recycling endosomes to the ApV conceivably provides an unlimited supply of host membrane material to allow for expansion of the AVM, which would be necessary to accommodate growing intravacuolar bacterial populations. Lastly, by coating the AVM with recycling endosome-associated Rab GTPases, the ApV camouflages itself as a recycling endosome, which is key to preventing maturation along the endosomal pathway and avoiding fusion with lysosomes. Support for this premise is evidenced by the lack of GFP-Rab7 association with the ApV, which is in agreement with the report that the ApV avoids lysosomal fusion (70). Additional support is provided by the observed rapid loss of GFP-tagged slow clathrin-independent endocytosis-associated Rabs from the ApV with concomitant acquisition of GFP-Rab5, GFP-Rab7 and LAMP-1 upon the addition of tetracycline.

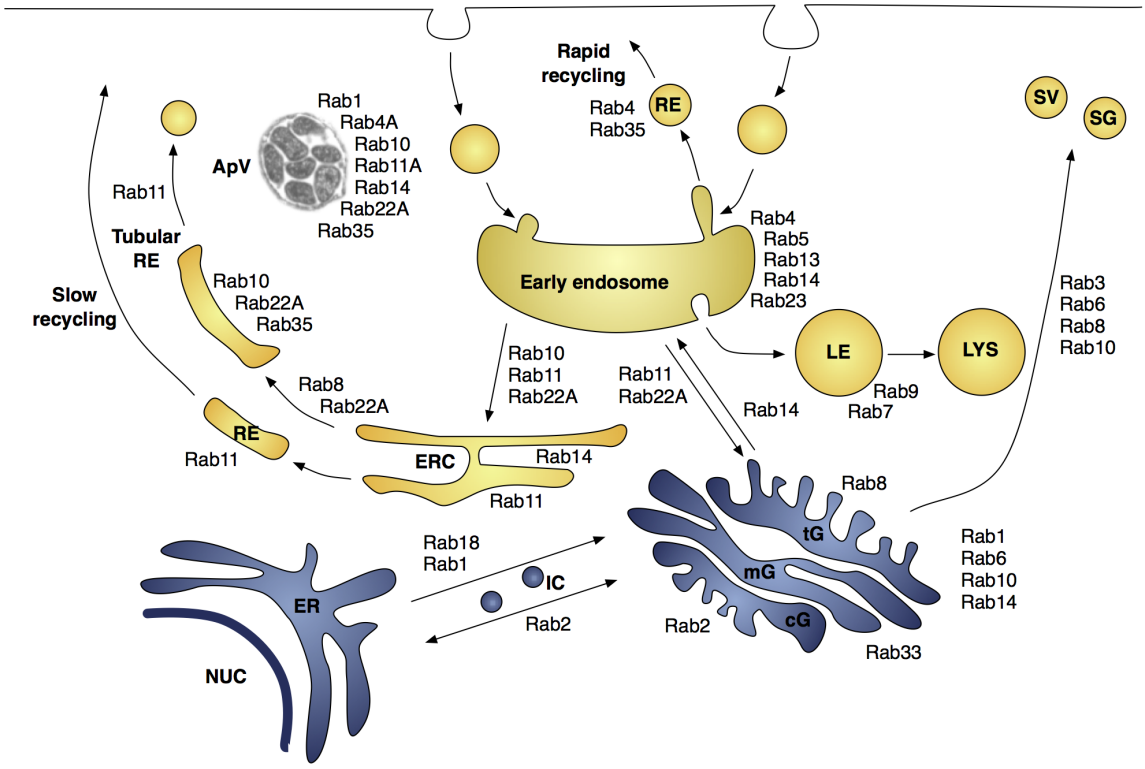

Figure 11. Model indicating the Rab GTPases and host cell membrane traffic pathways that are hijacked by the ApV.
ER, endoplasmic reticulum; cG, *cis*-Golgi; ERC, endocytic recycling centre; IC, pre-Golgi intermediate compartment; LE, late endosome; LYS, lysosome; mG, *medial*-Golgi; NUC, nucleus; RE, recycling endosome; SG, secretory granule; SV, synaptic vesicle; tG, *trans*-Golgi. This figure is partially adapted from Figure 1 presented by (76, 85).

The ApV's hijacking of recycling endosome traffic is consistent with the observation that that MHC class I and class II molecules, which are recycling endosome cargo, are found on the AVM (8, 129, 136). Further evidence that the ApV primarily acquires recycling endosome-derived traffic and does not acquire Golgi-derived vesicles comes from our observation that an intact Golgi network is not required for GFP-Rab10 or GFP-Rab14 to traffic to or maintain association with the ApV. This implies that GFP-Rab10 and GFP-Rab14 likely associate with the ApV by virtue of the ApV intercepting recycling endosome-derived traffic. BFA does not inhibit ApV recruitment of GFP-Rab10 and GFP-Rab14. This is consistent with a previous report that Golgi-derived markers are absent from the AVM and BFA exerts no aberrant effect on *A. phagocytophilum* intracellular survival (129). However, it cannot be completely ruled out that GFP-Rab10 and GFP-Rab14 are recruited to the ApV from cytosolic pools.

The ApV rapidly recruits recycling endosome-associated Rab GTPases and Rab1 very soon, if not immediately following bacterial entry and, with the exception of Rab14, which begins to dissociate by 24 h, continually recruits recycling endosome-associated Rabs throughout the duration of *A. phagocytophilum* intravacuolar development. At 4 h post-bacterial addition, the percentage of ApVs that are positive for GFP-Rab14 greatly exceeds those of all other ApV-associated GFP-Rabs, which indicates that Rab14 is the first Rab recruited to and/or it more stably associates with the bacterial inclusion. Initial hijacking of Rab14 may destine the ApV along the slow clathrin-independent endocytic recycling pathway. The fact that the ApV is positive for GFP-Rab14, but is negative for GFP-Rab5 supports previous observations that the ApV does not resemble an early endosome (129, 209). Perhaps the ApV hijacks Rab14 from a cytosolic pool or from an as yet defined Rab14-positive vacuole that is intermediate between early endosome and the endocytic recycling compartment. By 24 h, the number of GFP-Rab14-positive ApVs had declined, while the numbers of ApVs positive for GFP-Rab10, GFP-Rab11A, RFP-Rab22A and GFP-Rab35

had increased. Since the latter 4 Rabs are found on slow recycling endosomes and slow tubular recycling endosomes, while Rab14 is found on early endosomes and the endocytic recycling compartment, these data suggest that the ApV recruits traffic from the endocytic recycling compartment, slow recycling endosomes and slow tubular recycling endosomes through 18 h post infection, but draws less from the endocytic recycling compartment at 24 h post infection. How the ApV interacts with the recycling endosomes and membrane trafficking pathways beyond 24 h of infection cannot be extrapolated from this study.

Endogenous Rab14 localizes to a similar percentage of ApVs as its GFP-tagged counterpart. Attempts to localize endogenous Rab11 to the ApV in infected HL-60 cells were unsuccessful. Similarly, attempts to localize endogenous Rab4, Rab6 and Rab11 to the chlaymdial inclusion were also not feasible, even though their GFP-tagged counterparts localize to the chlaymdial inclusion (171). The inability to detect certain endogenous Rab GTPases at pathogen-occupied vacuolar membranes may be due to the fact that the levels of endogenous Rabs that are recruited to inclusions are too low to detect by indirect immunofluoresence microscopy or may simply reflect a limitation of available antibodies.

The ApV is fairly unique with respect to the composition of Rabs that it acquires and/or the fact that most ApV-recruited Rabs are retained for the duration of the infection. The ApV most closely resembles the *Mycobacteria* pathogen vacuole (MPV; occupied by *M. tuberculosis*), which recruits Rab11, Rab14 and Rab22 to obtain nutrients from the clathrin-independent recycling endosome pathway (24, 107, 108, 165). Unlike the MPV, which also acquires Rab5 (98), the ApV actively blocks Rab5 localization (129). The early and intermediate stages of the *Salmonella*-containing vacuole (SCV; occupied by *S. enterica* serovar Typhimurium) hijacks Rab4 and Rab11, respectively, along with other Rabs associated with early endosomes, late endosomes and pre-Golgi intermediate compartments that do not associate with the ApV (182, 183, 187). In contrast to inclusions occupied by *Chlamydia* spp., which recruit both recycling endosome- (Rab4, Rab11, Rab10, and Rab14)

and secretory pathway (Rab1, Rab6 and Rab10)-associated Rabs, the ApV does not intercept Golgi-derived traffic (27, 42, 170, 171). Furthermore, intercepting Golgi-derived traffic is essential for chlamydial (83, 159), but not *A. phagocytophilum* intracellular survival (129).

Fluorescent protein-tagged Rab10, Rab11A, Rab14, Rab22A and Rab35 localize to no more than $55.9 \pm 2.9\%$ of ApVs. Also, not all ApVs became positive for GFP-Rab5 or GFP-Rab7 upon the addition of tetracycline. Both phenomena are likely because endogenous Rabs are recruited to those ApVs to which the fluorescent protein-tagged Rabs have not localized. Also, because Rab GTPases dynamically cycle on and off target membranes, examining fixed *A. phagocytophilum*-infected cells only provides a snapshot of the Rab GTPases associated with the AVM at that instant. The presence of GFP-Rab4A on fewer ApVs than GFP-Rab10-, GFP-Rab11A-, GFP-Rab14-, RFP-Rab22A- or GFP-Rab35-positive ApVs indicates that the ApV intercepts rapid recycling endosomes but at a lower frequency than it intercepts slow tubular recycling endosomes. GFP-Rab1, which is normally found on endoplasmic reticulum exit sites and pre-Golgi intermediate compartments (153), localized to no more than $6.8 \pm 0.8\%$ of bacterial inclusions at any examined time point. Moreover, GFP-Rab2, which is found on pre-Golgi intermediate compartments (198), does not associate with the ApV. Thus, we can infer that a small percentage of ApVs hijack vesicles that emanate from endoplasmic reticulum exit sites. The low degree of GFP-Rab1 and GFP-Rab4A association with the ApV indicates that acquiring endogenous Rab1-positive endoplasmic reticulum-derived vesicles and/or Rab4A-positive rapid recycling endosomes either does not play a major role in *A. phagocytophilum* intracellular survival or that Rab1 and Rab4A rapidly cycle on and off the AVM and their transient associations cannot be accurately represented by the snapshot analyses utilized in this study. Alternatively, Rab1- or Rab4A-positive ApVs could have different complements of Rab GTPases and may have different intracellular fates. Despite the low percentages of ApVs to which GFP-Rab1 and GFP-Rab4A localize, these are likely real events since the GTPase-deficient versions of both GFP-Rab1 and

GFP-Rab4A each localize to significantly greater percentages of ApVs than their wild-type counterparts. This is presumably because the GTPase deficient Rabs are unable to cycle off the AVM once associated.

All GFP-Rab GTPases examined in this study are found on the ApV shortly, if not immediately following bacterial entry into HL-60 cells. Also, with the exception of GFP-Rab1, which localizes to very few inclusions throughout infection, and GFP-Rab14, which initially associates to a much greater percentage of ApVs than any other GFP- or RFP-Rab and begins to dissociate by 24 h, the GFP- and RFP-Rabs that are recruited to the ApV are found on increasing numbers of inclusions throughout the course of infection. This is in contrast to Rab GTPase recruitment to other pathogen-occupied vacuoles, such as those occupied by *Chlamydia* spp. and *S.* Typhimurium, which differentially recruit Rab GTPases over the duration of bacterial intravacuolar development (171, 183).

The observations that GTP-bound forms, but not GDP-bound forms of GFP-Rab1, GFP-Rab4A, GFP-Rab11A, GFP-Rab14 and GFP-Rab35 associate with the ApV indicate that these Rabs localize to the ApV as they would to their normal host cell target organelles. These GTP-bound Rabs may directly associate with the ApV by virtue of their interactions with *A. phagocytophilum*-encoded proteins presented on the AVM that mimic effectors of Rab1, Rab4, Rab11, Rab14 and/or Rab35. Alternatively, they may indirectly interact with the ApV through host-derived Rab effectors that are presented by the AVM by virtue of their interactions with *Anaplasma*-derived AVM proteins. Constitutively active GTPase-deficient GFP-Rab11A localizes to significantly fewer ApVs than wild-type GFP-Rab11A. We speculate that this is because a majority of GTP-locked GFP-Rab11A irreversibly associates with the membranes of recycling endosomes and the endocytic recycling compartment, which would effectively remove GTP-locked GFP-Rab11A from the cytosolic pool to be hijacked by the ApV. This premise is supported by the presence of considerably larger GFP-Rab11A-positive vacuoles in HL-60 cells expressing GTPase-deficient Rab11A as

compared with HL-60 cells expressing wild-type Rab11A (data not shown). The dominant negative GDP-locked Rab35 exhibited a decrease but not a complete loss of association to the ApV. We speculate this is due to a polybasic motif in the C-terminus of Rab35 that has been shown to be sufficient for targeting to the plasma membrane (81), which would explain why a reduction but not complete loss in ApV association of the GDP-locked Rab35 was observed. In addition, interference of Rab35 function has been shown to cause enlarged early endosomes and inhibit MHC class I recycling (6), suggesting that normal recycling and endocytic trafficking pathways are arrested. As a downstream effect, the activity of GAPs to remove membrane bound Rab35 could be delayed, which would prolong Rab35 association with the ApV. Alternatively, it is plausible that *Anaplasma* encodes a protein that has a functional role in Rab35 membrane cycling.

Our observations that the GDP-locked and nucleotide-free forms of GFP-Rab10 exhibit no and minimal defects, respectively, in localization to the ApV are striking and strongly suggest that *A. phagocytophilum*-derived proteins, presumably located on the AVM, mimic host GEF, GDI and/or GAP activities by regulating guanine nucleotide exchange on Rab10 to directly control Rab10 membrane cycling on/off the AVM. The precedents for such a remarkable phenomenon have been established by the identification of two *L. pneumophila* inclusion membrane proteins, DrrA/SidM and LepB. DrrA/SidM exhibits dual functionality as a GDF to displace Rab GDI such that Rab1 can be inserted into the *Legionella* containing vacuole membrane (LCVM) and as a GEF to stimulate Rab1 activation (92, 120, 134). LepB inactivates and removes Rab1 from the LCVM by functioning as a GAP to stimulate GTP hydrolysis (92). High-affinity binding to the nucleotide-free or GDP-bound form of a Rab GTPase is a characteristic feature of GDF/GEFs, while high-affinity binding to the GTP bound form is a signature of GAPs (24, 188). Thus, the association of nucleotide-free and GDP-bound GFP-Rab10 suggests that one or more *A. phagocytophilum*-derived proteins exhibit GDF/GEF activity. An alternative, albeit less likely, possibility is that the

ApV indirectly mediates Rab10 membrane cycling by hijacking one or more host-derived Rab10-specific GDIs, GEFs and/or GAPs. However, association of nucleotide-free and GDP-bound GFP-Rab10 with the ApV, which is inconsistent with how Rabs associate with eukaryotic target membranes, strongly argues in favor of these phenomena being dependent on bacterial-encoded AVM proteins.

To determine if any *A. phagocytophilum* proteins exhibit primary amino acid sequence homology to eukaryotic GAPs, GEFs and GDIs that interact with ApV-associated Rabs or to known bacterial PVM and effector proteins, we searched each protein's sequence against the annotated *A. phagocytophilum* proteome (57). No *A. phagocytophilum* protein exhibits primary sequence similarity to any known eukaryotic or bacterial pathogen Rab ligand (data not shown). This is not surprising since *Legionella*- and *Chlamydia*-derived Rab ligands and GEF/GDI/GAP mimics exhibit no primary amino acid sequence homology to any mammalian Rab effector, GAP or GEF (42, 92, 120, 134, 170, 175). Indeed, most bacterial effectors that mimic the activities of eukaryotic cellular proteins do so in the absence of detectable amino acid similarity (64). Thus, the *A. phagocytophilum* proteins that presumably regulate Rab10 membrane cycling are likely GEF/GDI/GAP homologues in functionality, but not in primary amino acid sequence.

This work advances our understanding of a key strategy by which *A. phagocytophilum* facilitates its survival within myeloid host cells. It actively controls the biogenesis of the vacuole in which it resides by selectively hijacking Rab GTPases that predominantly associate with recycling endosomes. In doing so, the ApV effectively disguises itself as a recycling endosome, which is requisite for avoiding endosomal maturation and lysosomal fusion. This strategy also likely contributes to the bacterium's acquisition of host membrane material, amino acids and cholesterol, each of which is important for bacterial growth and/or cell wall stability. This premise warrants further investigation. It will also be critical to identify and functionally assess the bacterial proteins that interact with each ApV-specific

Rab GTPase and those that regulate AVM cycling of Rab10. Further dissection of the mechanism of selective recruitment of Rab GTPases to the ApV will continue to enhance our understanding of how this unique pathogen survives within the primary effector cell of microbial killing.

A. phagocytophilum APH_1387 is expressed throughout bacterial intracellular development and localizes to the pathogen-occupied vacuolar membrane (PVM)

4.1 Introduction

Pathogen-encoded proteins that localize to the pathogen-occupied vacuolar membrane (PVM) play critical pathobiological roles, which include providing structural integrity to the PVM, hijacking vesicular traffic, and intercepting host signal transduction pathways. Because PVM alteration by pathogen-derived proteins is a paradigm of intracellular pathogenesis and at the time of this study there had been no previous reports of *A. phagocytophilum*-encoded proteins that localize to the AVM, we sought to identify and characterize such proteins. Since *A. phagocytophilum* is an obligate intracellular bacterium, we rationalized that bacterial proteins induced in host cells represent AVM candidate proteins. Storey et al. identified 3 such *A. phagocytophilum* proteins, P100, P130, and P160, which had apparent molecular masses of 100, 130, and 160 kDa, by screening an *A. phagocytophilum* genomic expression library with convalescent dog serum (190). Recombinant forms of these proteins were recognized by HGA patient antisera. P160, which has since been renamed AnkA because it carries a series of ankyrin repeats (32), is the first *A. phagocytophilum* type IV effector that was identified and does not localize to the AVM (95, 111, 161). P100 and P130 correspond to APH_1387 and APH_0032, respectively, in the annotated *A. phagocy-*

tophilum proteome (57). Both of these proteins are acidic, carry tandem direct repeats, and contain segments that putatively traverse the AVM. Because APH_1387 is induced upon infection and because it shares secondary structure characteristics with chlamydial inclusion membrane proteins (Inc), we performed detailed studies of APH_1387 and identified it as the first *A. phagocytophilum*-encoded protein that localizes to the AVM. This chapter presents the first direct evidence that *A. phagocytophilum* actively modifies the host cell-derived organelle in which it resides.

4.2 Results

4.2.1 APH_1387 has limited homology to any previously described protein.

APH_1387 is an acidic protein (pI 3.67) that contains 578 amino acids and has a predicted molecular mass of 61.4 kDa. It has 3 tandemly arranged direct repeats consisting of 93 amino acids (amino acids 180 to 272), 122 amino acids (amino acids 304 to 425), and 130 amino acids (amino acids 428 to 557) that together comprise 58% of the protein (**Figure 12A**). BLASTP searches using the entire APH_1387 sequence, the tandem repeat region (amino acids 180 to 557), or individual repeats identified no proteins that exhibited homology with APH_1387. A BLASTP search using the amino-terminal non-repeat region (amino acids 1 to 179) identified a 93-amino-acid stretch exhibiting 32.3% identity to AM_924 and AMF_1226 of the *A. marginale* St. Maries and Florida strains, respectively (21, 44). APH_1387 is predicted to consist largely of amphipathic alpha helices (**Figure 12B**). Chlamydial Inc proteins possess transmembrane and/or hydrophobic domains that facilitate insertion into the PVM (14, 15). Likewise, many PVM proteins possess hydrophilic domains that extend into the host cytoplasm to interact with host proteins (167). Although APH_1387 lacks a typical transmembrane domain, a 24-amino-acid sequence (AQVPVVAEAELPGVEAAEAIVPSL) that is part of each of the 3 direct repeats constitutes a bilobed hydrophobic domain (amino

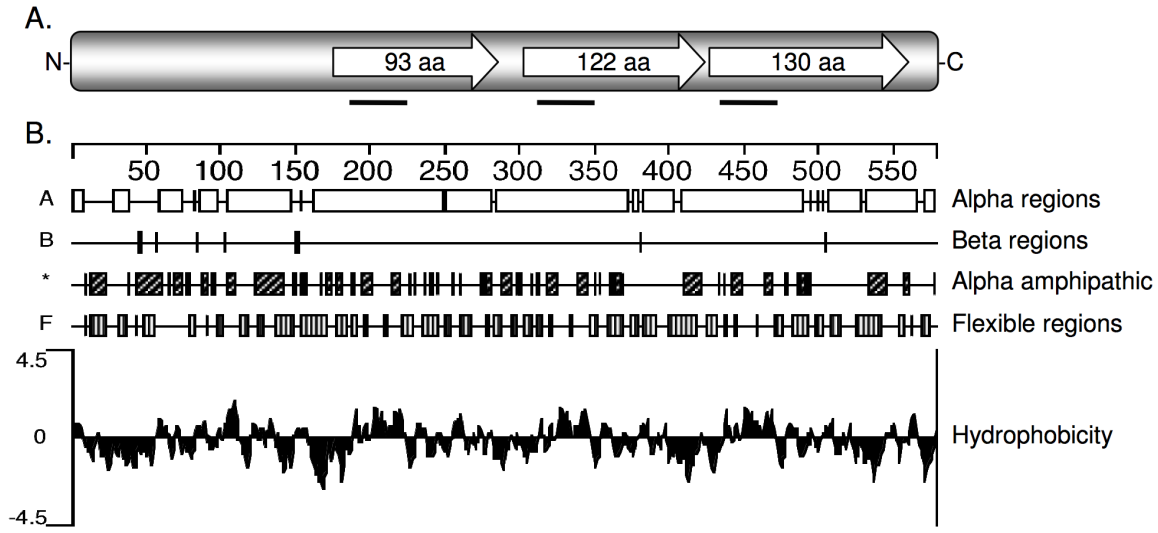

Figure 12. Schematic diagram of *A. phagocytophilum* APH_1387 and its secondary structure.

(**A**) The amino (N)-terminal region (amino acids [aa] 1 to 179) precedes the repeat region (aa 180 to 549), which precedes a short carboxy (C)-terminal region (aa 550 to 578). The repeat region consists of 3 tandem direct repeats (indicated by open arrows) consisting of 93, 122, and 130 aa. Underlining indicates the locations of the bilobed hydrophobic domains. (**B**) Diagram of the secondary structure of APH_1387. The scale indicates 50-aa intervals. The open and filled boxes indicate alpha helical (Alpha regions) and beta strand (Beta regions) regions, respectively, as determined using the Garnier-Osguthorpe-Robson algorithm. In the Alpha amphipathic diagram, striped boxes indicate regions that are predicted to form alpha helices and are comprised of amphipathic aa, as determined by the Eisenberg algorithm. For the Hydrophobicity diagram, the Kyte-Doolittle algorithm was used to determine hydrophobic (histogram above the x axis) and hydrophilic (histogram below the axis) regions. The 24-aa sequence constituting a bilobed hydrophobic domain occurs at aa 200 to 223, 324 to 347, and 448 to 471. All of the analyses were performed using Protean, which is part of the Lasergene software package, as described in Materials and Methods.

acids 200 to 223, 324 to 347, and 448 to 471) (**Figure 12B**). Bilobed hydrophobic domains are highly conserved among all chlamydial Inc proteins and are hypothesized to facilitate insertion of these proteins into the chlamydial inclusion membrane (167). Between the 3 hydrophobic domains are alpha-helical stretches that are largely hydrophilic. This periodicity of hydrophobic and hydrophilic domains could conceivably enable APH_1387 to traverse the AVM multiple times. Attempts to predict a tertiary structure for APH_1387 using SWISS-MODEL, ESyPred3D, 3Djigsaw, and GENO3D were unsuccessful because none of these programs was able to identify similar sequences with known structures on which to model the APH_1387 structure. Sequencing of the PCR products obtained for the entire *aph_1387* coding sequence of *A. phagocytophilum* strains NCH-1, HZ, and HGE-1 revealed that this gene's sequence is the same in these 3 strains and the USG3 strain, the strain in which it was originally sequenced (190) (data not shown).

4.2.2 APH_1387 is more abundant in *A. phagocytophilum* RC organisms than in DC organisms.

We initiated our characterization of APH_1387 by expressing it as a MBP fusion protein in *E. coli* and using the recombinant protein to raise rabbit polyclonal antiserum. To test the efficacy of anti-APH_1387 and to determine if APH_1387 is expressed during *A. phagocytophilum* infection of promyelocytic HL-60 cells, we performed Western blot analyses. Anti-APH_1387 recognized APH_1387 as a single band at ~115 kDa in an *A. phagocytophilum*-infected cell lysate but not in an uninfected HL-60 cell lysate (**Figure 13**). *A. phagocytophilum* has a biphasic developmental cycle in which an infectious DC organism binds, enters, and changes into a replicative RC organism that subsequently divides by binary fission (199). The numerous RC organisms, which are noninfectious, revert to DC organisms before they are released to infect naive host cells. We confirmed that a host cell-free population of *A. phagocytophilum* DC and RC organisms can be

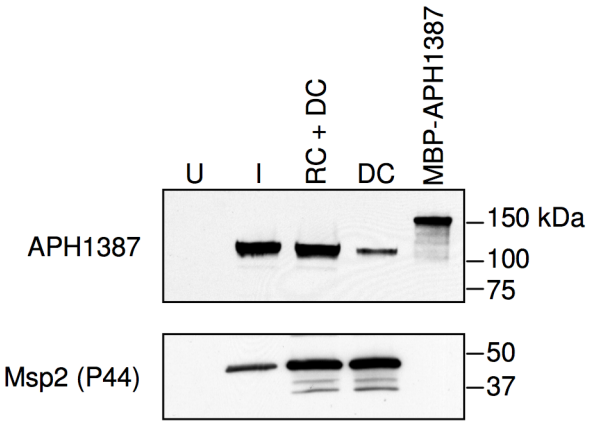

Figure 13. Screening of *A. phagocytophilum*-infected HL-60 cells and host cell-free bacterial populations with anti-APH_1387.
Western-blotted lysates of uninfected (lane U) and *A. phagocytophilum*-infected HL-60 cells (lane I), as well as host cell-free *A. phagocytophilum* populations consisting of RC and DC organisms (lane RC + DC) or only DC organisms (lane DC), were screened with anti-APH_1387. MBP-APH_1387 was used as a positive control. The blot was stripped and screened with anti-Msp2 (P44) to confirm that equivalent amounts of lysates derived from RC and DC organisms and from only DC organisms were used. The results are representative of the results of two separate experiments.

recovered following syringe lysis, which does not damage the fragile RC organisms, while a pure DC organism population can be recovered following sonication, which destroys the RC organisms (data not shown). To assess whether RC or DC organisms express more APH_1387, we screened Western-blotted lysates of host cell-free *A. phagocytophilum* organisms recovered following syringe lysis (DC and RC organisms) or sonication (only DC organisms) that were normalized using the levels of Msp2 (P44), which is a constitutively expressed outer membrane protein (71) (**Figure 13**). The intensity of the APH_1387 band was considerably higher for the lysate derived from DC and RC organisms than for the lysate generated from DC organisms. After longer exposures, additional anti-APH_1387 reactive bands at ~61 and 90 kDa were detected in lysates derived from the DC and RC organisms, as well as infected HL-60 cells (data not shown).

4.2.3 APH_1387 is induced following bacterial entry into host cells and localizes to the AVM.

We next screened *A. phagocytophilum*-infected HL-60 cells with anti-APH_1387 in conjunction with a mAb against Msp2 (P44) (149, 176) at 0.7, 8.5, and 24 h post infection and visualized the cells by confocal microscopy. At 0.7 h post infection, very little or no APH_1387 was detected on Msp2 (P44)-positive organisms that were bound to the HL-60 cell surface (**Figure 14A to D**). By 8.5 h, ApVs containing individual *A. phagocytophilum* bacteria were detected. At this time point, the AVM was positive for APH_1387 (**Figure 14E to H**). At 24 h, the AVM was strikingly distinguished from enclosed bacteria by exclusive staining for APH_1387 (**Figure 14I to L**). *A. phagocytophilum* bacteria within ApVs that were positive for both Msp2 (P44) and APH_1387 were green [corresponding to Msp2 (P44) staining] spheroid organisms, each of which was surrounded by a red ring (corresponding to APH_1387 staining) or a yellow ring [corresponding to APH_1387 and

Figure 14. *A. phagocytophilum* APH_1387 is detectable on the surfaces of intravacuolar bacteria and localizes to the AVM in infected host cells.
(**A–L**) HL-60 cells were synchronously infected with *A. phagocytophilum*. At 0.7 h (**A–D**), 8.5 h (**E–H**), and 24 h (**I–L**) post infection, the cells were fixed and viewed by confocal microscopy to determine immunoreactivity with antibodies against Msp2 (P44) (major bacterial surface protein; used to identify bacteria in panels **B, F,** and **J**) and APH_1387 (**C, G,** and **K**). Differential interfering contrast images are shown in panels **A, E,** and **I**. Merged fluorescent images are shown in panels **D, H,** and **L**. (**M–X**) *A. phagocytophilum*-infected THP-1 (**M–**P), HMEC-1 (**Q–T**), and ISE6 (**U–X**) cells were fixed and viewed by confocal microscopy to determine immunoreactivity with antibodies against Msp2 (P44) (**N, R,** and **V**) and APH_1387 (**O, S,** and **W**). Differential interfering contrast images are shown in panels **M, Q,** and **U**. Merged fluorescent images are shown in panels **P, T,** and **X**. In panel H the arrowheads indicate individual Msp2 (P44)-positive *A. phagocytophilum* organisms enclosed in APH_1387-positive vacuoles. In panels **L, P, T,** and **X** the arrows indicate representative AVMs or portions of AVMs that exhibit exclusive staining for APH_1387. Intravacuolar bacteria are positive for Msp2 (P44) or both Msp2 (P44) and APH_1387. The results are representative of the results of three separate experiments.

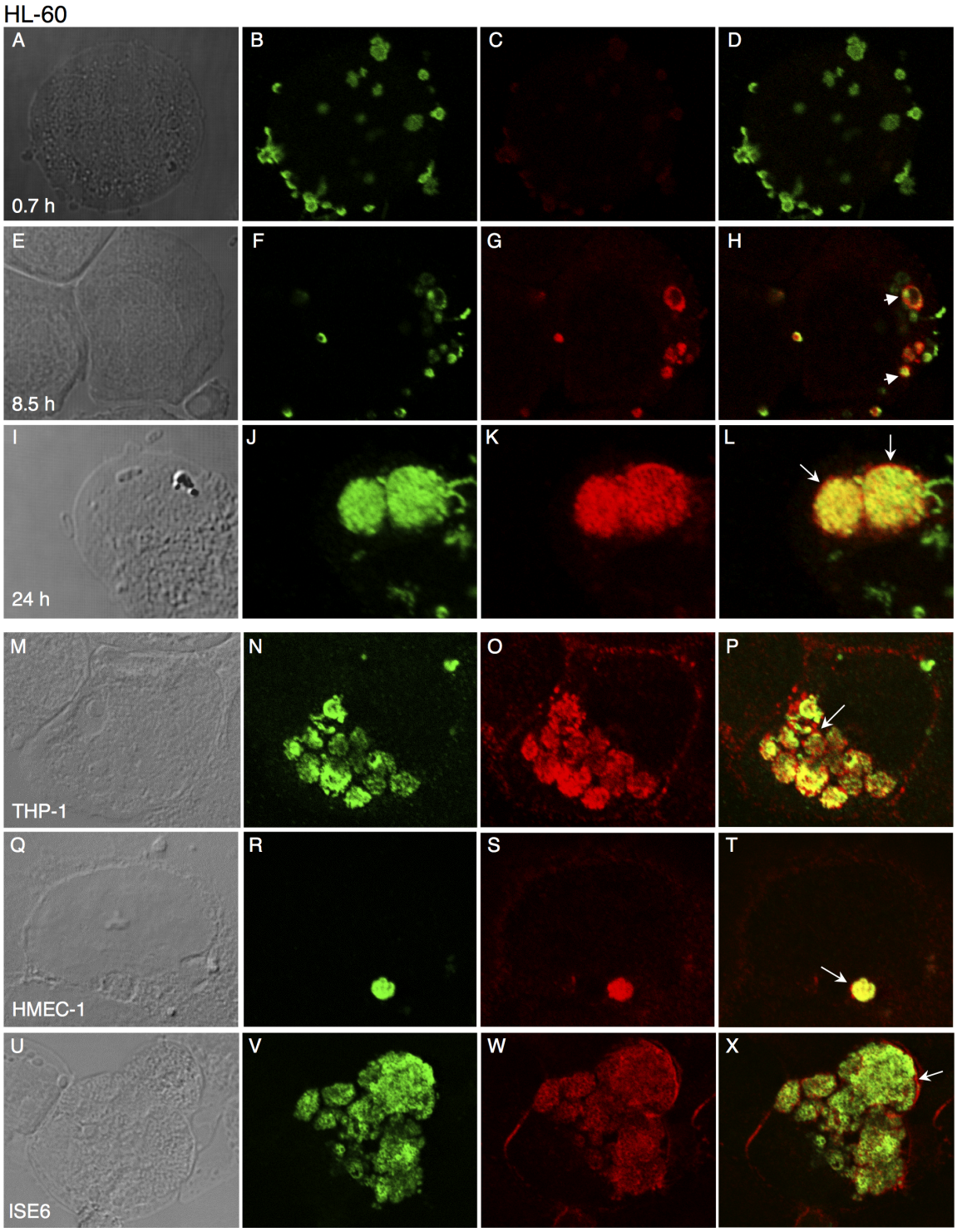
HL-60
A
B
C
D
0.7 h
E
F
G
H
8.5 h
I
J
K
L
24 h
M
N
O
P
THP-1
Q
R
S
T
HMEC-1
U
V
W
X
ISE6

Figure 14

Msp2 (P44) staining] (**Figure 14J to L**). At 24 h, 94.0 ± 3.5% of the ApVs were positive for APH_1387. The AVM was negative for Msp2 (P44) at all time points.

4.2.4 APH_1387 localizes to the AVM during *A. phagocytophilum* infection of human myeloid and endothelial cell lines and tick embryonic cell lines.

In addition to HL-60 cells, *A. phagocytophilum* infects and resides in ApVs in the human monocytic cell line THP-1, the human microvascular endothelial cell line HMEC-1, and the *I. scapularis* embryonic cell line ISE6 (65, 82, 133, 212). To determine if APH_1387 is expressed and localizes to the AVM in each of these cell lines, *A. phagocytophilum*-infected THP-1, HMEC-1, and ISE6 cells were examined by confocal microscopy at 24 h post infection. As observed for HL-60 cells, virtually all ApVs in each cell line were positive for APH_1387 (**Figure 14M to X**). Indeed, at 24 h post infection 93% of ApVs were positive for APH_1387 in THP-1 cells (data not shown). Notably, the plasma membranes of heavily infected THP-1 cells (**Figure 14O and P**), ISE6 cells (**Figure 14W and X**), and HL-60 cells (data not shown) and occasionally uninfected cells that were adjacent to the heavily infected cells were also positive for APH_1387.

4.2.5 APH_1387 is expressed and localizes to the AVM throughout *A. phagocytophilum* intracellular development in HL-60 cells.

We next assessed the temporal expression and AVM localization patterns of APH_1387 over the course of a synchronous *A. phagocytophilum* infection of HL-60 cells. Host cell-free bacteria were added to HL-60 cells and allowed to bind for 40 min, which was followed by removal of unbound organisms. We and others have determined that it takes 4 h for bound *A. phagocytophilum* DC organisms to internalize in nascent vacuoles (20, 28, 96). Beginning at 8 h after addition of bacteria, which corresponded to 4 h after entry, APH_1387 was weakly detected as a 115-kDa band by immunoblot analysis (**Figure 15A and B**). The intensity of

Figure 15. Kinetics of APH_1387 expression and AVM localization in *A. phagocytophilum*-infected cells.
HL-60 cells were synchronously infected with *A. phagocytophilum*. At the times post infection indicated, aliquots were processed and analyzed using Western blotting and densitometric analysis (**A–B**) or immunofluorescence microscopy (**C**). (**A**) Western blots of *A. phagocytophilum*-infected HL-60 whole-cell lysates screened with antibodies against APH_1387, Msp2 (P44) (infection control), and actin (loading control). (**B**) Densitometry to quantify the intensities of APH_1387 and actin bands. The ratio of the APH_1387 densitometric value to the actin densitometric value is shown for each time point. (**C**) Percentages of ApVs [based on the presence of Msp2 (P44)-positive *A. phagocytophilum* bacteria] that are positive for APH_1387 staining of intravacuolar bacteria and exclusive staining of the AVM. The data are the means and standard deviations for 3 separate experiments. At least 948 Msp2 (P44)-positive ApVs were scored for APH_1387 for each time point.

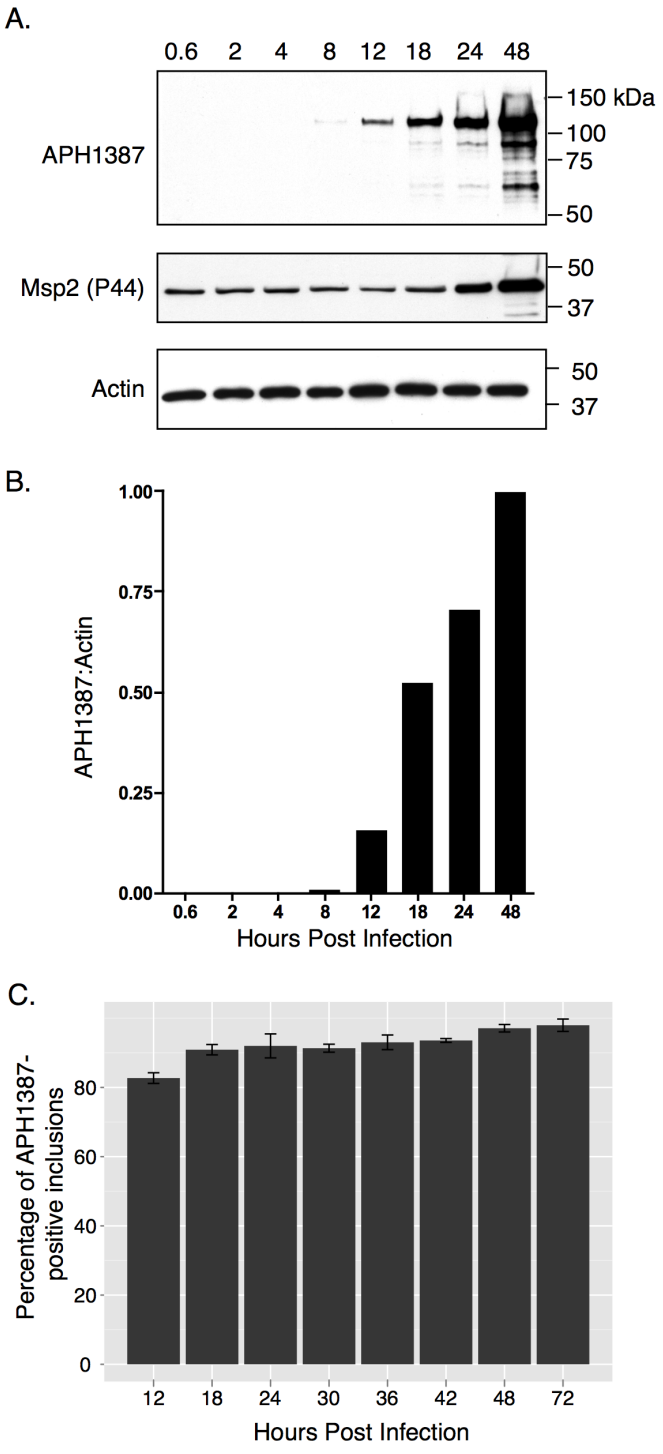
A.
0.6 2 4 8 12 18 24 48
APH1387
150 kDa
100
75
50
Msp2 (P44)
50
37
Actin
50
37
B.
APH1387:Actin
1.00
0.75
0.50
0.25
0.00
0.6 2 4 8 12 18 24 48
Hours Post Infection
C.
Percentage of APH1387-positive inclusions
80
60
40
20
0
12 18 24 30 36 42 48 72
Hours Post Infection

Figure 15

this band increased continually during the time course. Beginning at 18 h, several additional bands were also detected, and the primary bands were at ~61 and 90 kDa. As we have shown previously (31), the intensity of the Msp2 (P44) band, which is used as an infection control, increases throughout the course of an infection. APH_1387 was detected on >80% of the ApVs at 12 h and on >90% of the ApVs at all later time points by confocal microscopy (**Figure 15C**).

To more closely examine when APH_1387 is expressed and associates with the AVM during the course of infection, we screened synchronously infected HL-60 cells over a 48 h period by using immunoelectron microscopy. APH_1387-negative spheroid DC organisms were bound to the HL-60 cell surface at 0.7 h (**Figure 16A**), and some organisms had internalized into nascent vacuoles by 4 h (**Figure 16B**). By 8 h, which corresponded to ~4 h after entry, the internalized bacteria had changed into elongated, pleomorphic RC organisms and had begun to replicate. The surfaces of the replicating RC organisms were positive for APH_1387, as were portions of the AVM (**Figure 16C**). More APH_1387 was detected on the AVM and on intravacuolar *A. phagocytophilum* bacteria as the infection progressed (**Figure 16D to G**). At 24 h, individual HL-60 cells contained numerous ApVs, each of which harbored several DC organisms that had rough outer membranes or contained multiple mature RC organisms that were changing into DC organisms (**Figure 16F**), which is consistent with our previous report on the replication kinetics of *A. phagocytophilum* in HL-60 cells (199). At this time point, APH_1387 heavily decorated the AVM, as well as the surfaces of intravacuolar DC and RC organisms. APH_1387 labeling of the AVM was most pronounced for mature ApVs that contained several *A. phagocytophilum* bacteria at 48 h (**Figure 16G and H**).

Figure 16. Assessment of *A. phagocytophilum* APH_1387 expression and localization to the AVM by immunoelectron microscopy.
HL-60 cells were synchronously infected with *A. phagocytophilum*. At 0.7 h (**A**), 4 h (**B**), 8 h (**C**), 12 h (**D**), 18 h (**E**), 24 h (**F**), and 48 h (**G** and **H**) after addition of bacteria, samples were fixed and screened with anti-APH_1387 followed by goat anti-rabbit IgG conjugated to 6-nm gold particles and examined by electron microscopy. Representative results of two separate experiments are shown. (**A–B**) Asterisks indicate bound or newly internalized *A. phagocytophilum* DC organisms. (**C–F**) Arrows indicate representative portions of the AVM that are labeled with gold particles. (**H**) Magnification of the region in panel **G** indicated by a box. Scale bars, 0.5 μm.

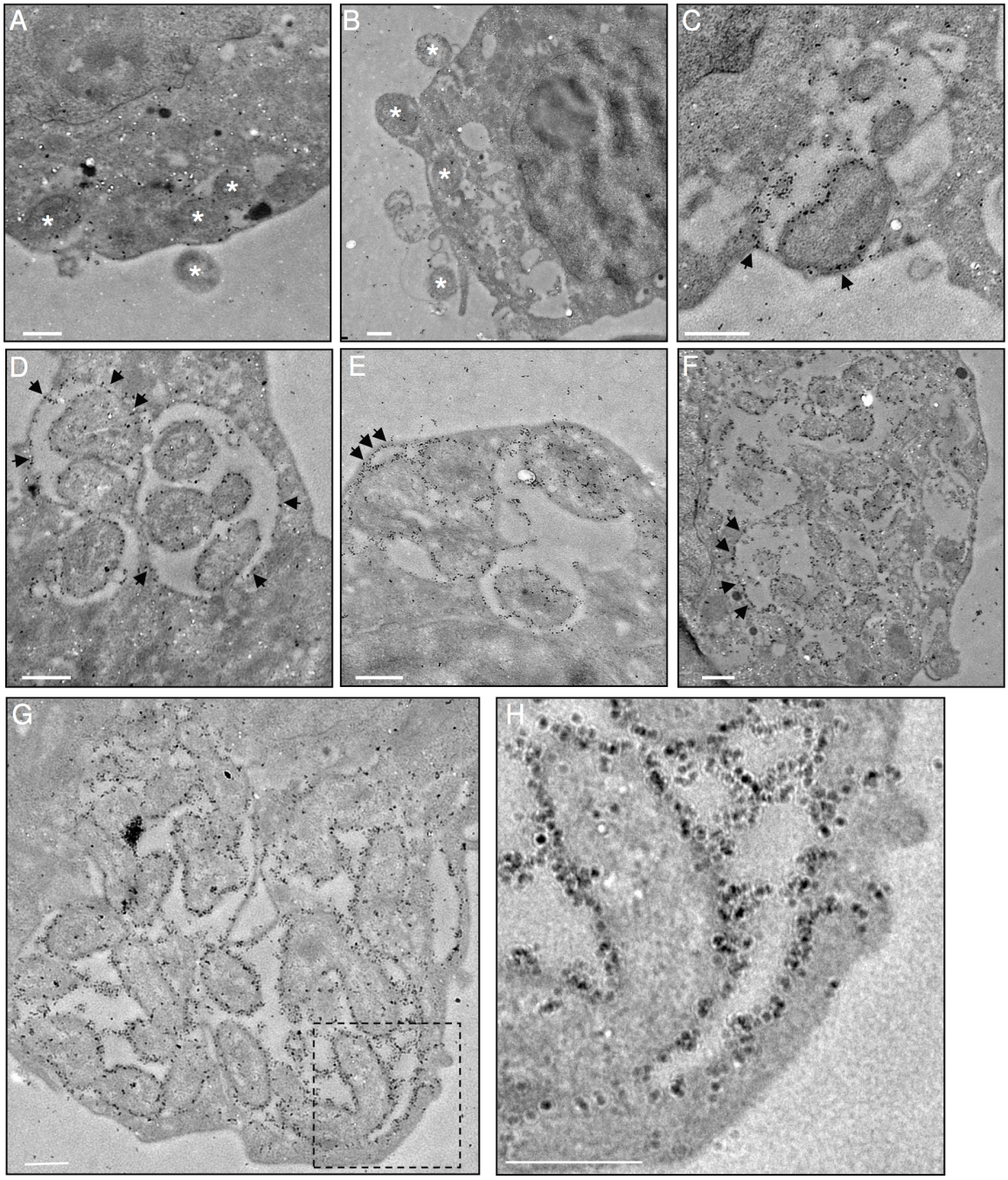

Figure 16

4.2.6 APH_1387 is expressed and localizes to the AVM *in vivo*.

Next, we investigated APH_1387 expression *in vivo*. MBP-APH_1387, but not MBP alone, was recognized by antiserum from an HGA patient (**Figure 17A**), which confirmed a previous report by Storey and colleagues (190). Likewise, Msp2 (P44)- and APH_1387-positive ApVs were detected by confocal microscopy in murine buffy coats isolated from *A. phagocytophilum*-infected mice at 8 days post infection (**Figure 17B to E**).

4.3 Discussion

APH_1387 is expressed and modifies the AVM *in vivo* in neutrophils during murine infection and *in vitro* during intracellular residence in human HL-60, THP-1, HMEC-1, and tick ISE6 cells, and it is expressed throughout the course of intracellular development. The examination of *A. phagocytophilum* whole-genome transcription profile data that was performed by Nelson and colleagues for infected HL-60, HMEC-1, and ISE6 cells revealed that *aph_1387* is transcribed in each cell line (137), which corroborates the findings of our protein expression analyses. Thus, APH_1387 is conceivably important for *A. phagocytophilum* survival in all eukaryotic host cells that this bacterium infects. This hypothesis is further supported by the high degree of sequence conservation in at least 4 geographically diverse *A. phagocytophilum* strains (190). Notably, anti-APH_1387 stains the plasma membranes of heavily infected host cells and uninfected host cells that are adjacent to heavily infected cells, which suggests that APH_1387 may associate with the host cell plasma membrane.

Tandem repeat proteins of pathogenic bacteria have been implicated in a wide range of host-pathogen interactions (38, 63, 90, 95, 111, 205, 211, 219). A protein alignment of APH_1387 and the *E. chaffeensis* tandem repeat protein P120 (encoded by ECH_0039 in the annotated *E. chaffeensis* genome) (215) that was performed by Storey and colleagues revealed that two short repeat segments that help comprise each APH_1387 tandem repeat

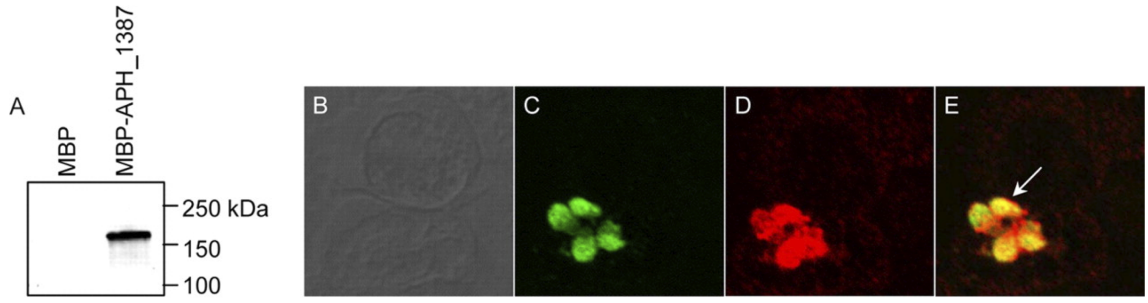

Figure 17. *A. phagocytophilum* APH_1387 is expressed and associates with the AVM during *in vivo* infection.
(**A**) Antiserum from an HGA patient recognized MBP-APH_1387 but not MBP alone. (**B–E**) Buffy coats isolated from an *A. phagocytophilum*-infected mouse on day 8 post infection were fixed and viewed by confocal microscopy to determine immunoreactivity with antibodies against Msp2 (P44) (**C**) and APH_1387 (**D**). A differential interfering contrast image is shown in panel **B**. A merged fluorescent image is shown in panel **E**. The arrow indicates exclusive APH_1387 staining of the AVM. The results are representative of the results of three separate experiments for each analysis.

region share sequence similarity with portions of the tandem repeat region of P120 (190). *E. chaffeensis* P47 is an acidic (pI 4.2) tandem repeat carrying protein that interacts with host molecules involved in cell signaling, transcriptional regulation, and vesicle trafficking (119, 205, 218). The target host molecules with which APH_1387 presumably interacts and/or the pathobiological role of APH_1387 is likely unique to *A. phagocytophilum* intracellular survival, as APH_1387 exhibits very little to no homology with any previously described protein. Alternatively, APH_1387 may be important for adding structural integrity to the AVM and may have no target ligand.

Upon electrophoresis APH_1387 migrates primarily as a 115 kDa band and also produces less prominent bands; the primary less prominent bands are a 90 kDa band and a band at the predicted molecular mass of 61.4 kDa. While other workers have attributed this aberrant migration to glycosylation (47), our assessments of both native and recombinant APH_1387 indicate that neither protein is glycosylated (unpublished data). All Anaplasmataceae acidic tandem repeat proteins analyzed to date migrate at molecular weights considerably higher than their predicted molecular weights. Alternatively, the acidic nature of APH_1387 may prevent it from amply binding SDS, which would retard proper SDS-PAGE resolution, as has been observed for other acidic proteins and was reported for *E. chaffeensis* P47 by Wakeel and colleagues (127).

Large amounts of APH_1387 associated with the surfaces of intravacuolar *A. phagocytophilum* RC and DC organisms are detected by indirect immunofluorescence and immunoelectron microscopy. Yet APH_1387 was not detected on the surfaces of glutaraldehyde-fixed host cell-free *A. phagocytophilum* bacteria that were recovered following mechanical disruption of infected HL-60 cells, washed with PBS, and added to naive HL-60 cells, and it was only weakly detected on methanol-permeabilized bacteria by immunofluorescence analysis. Accordingly, we hypothesize that APH_1387 is not integrated into the *A. phagocytophilum* outer membrane but instead is loosely associated with it and is easily washed away during

the isolation procedure. We further hypothesize that this is because APH_1387 is transiently associated with the surfaces of intravacuolar bacteria while it is being secreted and that it subsequently integrates into the AVM.

Dissecting the role of APH_1387, confirming its route of delivery, and identifying its eukaryotic host cell ligands are essential for fully comprehending the intracellular survival strategies of this unusual bacterial pathogen.

A. phagocytophilum APH_0032 is expressed late during infection and localizes to the pathogen-occupied vacuolar membrane

5.1 Introduction

Multiple pathogen-encoded PVM proteins have been found for a diverse array of obligate vacuolar pathogens. Indeed, $\geq$45 and $\geq$65 Inc proteins have been confirmed and/or are predicted for *C. pneumoniae* and *C. trachomatis*, respectively (167). Thus, APH_1387 is likely one of a multitude of AVM proteins that are waiting to be identified and functionally characterized. APH_0032 is another *A. phagocytophilum* acidic tandem repeat protein that, along with APH_1387, is induced during *A. phagocytophilum* infection of dogs and humans (190). In their abstract presented at the American Society for Rickettsiology-Bartonella as an Emerging Pathogen Group 2001 Joint Conference, Nelson, Ahn, Herron, and Goodman reported that antisera against APH_0032 recognized the AVM, which implicates APH_0032 as a bacterial-encoded AVM protein. Because of the relevance of bacterial PVM proteins to intravacuolar pathogens and to gain further insight into how *A. phagocytophilum* modifies its host cell-derived vacuole, we set out to confirm whether APH_0032 is a bona fide AVM protein and characterize its expression pattern in a variety of host cells.

5.2 Results

5.2.1 APH_0032 displays limited similarity to other known proteins but exhibits predicted secondary structural characteristics that are suggestive of AVM localization.

APH_0032 is a 619 aa acidic protein (pI = 3.6) with a predicted molecular weight of 66.1 kDa. Amino acids 313-597 (46.0% of the protein's sequence) encode a tandem repeat region (**Figure 18A and C**). Eight direct repeats, which are nearly identical and range from 33 to 35 amino acids long, are preceded by a truncated segment that is homologous to the last 10 amino acids of each repeat and followed by a truncated segment that is homologous to the first 3 amino acids of each repeat (**Figure 18A and C**). BLASTP searches using the entire APH_0032 sequence or the repeat-region revealed that amino acids 341-609 exhibit 30% identity to PY03917, which is a hypothetical protein of *Plasmodium falciparum*. A BLASTP search using the N-terminal non-repeat region (amino acids 1-312) yielded hits to hypothetical proteins of *Microcoleus chthonoplastes* and *Entamoeba dispar* and a putative RNA methylase from *Methanococcus voltae* that ranged from 22 to 30% identity. APH_0032 is predicted to be largely hydrophilic (**Figure 18B**). Chlamydial Inc proteins possess transmembrane domains (TMD) that facilitate insertion into the PVM and often carry hydrophilic domains that extend into the host cell cytoplasm to interact with host proteins (14, 15). TMPred analysis predicts APH_0032 to carry a TMD that spans amino acids 144-162 (**Figure 18B**) (47). Attempts to predict a tertiary structure for APH_0032 using SWISS-MODEL, ESyPred3D, 3Djigsaw, and GENO3D were unsuccessful because none of these programs were able to identify similar sequences of known structure on which to model APH_0032. Sequencing of PCR products of the *aph_0032* coding sequence amplified from *A. phagocytophilum* strains NCH-1, HZ, and HGE-1 revealed that this gene's sequence is identical among the 3 strains, as well as the USG3 strain for which it was

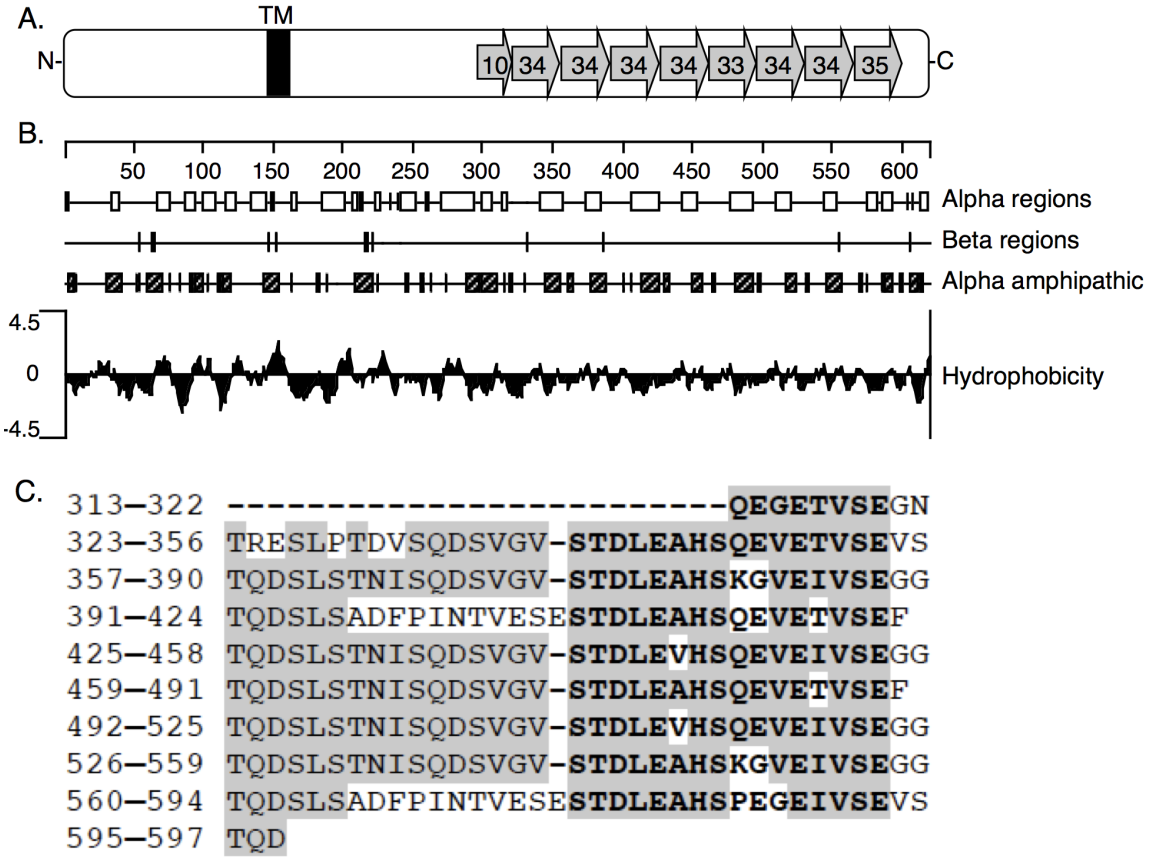

Figure 18. Schematic representation of *A. phagocytophilum* APH_0032, sequence, and secondary structure analyses.

(**A**) The amino (N)-terminal region (amino acids 1–312) precedes the repeat region (amino acids 313–597), which precedes a short carboxy (C)-terminal region (amino acids 598–619). The repeat region consists of 8 imperfect direct repeats (denoted by grey arrows) of 34, 34, 34, 34, 33, 34, 34, and 35 amino acids that are arranged in tandem. The 8 direct repeats are preceded by a truncated segment that is homologous to the last 10 amino acids of each repeat and followed by a truncated segment that is homologous to the first 3 amino acids of each repeat. The black bar and TMD designation denote the predicted transmembrane domain encoded by amino acids 144–162, as determined by the TMPRED algorithm. (**B**) Hydrophobicity analysis of APH_0032. The numerical scale demarcates the protein sequence at 50-amino acid intervals. The Kyte-Doolittle algorithm was used to denote hydrophobic (black filled histogram above the x-axis) and hydrophilic (black filled histogram below the axis) regions. (**C**) APH_0032 tandem repeat sequence alignment. The amino acid (aa) positions and sequence of each repeat are provided. Dashes denote gaps in the alignment. Grey highlighting denotes identical amino acids. Bolded amino acid segments are those that are homologous to a segment that occurs 4 times in the *E. chaffeensis* ECH0039 (P120) tandem repeat region (57, 190).

originally sequenced (190) (data not shown).

5.2.2 APH_0032 is present in higher abundance in *A. phagocytophilum* RC organisms than in DC organisms.

We performed Western blot analysis to determine if APH_0032 is expressed during *A. phagocytophilum* infection of promyelocytic HL-60 cells. Anti-APH_0032 recognized APH_0032 as a single band of ∼130 kDa in an *A. phagocytophilum*-infected, but not an uninfected HL-60 cell lysate (**Figure 19A**). APH_0032's apparent MW is considerably larger than its predicted size of 66.1 kDa. Likewise, MBP-APH_0032 (pI = 4.1) migrates with an apparent MW of 160 kDa, which is larger than its predicted MW of 109.3 kDa.

A. phagocytophilum undergoes a biphasic developmental cycle in which an infectious DC organism binds, invades, and develops into a replicative RC organism that divides by binary fission (199). The numerous RC bacteria, which are non-infectious, revert to DC organisms before being released to infect naive host cells. We have determined that a host cell-free population of *A. phagocytophilum* DC and RC organisms can be recovered following syringe lysis, which does not damage the fragile RC, while a pure DC population can be recovered following sonication, which destroys the RC (data not shown). To assess whether DC or RC organisms express more APH_0032, we screened Western-blotted lysates of host cell-free *A. phagocytophilum* organisms recovered following syringe lysis (RC and DC) or sonication (DC only) that were normalized according to the levels of Msp2 (P44), which is a constitutively expressed outer membrane protein (71). APH_0032 was detected in lysates derived from RC and DC organisms and from DC organisms alone (**Figure 19A**). Densitometric analyses of two separate experiments revealed that there is 2.37-2.74 times more APH_0032 in lysates derived from RC and DC organisms as compared to lysates derived from DC organisms (**Figure 19B**).

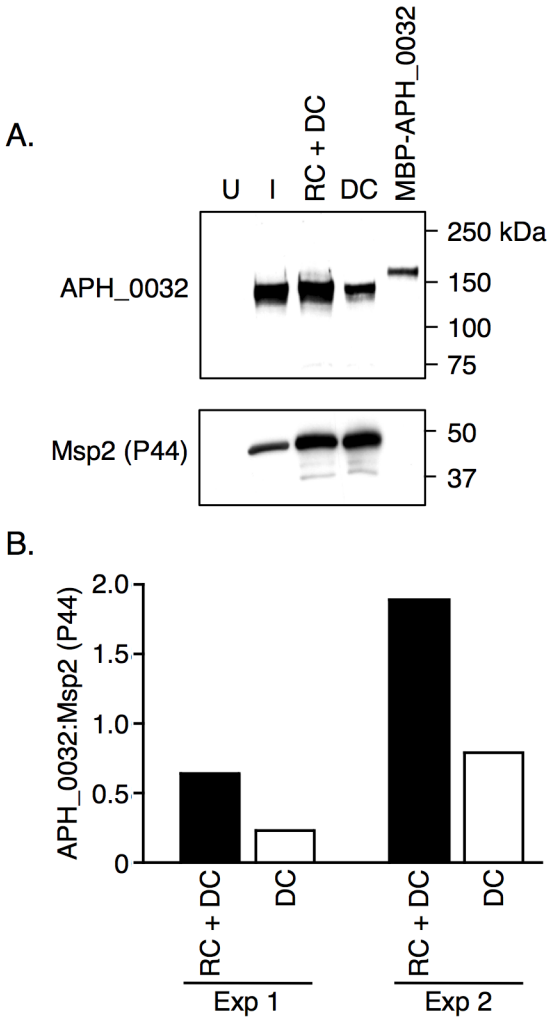

Figure 19. APH_0032 is present in greater abundance in lysates of *A. phagocytophilum* RC organisms compared to DC organisms.
(**A**) Western-blotted lysates of uninfected (U) and *A. phagocytophilum*-infected HL-60 cells (I) as well as host cell-free *A. phagocytophilum* populations consisting of RC and DC organisms (RC + DC) or only DC organisms (DC) was screened with anti-APH_0032. MBP-APH_0032 served as a positive control. The blot was stripped and screened with anti-Msp2 (P44) to confirm that equivalent amounts of lysates derived from RC and DC organisms and only DC organisms were used. The results are representative of two separate experiments. (**B**) Densitometry to quantify the intensities of APH_0032 and Msp2 (P44) bands. The ratio of the APH_0032 densitometric value to the Msp2 (P44) densitometric value is shown for RC + DC and DC lysates for two separate experiments.

5.2.3 APH_0032 is not detected until 24 h post infection and localizes to the AVM.

Next, we screened *A. phagocytophilum*-infected HL-60 cells with anti-APH_0032 in conjunction with a mAb against Msp2 (P44) (149, 176) and at 0.7, 8.5, and 24 h post infection and examined the cells by confocal microscopy. At 0.7 h post infection, essentially no APH_0032 was detected on Msp2 (P44)-positive organisms that were bound to the HL-60 cell surface (**Figure 20A-D**). By 8.5 h, some *A. phagocytophilum* organisms that were positive for both Msp2 (P44) and APH_0032 were detectable (**Figure 20E-H**). At 24 h, the AVM was strikingly distinguishable from enclosed bacteria by exclusive staining for APH_0032 (**Figure 20I-L**). *A. phagocytophilum* organisms within inclusions that were positive for both Msp2 (P44) and APH_0032 appeared as green (corresponding to Msp2 [P44] staining) spheroid organisms, each of which was surrounded by a red ring (corresponding to APH_0032 staining; **Figure 20J-L**) or as yellow organisms. At 24 h, 56.6 $\pm$ 3.1% of *A. phagocytophilum* inclusions were positive for APH_0032 (**Figure 20L**). The AVM was negative for Msp2 (P44) at all time points.

5.2.4 APH_0032 localizes to the AVM during *A. phagocytophilum* infection of human myeloid and endothelial cell lines and tick embryonic cell lines.

In addition to HL-60 cells, *A. phagocytophilum* infects and resides within host cell-derived inclusion in the human monocytic cell line, THP-1, the human microvascular endothelial cell line, HMEC-1, and the *I. scapularis* embryonic cell line, ISE6. To confirm whether APH_0032 is expressed and localizes to the AVM within each of these cell lines, *A. phagocytophilum*-infected THP-1, HMEC-1, and ISE6 cells were examined by confocal microscopy at 24 h post infection. APH_0032-positive inclusions were detected within each cell line (**Figure 20M-X**). As observed for HL-60 cells, a notable number of ApVs were negative for APH_0032 staining (**Figure 20P, T, and X**). Indeed, at 24 h post infection only 54% of

Figure 20. *A. phagocytophilum* APH_0032 is detectable on the surfaces of intravacuolar bacteria and localizes to the AVM in infected host cells.
(**A–L**) HL-60 cells were synchronously infected with *A. phagocytophilum*. At 0.7 (**A–D**), 8.5 h (**E–H**), and 24 h post infection (**I–L**), the cells were fixed and viewed by confocal microscopy for immunoreactivity with antibodies against Msp2 (P44) (major bacterial surface protein; used to denote bacteria in **B, F,** and **J**) and APH_0032 (**C, G,** and **K**). DIC images are presented in panels **A, E,** and **I**. Merged fluorescent images are presented in **D, H,** and **L**. (**M–X**) *A. phagocytophilum*-infected THP-1 (**M–P**), HMEC-1 (**Q–T**), and ISE6 (**U–X**) cells were fixed and viewed by confocal microscopy for immunoreactivity with antibodies against Msp2 (P44) (**N, R,** and **V**) and APH_0032 (**O, S,** and **W**). DIC images are presented in panels **M, Q,** and **U**. Merged fluorescent images are presented in panels **P, T,** and **X**. (**L, P, T,** and **X**) Arrows denote representative AVMs that exhibit exclusive staining for APH_0032 surrounding Msp2 (P44)-positive or Msp2 (P44)- and APH_0032-dual-positive intravacuolar bacteria. The results are representative of three separate experiments.

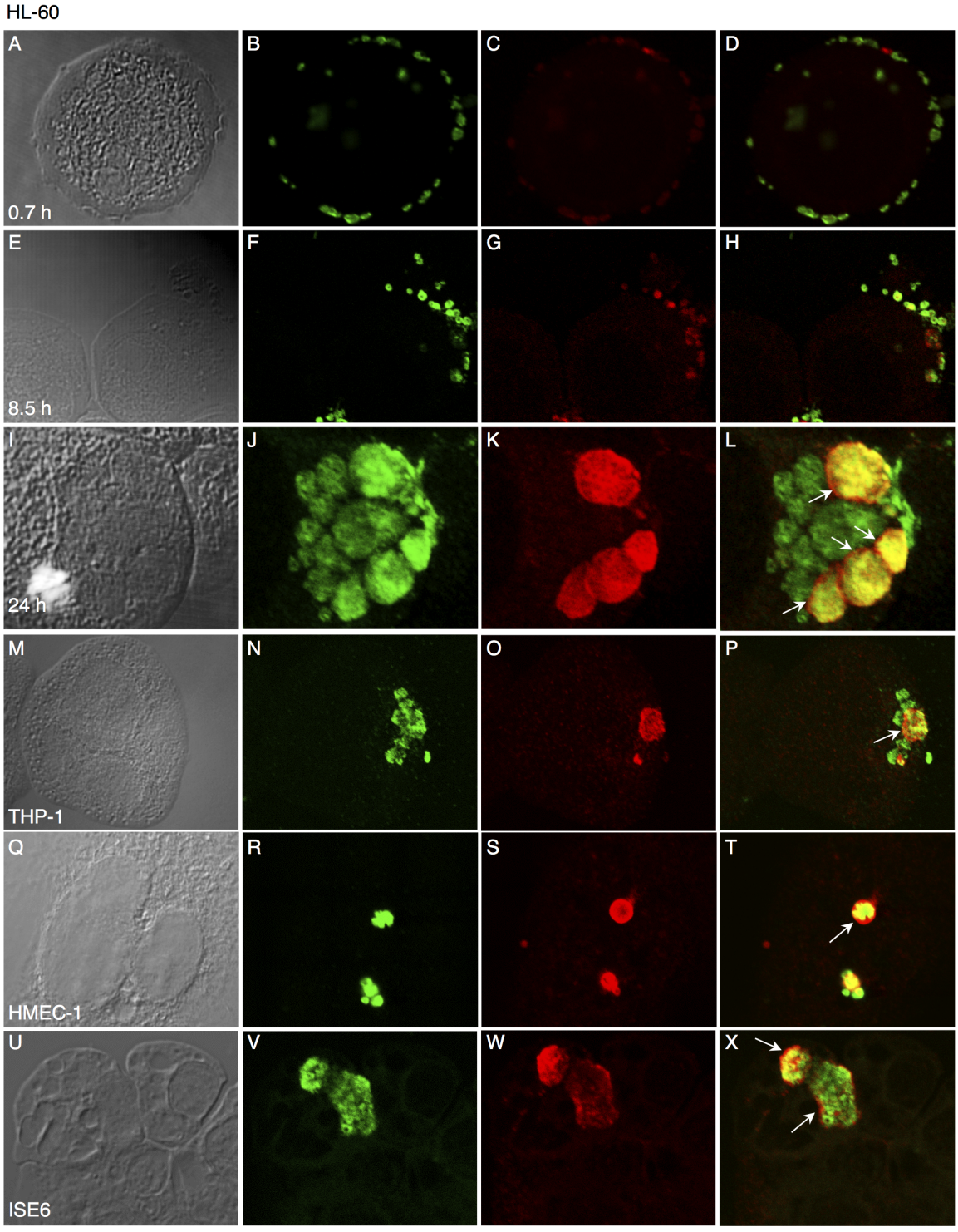
HL-60
A
B
C
D
0.7 h
E
F
G
H
8.5 h
I
J
K
L
24 h
M
N
O
P
THP-1
Q
R
S
T
HMEC-1
U
V
W
X
ISE6

Figure 20

ApVs were positive for APH_0032 in THP-1 cells (data not shown).

5.2.5 APH_0032 is not amply expressed by *A. phagocytophilum* and does not localize to the AVM until 24 h post infection of HL-60 cells.

We next monitored the temporal expression and AVM localization kinetics of APH_0032 over the course of a synchronous *A. phagocytophilum* infection of HL-60 cells. Host cell-free organisms were added to HL-60 cells and allowed to bind for 40 min after which unbound bacteria were removed. Our and other laboratories have shown that it takes approximately 4 h for bound *A. phagocytophilum* DC organisms to enter into nascent vacuoles (20, 28, 96). APH_0032 is not detectable by Western blot analysis until 24 h post-bacterial addition, which corresponds to ~20 h post entry (**Figure 21A**). At 48 h, the intensity of the APH_0032 130 kDa band is considerably stronger and additional less intense bands of higher and lower apparent molecular weights are also detected. One of the lower molecular weight bands is ~66 kDa, which is in agreement with the predicted size for APH_0032. Consistent with what we have shown previously (31), the intensity of the Msp2 (P44) band, which serves as an infection control, increases throughout the course of infection. APH_0032 is detectable on 9.8 ± 4.3% and 15.5 ± 2.0% of ApVs at 12 and 18 h, respectively (**Figure 21B**). By 24 h, the number of APH_0032-positive ApVs had increased to 56.6 ± 3.1%. The percentage of APH_0032-positive ApVs fluctuated between 41.4 ± 16.2% and 61.1 ± 1.4% for the remainder of the time course. The decrease in the percentage of APH_0032-positive ApVs that occurs at 42 h is likely due to reinfection, which we have shown occurs by or shortly after 36 h (199).

We utilized immunoelectron microscopy to screen synchronously infected HL-60 cells over a 48 h period to further examine when APH_0032 is expressed and when it localizes to the AVM during *A. phagocytophilum* infection. APH_0032-negative DC organisms were bound to the HL-60 cell surface at 0.7 h (**Figure 22A**) and had internalized into nascent

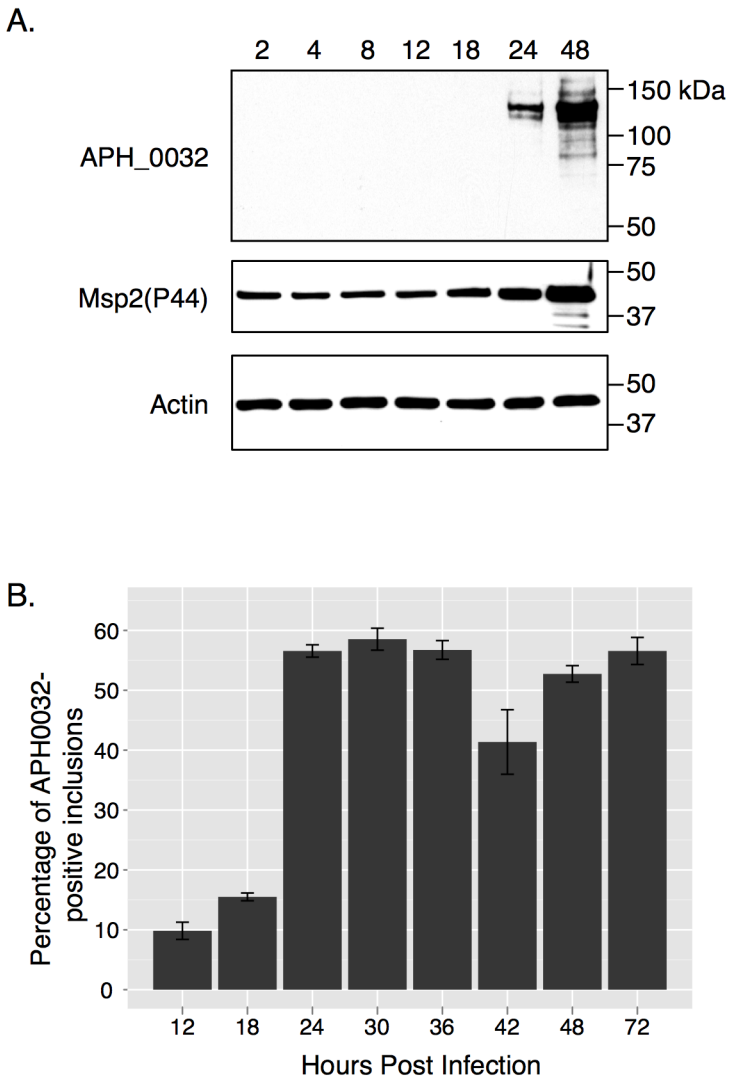

Figure 21. Kinetics of APH_0032 expression and AVM localization in *A. phagocytophilum*-infected HL-60 cells.

HL-60 cells were synchronously infected with *A. phagocytophilum*. At the indicated post infection time points, aliquots were processed and analyzed by Western blot analysis (**A**) or immunofluorescence microscopy (**B**). (**A**) Western blots of *A. phagocytophilum*-infected HL-60 whole cell lysates were screened with antibodies against APH_0032, Msp2 (P44) (infection control), and actin (loading control). (**B**) Percentages of ApVs [based on the presence of Msp2 (P44)-positive *A. phagocytophilum* organisms] that are also positive for APH_0032 exclusive staining of the AVM. Results are the mean (±SD) of 3 separate experiments. 828–1471 Msp2 (P44)-positive inclusions were scored for APH_0032 staining per time point.

Figure 22. Assessment of *A. phagocytophilum* APH_0032 expression and localization to the AVM by immunoelectron microscopy.
HL-60 cells were synchronously infected with *A. phagocytophilum*. At 0.7 (**A**), 4 (**B**), 8 (**C**), 12 (**D**), 18 (**E**), 24 (**F**), and 48 h (**G**) post-bacterial addition, samples were fixed and screened with anti-APH_0032 followed by goat anti-rabbit IgG conjugated to 6 nm gold particles and examined by transmission electron microscopy. Representative results of two separate experiments are shown. (**A–B**) Asterisks denote bound or newly internalized *A. phagocytophilum* DC organisms. (**F–H**) Arrowheads denote representative portions of the AVM that are labeled with gold particles. (**H**) Magnified view of the region in panel **G** that is demarcated by a hatched box. Scale bars, 0.5 μm.

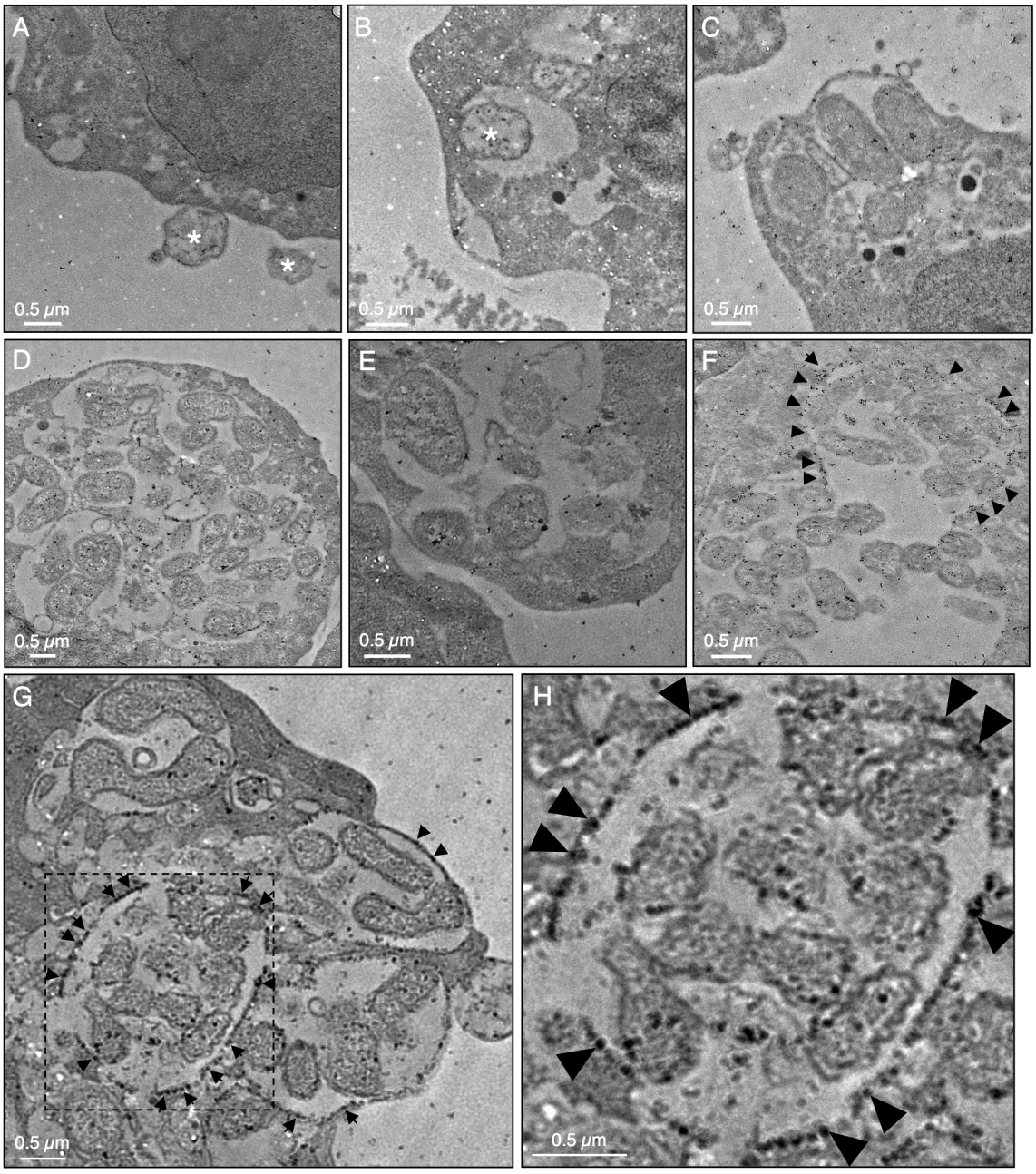

Figure 22

vacuoles by 4 h (**Figure 22B**). By 8 h, which corresponds to 4 h post entry, internalized bacteria had transitioned into elongated, pleomorphic RC and initiated replication (**Figure 22C**). Consistent with our observations obtained using Western blot analysis and confocal microscopy, *A. phagocytophilum* organisms exhibited little anti-APH_0032 reactivity and the AVM was negative for APH_0032 at 8, 12, and 18 h (**Figure 22C-E**). APH_0032 was not convincingly detected at the AVM of any inclusion through 18 h. At 24 h, individual HL-60 cells contained numerous ApVs that harbored several APH_0032-positive *A. phagocytophilum* organisms; and the AVM was heavily decorated by APH_0032 (**Figure 22F**). We have previously demonstrated that an *A. phagocytophilum* infection of HL-60 cells that was synchronously initiated becomes asynchronous after 24 h due to reinfection by DC organisms (199). **Figure 22G** presents a representative example of an asynchronously infected HL-60 cell at 48 h that harbors numerous ApVs differing in their maturities. Immature inclusions are those that contain either an individual DC organism or those that contain few RC organisms. A mature inclusion containing several DC organisms having rough outer membranes is also present. APH_0032 heavily labels the AVM of the mature ApV, while little to no APH_0032 is detected on the AVMs of less mature inclusions (**Figure 22G and H**).

5.2.6 APH_0032 is expressed and localizes to the AVM during *in vivo A. phagocytophilum* infection and *aph_0032* and *aph_1387* are transcribed during *A. phagocytophilum* residence in tick salivary glands.

APH_0032 is expressed and elicits a humoral immune response during HGA as MBP-APH_0032, but not MBP alone is recognized by antiserum from an HGA patient (**Figure 23A**). This is in agreement with our results obtained using another HGA patient's antiserum (data not shown) and with a report by Storey and colleagues (190). Seronegative normal human serum recognizes neither MBP-APH_0032 nor MBP alone (data not shown). We

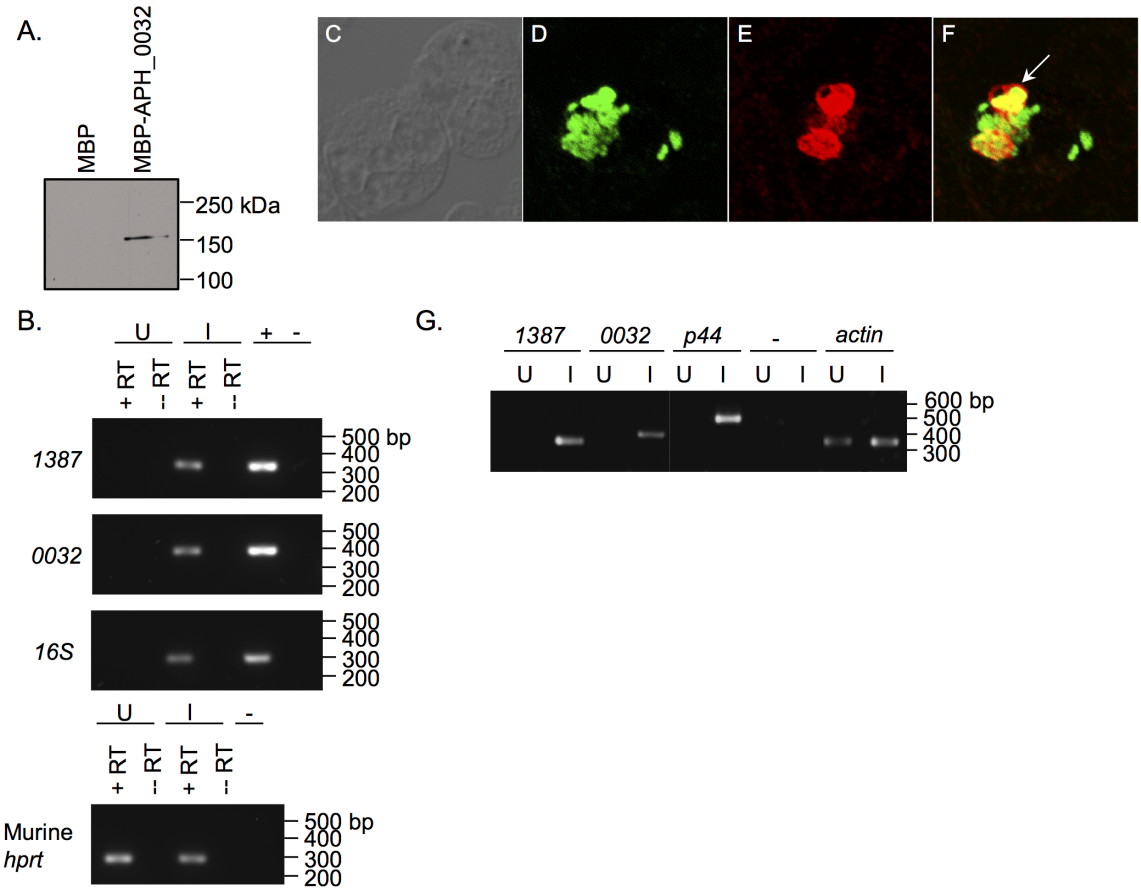

Figure 23. *A. phagocytophilum* APH_0032 is expressed and modifies the AVM during *in vivo* infection.

(**A**) Antiserum from an HGA patient recognizes MBP-APH_0032, but not MBP alone. (**B**) RT-PCR utilizing primers targeting *aph_1387* (1387), *aph_0032* (0032), murine *hprt* (loading control), and the *A. phagocytophilum* 16S rRNA gene (infection control) and total RNA isolated from neutrophils recovered from *A. phagocytophilum*-infected mice on day 8 was performed in the presence (+RT) and absence (–RT) of reverse transcriptase. *A. phagocytophilum* DNA and water served as positive and negative controls, respectively. (**C–F**) Buffy coats isolated from an *A. phagocytophilum*-infected mouse on day 8 post infection were fixed and viewed by confocal microscopy for immunoreactivity with antibodies against Msp2 (P44) (**D**) and APH_0032 (**E**). DIC images are presented in panel **C**. A merged fluorescent image is presented in **F**. The arrow denotes exclusive APH_0032 staining of the AVM. (**G**) RT-PCR targeting *aph_1387*, *aph_0032*, *msp2 (p44)* (infection control), and human *actin* (loading control) was performed on total RNA isolated from uninfected (U) and *A. phagocytophilum*-infected (I) *I. scapularis* nymph salivary glands. Reactions performed in the absence of reverse transcriptase (–) served as negative controls. The results are representative of two to three separate experiments for each analysis.

next investigated transcription of *aph_0032* and *aph_1387*, which encodes another bacterial AVM protein (87), during murine infection. Both transcripts are detected in total RNA recovered from GR-1-positive neutrophils isolated from *A. phagocytophilum*-infected mice on day 8 post infection (31) (**Figure 23B**). Moreover, Msp2 (P44)- and APH_0032-positive inclusions are detectable by confocal microscopy in murine buffy coats obtained from *A. phagocytophilum*-infected mice at 8 days post infection (**Figure 23C-F**). Consistent with our observations of *A. phagocytophilum*-infected mammalian cell lines, multiple APH_0032-negative inclusions are also present within murine buffy coat cells (**Figure 23F**). Because APH_0032 (**Figure 20**) and APH_1387 (87) are expressed in ISE6 cells, we investigated whether *aph_0032* and *aph_1387* are transcribed by *A. phagocytophilum* during its residence in *I. scapularis* nymphal salivary glands. RT-PCR analysis revealed that both genes are expressed in tick salivary glands (**Figure 23G**).

5.3 Discussion

We have confirmed APH_0032 as an *A. phagocytophilum*-derived protein that localizes to the AVM during infection of human myeloid, human microvascular endothelial and *I. scapularis* embryonic cell lines and murine neutrophils. A recent whole genome transcription profiling study that demonstrated *aph_0032* transcription in HL-60, HMEC-1, and ISE6 cells (137) corroborates these results. *aph_0032*, along with *aph_1387*, is transcribed in *I. scapularis* salivary glands. *aph_0032* exhibits a high degree of nucleotide sequence conservation among at least 4 geographically diverse *A. phagocytophilum* strains (190). APH_0032 may exert a function that is unique to *A. phagocytophilum*, as it exhibits very little to no sequence similarity to any other known protein. APH_0032 is expressed in high abundance beginning $\sim$20 h post invasion and is retained on the AVM for the remainder of the infection. A plausible speculation is that it may play an important role during late-stage infection of

mammalian and tick host cells, such as preparing the ApV for eventual release of infectious DC organisms, and is less likely important for preventing early host cell-mediated killing. APH_0032 can serve as a marker for distinguishing more mature ApVs that contain DC organisms and/or RC organisms that are transitioning to DC organisms (APH_0032-positive) from less mature ApVs that contain RC organisms (APH_0032-negative). It is important to note that not all AVMs are positive for APH_0032 at any given time point, which may be directly related to the maturity of the ApVs. For instance, the majority of the APH_0032-negative ApVs in **Figure 20L** are smaller and presumably contain fewer and less mature organisms than those ApVs that are APH_0032-positive. Likewise, the AVM that is heavily decorated by APH_0032 in **Figure 22G** encloses the most bacteria of any ApV in that cell. The bacteria within that strongly APH_0032-positive vacuole display ruffled outer membranes and are $\sim$0.5 μm in diameter, both characteristics of which are consistent with DC organisms and late-stage RC organisms (199). An alternative explanation is that APH_0032 may be dispensable for *A. phagocytophilum* intracellular survival, perhaps because it shares a redundant function with another *Anaplasma* AVM protein.

Acidic tandem repeat proteins are emerging as key effectors and AVM proteins of Anaplasmataceae pathogens. A protein alignment of APH_0032 and the *E. chaffeensis* tandem repeat protein P120 (ECH_0039 in the annotated *E. chaffeensis* genome) (215) revealed that a short amino acid segment that occurs in each of the full-length tandem repeats of APH_0032 (**Figure 18C**) shares sequence similarity to a segment that occurs 4 times in the tandem repeat region of P120 (190). *E. chaffeensis* P47 is another acidic (pI 4.2) tandem repeat carrying protein that interacts with host molecules involved in cell signaling, transcriptional regulation, and vesicle trafficking (119, 205, 218).

APH_0032 migrates predominantly as a 130 kDa band in SDS-polyacrylamide gels, which is considerably larger than its predicted MW of 66.1 kDa. Others have proposed that this phenomenon is due to APH_0032 being a glycoprotein (47). However, we find

no evidence of glycosylation of APH_0032 (data not shown). The anomalous migration of APH_0032 is likely due to its acidic nature, which conceivably prevents SDS from amply coating the protein and thereby inhibits its proper electrophoretic mobility. This phenomenon has been demonstrated for other acidic proteins in SDS-polyacrylamide gels, including *E. chaffeensis* P47 (206). Indeed, Wakeel and colleagues showed that recombinant forms of the full-length and C-terminal region of P47, both of which have overall acidic pIs, but not the N-terminal region, which has a near neutral pI, exhibit slower than predicted electrophoretic mobilities upon SDS-PAGE (206).

Even though APH_0032 is detected on the surfaces of intravacuolar *A. phagocytophilum* organisms and is detected in great abundance at the AVM, it is not detected on bacteria that were bound at the HL-60 cell surface by immunofluorescence microscopy. A similar trend was observed for APH_1387 (87). Because these bacteria had been recovered following disruption of infected HL-60 cells, washed with PBS, and added to naive HL-60 cells, we propose that APH_0032 and APH_1387 are not integral membrane proteins, but are instead loosely associated with the *Anaplasma* outer membrane while being secreted and are easily washed away during bacterial isolation. APH_0032 is more abundantly detected in an *A. phagocytophilum* lysate of RC and DC organisms as compared to a lysate derived from only DC organisms. RC organisms are metabolically active and therefore actively express APH_0032, while metabolically inert DC will presumably have less APH_0032 protein.

APH_0032 is the second confirmed AVM protein. APH_1387 is the first (87). Their differential expression patterns during the course of infection suggest that they play distinct pathobiological roles. Elucidating the host cell ligands and/or signaling pathways with which APH_0032 and APH_1387 interact and confirming the mechanism by which they are delivered to the AVM, as well as identifying additional bacterial-derived AVM proteins represent ongoing efforts in our laboratory. Achieving these goals will be critical to understanding how *A. phagocytophilum* facilitates its intracellular survival.

A. phagocytophilum proteins APH_1387 and APH_0032 are expressed on the cytoplasmic face of the AVM and are critical for ApV development.

6.1 Introduction

A. phagocytophilum-encoded proteins actively modify the vacuole in which it resides. As a result, the ApV becomes a unique compartment by which *A. phagocytophilum* can acquire nutrients, replicate, and interact with multiple host vesicular pathways. The bacterial and corresponding host cell factors that mediate the intracellular trafficking and fusogenicity of the ApV are not fully understood. However, pathogen-derived proteins that localize to the PVM likely contribute to the molecular mechanisms that underlie the establishment of a protective niche. We identified the first two *A. phagocytophilum*-encoded proteins that localize to the AVM, APH_1387 and APH_0032 (86, 87). APH_0032 presumably traverses the AVM by means of its predicted N-terminal TMD. The region of the protein that is C-terminal to the TMD likely projects into the host cell cytoplasm since it is highly hydrophilic and lacks additional TMDs or hydrophobic stretches that are of requisite length ($\geq$20 aa) to traverse the AVM (152). This is in agreement with a theme among bacterial-encoded PVM proteins; the cytoplasmic domains interact with host cell signaling cascades and vesicular traffic. In contrast, APH_1387 does not carry a traditional TMD, but it contains a stretch of amino acids in the N-terminal non-repeat region that form a hydrophobic β-sheet

and 3 additional bilobed hydrophobic domains that could conceivably facilitate insertion into the AVM. In addition, APH_1387 carries predicted "surface exposed" regions that are presumably exposed on the cytoplasmic face.

The functional roles of APH_1387 and APH_0032 remain largely unknown, in part because both proteins exhibit limited to no homology with any previously described protein. However, many bacterial effectors have been shown to mimic the activities of cellular proteins without detectable amino acid sequence similarity (186). While targeted gene deletion would be the most direct way to decipher their respective functions, the lack of genetic techniques for knock-out, complementation or site directed mutagenesis of *Anaplasma* requires the use of alternative and less direct approaches. In this chapter we identify the regions of APH_1387 and APH_0032 that facilitate membrane association and determine that the proteins are exposed on the cytoplasmic face of the AVM. In addition, we demonstrate that ectopic expression of the GFP-tagged repeat regions of APH_1387 and APH_0032 interfere with the intracellular development of *A. phagocytophilum* containing vacuoles.

6.2 Results

6.2.1 GFP tagged APH_1387 and APH_0032 constructs used in this study.

In this study we generated a series of GFP-tagged APH_0032 and APH_1387 truncations (**Figure 24A** and **Figure 25A**). To confirm expression and test the immunoreactivity of anti-APH_0032 and anti-APH_1387 against selected fusion proteins, HeLa cells were transfected, lysates were resolved by SDS-PAGE, and immunoblots were probed with anti-APH_0032 or anti-APH_1387. Robust expression of full-length GFP-APH_0032, GFP-APH_0032$_{\Delta 313-620}$, and GFP-APH_0032$_{\Delta 1-301}$ were detected with APH_0032 antisera (**Figure 24B**). In contrast, APH_1387 antisera failed to recognize expression of the N-

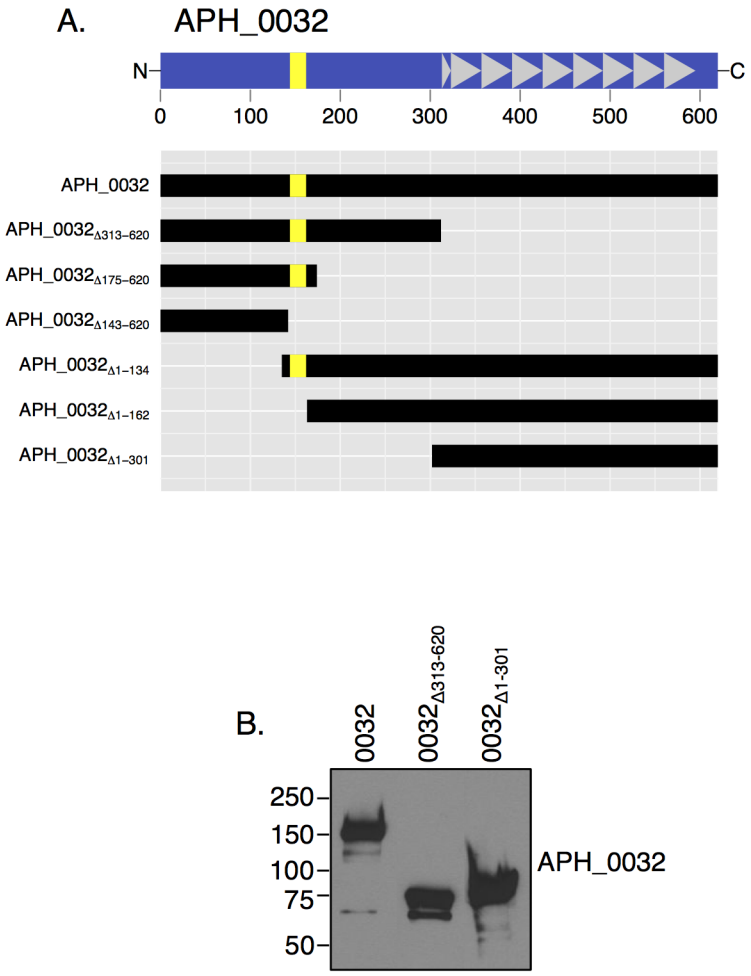

Figure 24. Schematic representation of APH_0032 gene constructs used in this study. (**A**) Diagram of APH_0032 deletion constructs N-terminally fused to GFP. Amino acids 144-162 represent the predicted transmembrane domain, denoted by the yellow bar.The C-terminal region consists of 8 imperfect tandem direct repeats (denoted by grey arrows). (**B**) HeLa cells transfected with plasmids encoding GFP fusions to full length APH_0032, APH_0032$_{\Delta 313-620}$, and APH_0032$_{\Delta 1-301}$. Lysates were resolved by SDS-PAGE and the immunoblot was probed with anti-APH_0032.

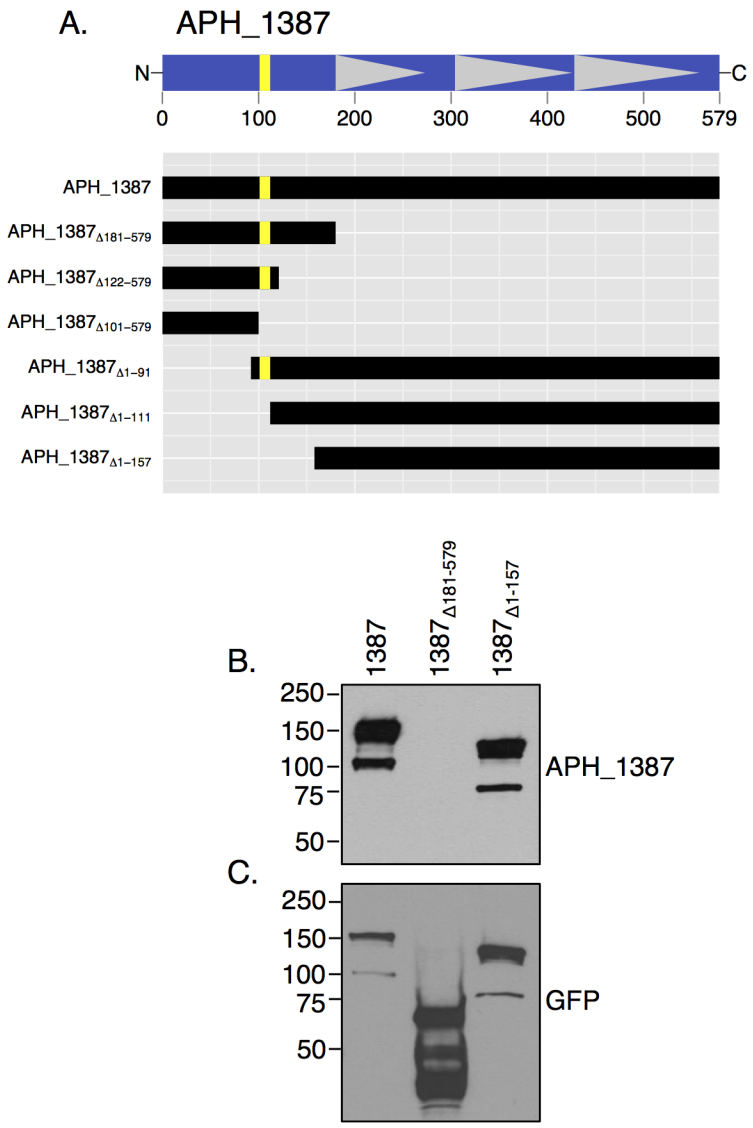

Figure 25. Schematic representation of APH_1387 gene constructs used in this study. (**A**) Diagram of APH_1387 deletion constructs N-terminally fused to GFP. Amino acids 101-112 form a hydrophobic β-pleated sheet, indicated by the yellow bar. The C-terminal repeat region consists of 3 tandem direct repeats (denoted by grey arrows) consisting of 93, 122, and 130 amino acids. (**B**) HeLa cells were transfected with plasmids encoding GFP fusions to full length APH_1387, APH_1387$_{\Delta 181-579}$, and APH_1387$_{\Delta 1-157}$. Lysates were resolved by SDS-PAGE and the immunoblot was probed with anti-APH_1387. (**C**) The blot was stripped and screened with anti-GFP to confirm the expression of all fusion proteins in HeLa cells. The results are representative of 3 separate experiments.

terminal non-repeat portion of APH_1387, GFP-APH_1387$_{\Delta 181-579}$ (**Figure 25B**). Only when the immunoblot was stripped and re-probed with an anti-GFP antibody was GFP-APH_1387$_{\Delta 181-579}$ detected, indicating it is the C-terminal repeat region of APH_1387 that is immunoreactive (**Figure 25C**).

6.2.2 *A. phagocytophilum* AnkA, but not APH_0032 or APH_1387 can be heterologously secreted by the *L. pneumophila* Dot/Icm T4SS secretion system.

The presence of APH_0032 (86) and APH_1387 (87) at the AVM indicates that the proteins are secreted. *A. phagocytophilum* encodes a VirB/D T4SS that is similar to that of *A. tumefaciens* (140). Indeed, a GFP-tagged version of the *A. phagocytophilum* T4SS effector, AnkA (APH_0470), can be secreted by *A. tumefaciens* (111). To determine whether APH_0032 or APH_1387 are T4SS substrates, each was N-terminally fused to the enzymatic reporter, *Bordetella pertussis* CyaA, and expressed in the surrogate host, *L. pneumophila*, which utilizes its Dot/Icm secretory apparatus to export T4SS substrates (180). The ability of a surrogate host that uses the Dot/Icm system to secrete VirB/D substrates has been previously reported (46). THP-1 cells were infected with *L. pneumophila* transformants expressing CyaA-fusions of APH_0032, APH_1387, *A. phagocytophilum* AnkA, RalF (*L. pneumophila* Dot/Icm effector; positive control), or CyaA alone (negative control) and changes in host cAMP levels were measured. Expression of each CyaA-tagged protein in infected THP-1 cells was confirmed by Western blot analysis (data not shown). As presented in **Figure 26**, cAMP levels were substantially elevated relative to that in *L. pneumophila* expressing CyaA alone (negative control) when cells were infected with bacteria producing CyaA-RalF or CyaA-AnkA, but not CyaA-APH_0032 or CyaA-APH_1387. As anticipated, cAMP levels were low for host cells infected with transformants of a *L. pneumophila* DotA mutant.

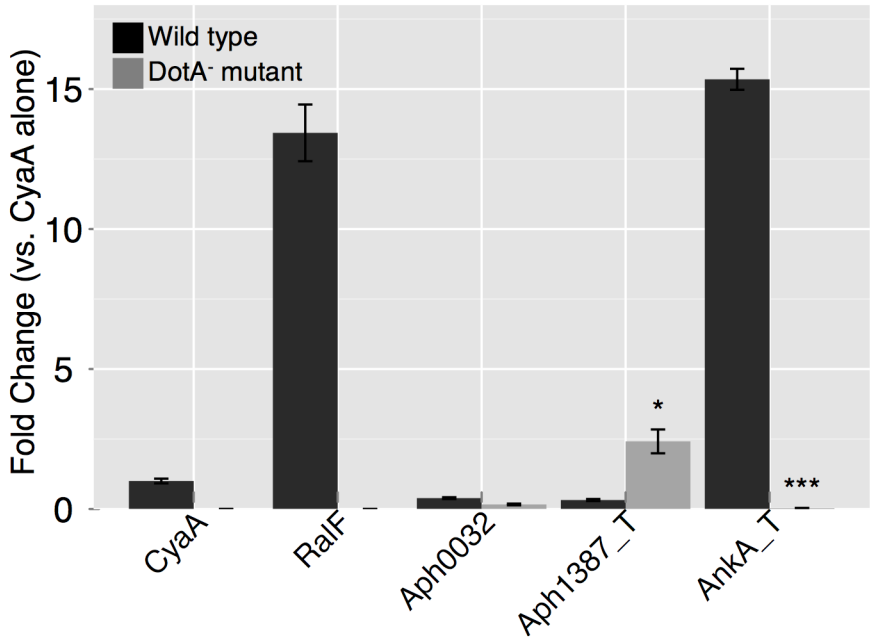

Figure 26. ***A. phagocytophilum*** **AnkA, but not APH_0032 or APH_1387 can be secreted by the** ***Legionella pneumophila*** **Dot/Icm secretion system.**
PMA-stimulated THP-1 cells were infected with *L. pneumophila* transformants expressing CyaA-tagged RalF, APH_0032, or N-terminally truncated APH_1387 (APH_1387-T), and N-terminally truncated AnkA (AnkA-T). Black bars present the fold change in intracellular [cAMP] for THP-1 cells infected with wild type *L. pneumophila* transformants expressing CyaA-fusions relative to control cells infected with transformants expressing CyaA alone. Grey bars correspond to the fold change in intracellular [cAMP] measured for THP-1 cells infected with T4SS-defective *L. pneumophila* DotA$^-$ transformants. Results are representative of three independent experiments. Statistically significant (*$P < 0.05$; ***$P < 0.001$) values are indicated.

6.2.3 The N-terminal non-repeat regions of APH_0032 and APH_1387 possess domains that facilitate association with host cell membranes.

We identified the residues required for membrane localization of APH_0032 and APH_1387 by deletion analysis and use of a fluorescence-based technique. The TMPred algorithm predicts a putative transmembrane domain for APH_0032 that spans amino acids 144-162. To investigate the potential contribution of this region for membrane association, we constructed GFP-tagged APH_0032 constructs (**Figure 24A**) and ectopically expressed them in HeLa cells (**Figure 27B**). The cells were washed with PBS to confirm expression, which does not permeabilize the cells so that transfected cells retained the GFP proteins. Duplicate samples were digitonin permeabilized prior to fixation so that any GFP protein not associated with host membranes was washed out. Digitonin is a cholesterol binding drug that targets and perforates the plasma membrane. The selectivity is due to the plasma membrane having the highest concentration of cholesterol, containing approximately 65-80% of free cellular cholesterol (115). Following digitonin permeabilization, loss of intracellular GFP signal from the cells indicated that the fusion protein was not membrane associated. By contrast, GFP signals that were retained upon cell permeabilization indicated the fusion protein was membrane bound. Retention was determined as the percentage of cells that remained GFP-positive after digitonin permeabilization. Deletion of the C-terminal repeat region, GFP-APH_0032$_{\Delta 313-620}$, did not impact retention relative to full-length GFP-APH_0032. In contrast, upon digitonin permeabilization, deletion of the N-terminal non-repeat region, GFP-APH_0032$_{\Delta 1-301}$, resulted in almost complete loss of GFP signal, indicating that region of APH_0032 was not membrane associated (**Figure 27A**). Further analysis revealed that in cells producing GFP-APH_0032$_{\Delta 1-162}$ or GFP-APH_0032$_{\Delta 143-620}$, both of which lack the putative transmembrane domain, there was a pronounced decrease in retention compared to full-length GFP-APH_0032. However, retention was partially restored in

Figure 27. Deletion analysis of APH_0032 reveals a N-terminal domain necessary for host cell membrane association.
(**A**) HeLa cells were transiently transfected to ectopically express GFP alone, GFP-APH_0032 or GFP-APH_0032 deletion constructs. To confirm expression the cells were washed with PBS, which does not permeabilize the host cell membrane so that the GFP proteins were retained. Duplicate samples were digitonin permeabilized prior to fixation so that any GFP proteins not specifically associated with host organelle membranes were washed out. Retention was calculated as the percentage of cells that remained GFP-positive after digitonin permeabilization and PBS washing. The data are representative of 3 separate experiments. A schematic diagram of the APH_0032 protein sequence shows the different deletion constructs with the predicted transmembrane domain indicated by the yellow bar. The predicted N-terminal transmembrane domain was found to be critical for membrane association of ectopically expressed APH_0032. (**B**) Representative images of HeLa cells ectopically expressing GFP-APH_0032 constructs. DAPI stained host and bacterial are blue and are present in all panels.

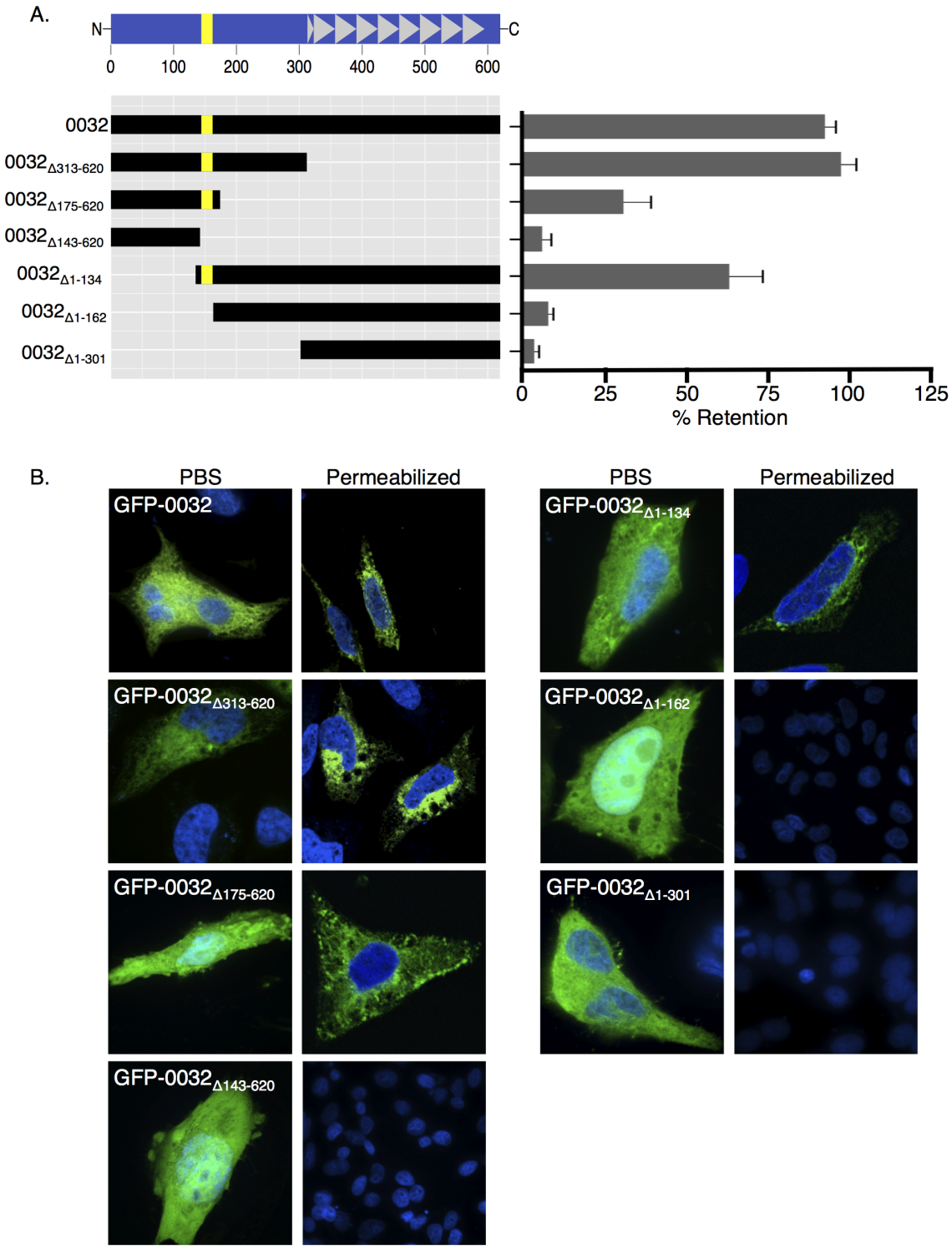
A.
N
C
0
100
200
300
400
500
600
0032
0032Δ313-620
0032Δ175-620
0032Δ143-620
0032Δ1-134
0032Δ1-162
0032Δ1-301
0
25
50
75
100
125
% Retention
B.
PBS
Permeabilized
PBS
Permeabilized
GFP-0032
GFP-0032Δ1-134
GFP-0032Δ313-620
GFP-0032Δ1-162
GFP-0032Δ175-620
GFP-0032Δ1-301
GFP-0032Δ143-620

Figure 27

cells producing the transmembrane containing constructs, GFP-APH_0032$_{\Delta 1-134}$ and GFP-APH_0032$_{\Delta 175-620}$, indicating that region is necessary for the association of APH_0032 with host cell membranes (**Figure 27A**).

Although APH_1387 lacks a predicted transmembrane domain, it contains a stretch of amino acids, 101-112, in the N-terminal non-repeat region that form a hydrophobic β-pleated sheet and 3 bilobed hydrophobic domains that could conceivably facilitate insertion into the AVM. To investigate the potential contribution of either region to membrane localization of APH_1387, GFP-tagged APH_1387 constructs (**Figure 25A**) were ectopically expressed in HeLa cells (**Figure 28B**) and washed with either PBS or permeabilized with digitonin. Similar to APH_0032, deletion of the C-terminal repeat region, GFP-APH_1387$_{\Delta 181-579}$, did not impact retention relative to full-length GFP-APH_1387 (**Figure 28A**). However, upon digitonin permeabilization, deletion of the N-terminal non-repeat region, GFP-APH_1387$_{\Delta 1-157}$, resulted in almost complete loss of GFP protein (**Figure 28A**). These results indicate the 3 bilobed hydrophobic domains are not critical for membrane association. Further analysis to confirm the involvement of the hydrophobic β-pleated sheet revealed that in cells producing GFP-APH_1387$_{\Delta 1-111}$ or GFP-APH_1387$_{\Delta 101-579}$, both of which lack the putative membrane associating domain, there was a pronounced decrease in retention compared to full-length GFP-APH_1387. However, retention was partially restored in cells producing GFP-APH_1387$_{\Delta 1-91}$ or GFP-APH_1387$_{\Delta 122-579}$, indicating that the hydrophobic β-pleated sheet domain is essential for the localization of APH_1387 to host cell membranes (**Figure 28A**).

6.2.4 APH_1387 and APH_0032 are exposed on the cytoplasmic face of the AVM.

Because vesicular trafficking is regulated by protein-protein interactions at the surface of transport vesicles and their appropriate target membrane, we investigated whether APH_1387 and/or APH_0032 are exposed on the cytoplasmic face of the AVM. *A. phagocytophilum*

Figure 28. Deletion analysis of APH_1387 identifies a N-terminal domain, residues 101-112, necessary for host cell membrane association.
(**A**) HeLa cells were transiently transfected to ectopically express GFP alone, GFP-APH_1387 or GFP-APH_1387 deletion constructs. To confirm expression the cells were washed with PBS, which does not permeabilize the host cell membrane so that the GFP-proteins were retained. Duplicate samples were digitonin permeabilized prior to fixation so that any GFP proteins not specifically associated with host organelle membranes were washed out. Retention was calculated as the percentage of cells that remained GFP-positive after digitonin permeabilization and PBS washing. The data are representative of 3 separate experiments. A schematic diagram of the APH_1387 protein sequence shows the different deletion constructs with the stretch of amino acids that form a hydrophobic β-sheet denoted by the yellow bar. The region containing amino acids 101-112 was found to be critical for membrane association of ectopically expressed APH_1387. (**B**) Representative images of HeLa cells ectopically expressing GFP-APH_1387 constructs. DAPI stained host and bacterial nuclei are blue and are present in all panels.

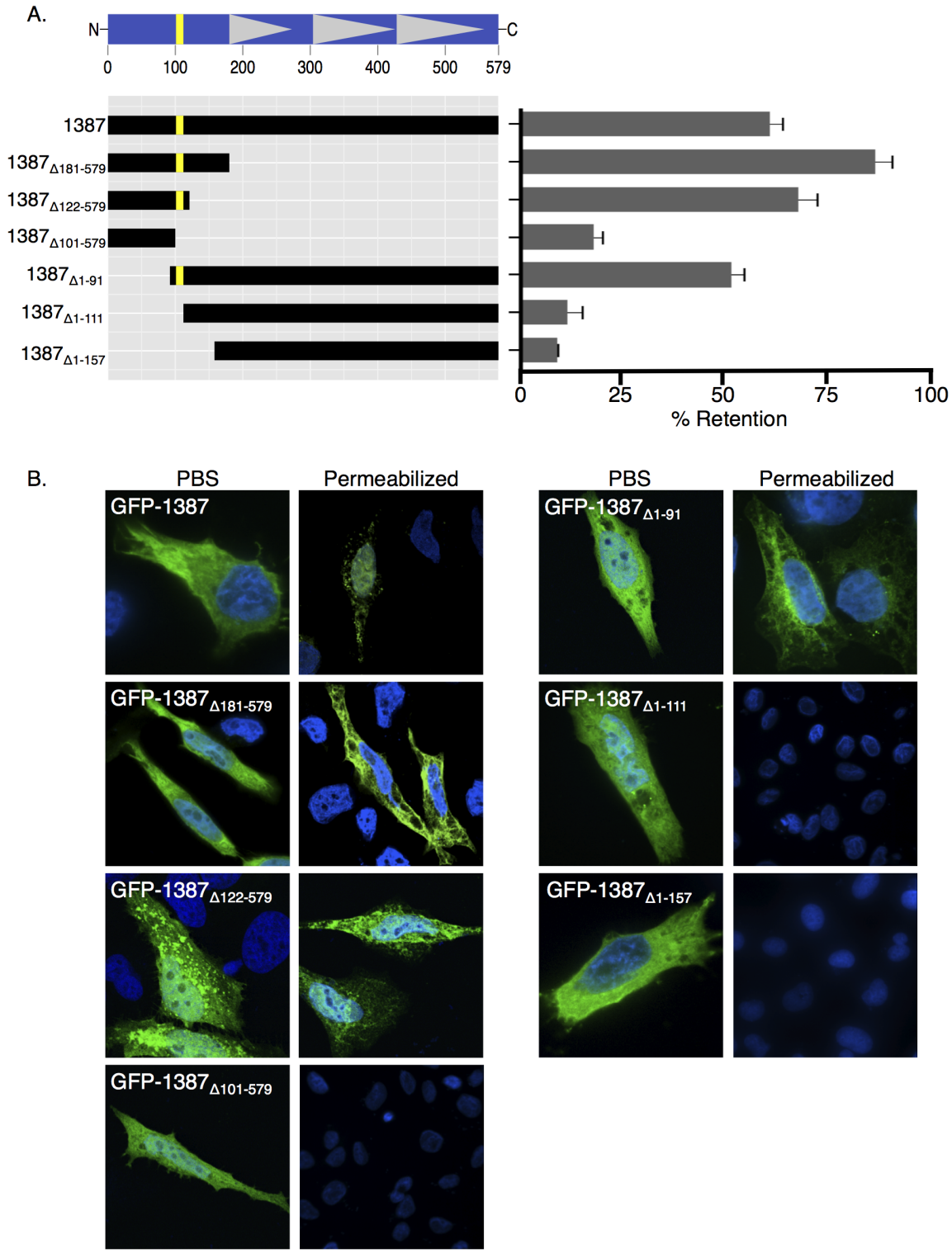
A.
N
C
0
100
200
300
400
500
579
1387
1387Δ181-579
1387Δ122-579
1387Δ101-579
1387Δ1-91
1387Δ1-111
1387Δ1-157
0
25
50
75
100
% Retention
B.
PBS
Permeabilized
PBS
Permeabilized
GFP-1387
GFP-1387Δ1-91
GFP-1387Δ181-579
GFP-1387Δ1-111
GFP-1387Δ122-579
GFP-1387Δ1-157
GFP-1387Δ101-579

Figure 28

infected RF/6A cells were differentially permeabilized with digitonin and saponin to distinguish between proteins exposed to the cytoplasm and proteins enclosed within membrane bound vacuoles or organelles. Digitonin perforates the plasma membrane and allows antibodies to diffuse into the host cell while organelle membranes remain intact (34). To determine whether APH_1387 and/or APH_0032 are exposed to the host cell cytosol, anti-APH_1387 and anti-APH_0032 antibodies were introduced into *A. phagocytophilum* infected RF/6A cells following digitonin permeabilization. Next, the cells were fixed and bound intracellular antibodies were detected with an Alexa Fluor conjugated secondary antibody. The positive APH_1387 and APH_0032 signals detected at the periphery of the ApV indicated that the anti-APH_1387 and -APH_0032 antibodies recognized portions of their respective proteins that were accessible in the host cell cytoplasm (**Figure 29M-R**). To confirm that digitonin did not compromise the integrity of the AVM, an antibody against the *A. phagocytophilum* major outer surface protein Msp2 (P44) was used. Msp2 (P44) is only expressed on bacterial membranes and not the vacuolar membrane. The lack of staining with anti-Msp2 (P44) in digitonin permeabilized cells demonstrated the AVM was intact (**Figure 29J-L**). To confirm that the antibodies were immunoreactive with their appropriate targets, *A. phagocytophilum* infected RF/6A cells were permeabilized with saponin, which permeabilizes all membranes, and stained with each antibody. Consistent with previous studies (86, 87), vacuolar-enclosed bacteria were positive for P44, APH_1387 and APH_0032, while the AVM was also positive for APH_1387 and APH_0032 (**Figure 29A-I**). Thus, positive staining after digitonin permeabilization indicates APH_1387 and APH_0032 are present on the cytoplasmic face of the AVM.

Figure 29. APH_1387 and APH_0032 contain portions exposed on the cytoplasmic face of the AVM.

A. phagocytophilum infected RF/6A cells were permeabilized with digitonin (**J-R**) or saponin (**A-I**) as described in the Materials and Methods and viewed by confocal microscopy. DAPI stained host and bacterial nuclei blue and was used to delineate *A. phagocytophilum* inclusions. Merged fluorescent images are presented in panels **C, F, I, L, O,** and **R**. To determine whether APH_1387 and APH_0032 are exposed on the cytoplasmic face of the AVM, cells were permeabilized with digitonin (**J-R**) and subsequently incubated with APH_1387 (**N**) or APH_0032 (**Q**) antibodies. Bound antibodies were detected with an Alexa fluor 594 conjugated secondary antibody (red). In **O** and **R**, punctate staining around the periphery of the ApV represent positive APH_1387 and APH_0032 detection. The integrity of the AVM was confirmed after digitonin permeabilization by the lack of ApV staining with the Msp2 (P44) antibody. To confirm that the antibodies were immunoreactive, *A. phagocytophilum* infected RF/6A cells were fixed and permeabilized with saponin (**A-I**).

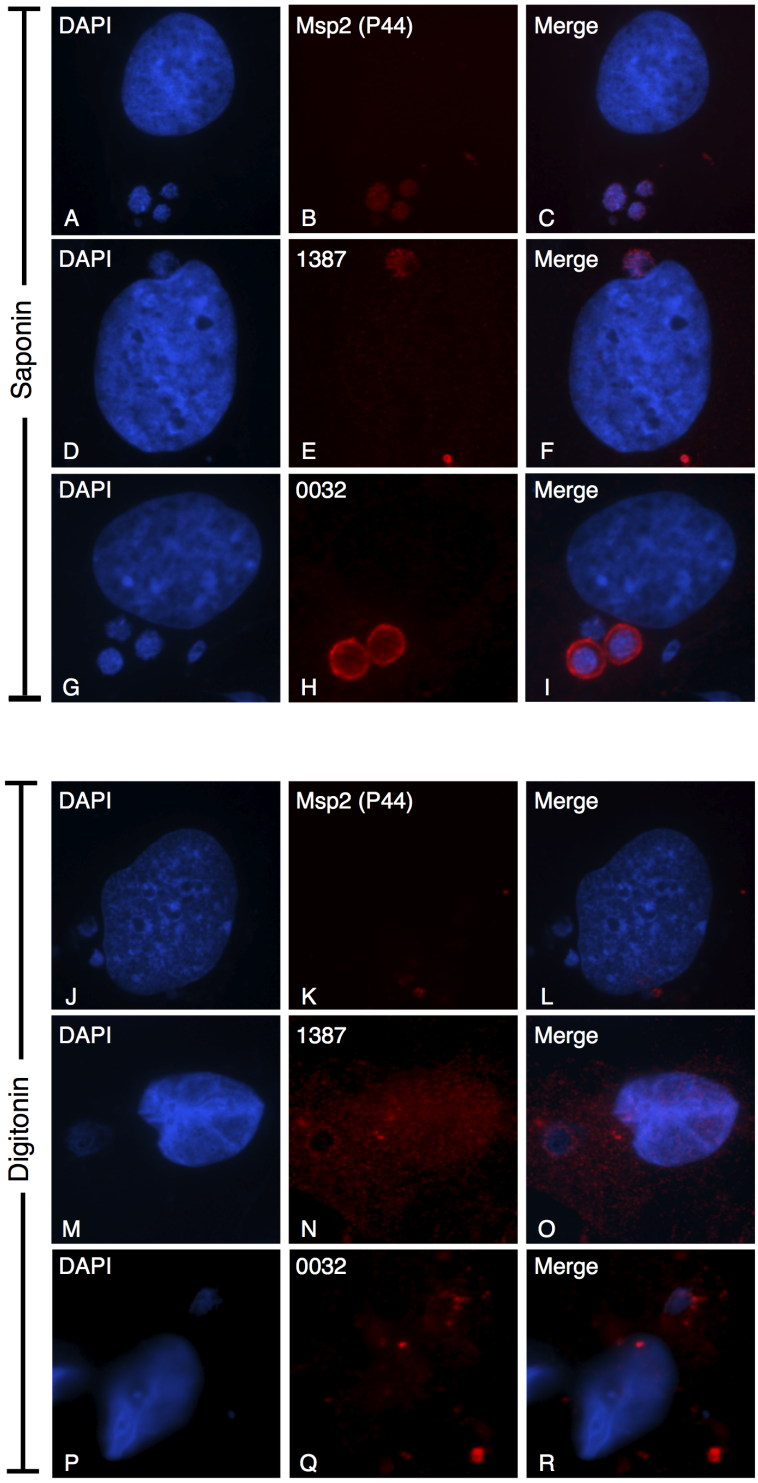
Saponin
DAPI
Msp2 (P44)
Merge
A
B
C
DAPI
1387
Merge
D
E
F
DAPI
0032
Merge
G
H
I
Digitonin
DAPI
Msp2 (P44)
Merge
J
K
L
DAPI
1387
Merge
M
N
O
DAPI
0032
Merge
P
Q
R

Figure 29

6.2.5 Ectopic expression of GFP-tagged APH_1387 and APH_0032 interferes with *A. phagocytophilum* development in RF/6A cells.

Because APH_1387 and APH_0032 are on the cytoplasmic face of the AVM, we assessed the abilities of ectopically expressed proteins to competitively inhibit *A. phagocytophilum* infection. We rationalized that if APH_1387 or APH_0032 established interactions with host proteins critical for ApV development then ectopic expression of APH_1387 or APH_0032 might competitively inhibit infection. To test this, GFP fusions of APH_1387 or APH_0032 were transfected into RF/6A cells and then infected with *A. phagocytophilum*. Twenty four h post infection, the number of ApVs and the ApV morphology were assessed by confocal microscopy. Expression of GFP-APH_1387 led to an observable decrease in ApV size relative to ApVs in untransfected cells or cells expressing GFP-APH_0032 or GFP. These data were quantified by measuring the diameter of ApVs in transfected cells (**Figure 30**). In cells expressing GFP-APH_1387, ApV diameters were 2.3 $\pm$ 0.9 μm compared with 3.5 $\pm$ 1.2 μm and 4.3 $\pm$ 1.2 μm in cells expressing GFP-APH_0032 and GFP alone, respectively. Next, we wanted to identify regions of APH_1387 that might be important in facilitating the developmental block. To do this, we assessed ApV morphology in *A. phagocytophilum* infected cells expressing amino- and carboxy-terminal deletions of APH_1387. In cells expressing the C-terminal repeat region, GFP-APH_1387$_{\Delta 1-157}$, the average ApV was 2.4 $\pm$ 1.1 μm, similar to what was observed in cells expressing full-length GFP-APH_1387 (**Figure 30**). In contrast, when the N-terminal non-repeat region of APH_1387 was expressed, GFP-APH_1387$_{\Delta 181-579}$, the average ApV size was 4.2 $\pm$ 1.4 μm, similar to that observed in GFP expressing cells, indicating ApV development was not blocked. These results suggest that the C-terminal repeat region of APH_1387 is interacting with host proteins and consequently interfering with *A. phagocytophilum* infection. It should be noted that although ectopic expression of vacuolar membrane proteins

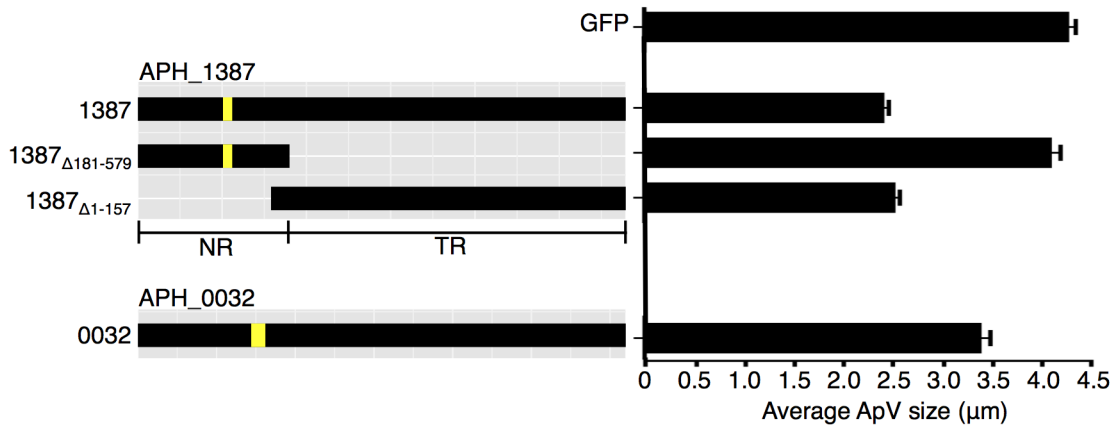

Figure 30. Ectopically expressed GFP-APH_1387 interferes with ApV development at 24 h post infection.

RF/6A cells transiently expressing the indicated APH_0032 or APH_1387 constructs N-terminally fused to GFP were infected with *A. phagocytophilum*. At 24 h post infection cells were fixed and the ApVs from transfected cells were measured. A schematic representation of the APH_1387 and APH_0032 protein sequences illustrate the different truncation constructs. The C-terminal region of APH_1387 was found to be involved in the ApV developmental block. NR: non-repeat region; TR: tandem repeat region.

from other pathogens have been shown to localize to the PVM, we were unable to detect GFP-APH_1387 or GFP-APH_0032 at the AVM in *A. phagocytophilum* infected RF-6A cells (138).

Because APH_0032 is not expressed in high abundance until 24 h post infection, we speculated that a block in *A. phagocytophilum* development would not be detectable until time points beyond 24 h. To investigate this, we infected RF/6A cells with *A. phagocytophilum* for 24 h, then transfected the cells. At forty-eight h post infection the resulting effects on infection and ApV morphology were examined by confocal microscopy (**Figure 31B-H**). Similar to the results observed at 24 h post infection, cells expressing GFP-APH_1387 yielded atypical ApVs that were smaller than those in GFP expressing cells (**Figure 31A-E**). In cells expressing GFP-APH_1387 the average ApV was 1.9 ± 0.7 μm, compared with 4.0 ± 1.4 μm in cells expressing GFP (**Figure 31A-C**). Furthermore, the developmental block was only seen in cells expressing full-length APH_1387 or the C-terminal repeat region. Notably, at 48 h post infection the ApVs in GFP-APH_0032 expressing cells were also significantly smaller in size, with the average ApV 1.9 ± 0.5 μm (**Figure 31A and F-H**). To identify the region of APH_0032 responsible for the atypical ApV morphology we used GFP-fusions expressing the N-terminal non-repeat and C-terminal repeat regions of APH_0032. In cell expressing the APH_0032 repeat region, GFP-APH_0032$_{\Delta 1-301}$, the ApVs were 2.1 ± 0.6 μm (**Figure 31A and G**). In contrast, the atypical ApV phenotype was less pronounced in cells expressing the APH_0032 non-repeat region, GFP-APH_0032$_{\Delta 313-620}$, with the average ApV 2.7 ± 0.9 μm (**Figure 31A and H**). Therefore, the C-terminal repeat regions of APH_1387 and APH_0032 are important for competitively inhibiting *A. phagocytophilum* infection.

Figure 31. Ectopically expressed GFP-APH_1387 and GFP-APH_0032 competitively inhibit ApV development at 48 h post infection.
RF/6A cells were infected with *A. phagocytophilum*. At 24 h post infection, cells were transiently transfected to express the indicated APH_0032 or APH_1387 constructs N-terminally fused to GFP. At 48 h post infection the cells were fixed, stained with antibodies against Msp2 (P44) (major *A. phagocytophilum* outer membrane protein) to identify bacteria, and viewed by confocal microscopy. (**A**) To assess the block in ApV development, the ApV in transfected cells was measured. A schematic representation of the APH_1387 and APH_0032 protein sequences illustrate the different truncation constructs. The C-terminal regions of APH_1387 and APH_0032 were found to be involved in the ApV developmental block at 48 h post infection. (**B-H**) Representative confocal micrographs depicting transiently transfected RF/6A cells infected with *A. phagocytophilum*. *A. phagocytophilum* organisms were delineated by staining with Msp2 (P44), which recognizes the *A. phagocytophilum* surface protein. NR: non-repeat region; TR: tandem repeat region. The scale bar represents 4 μm.

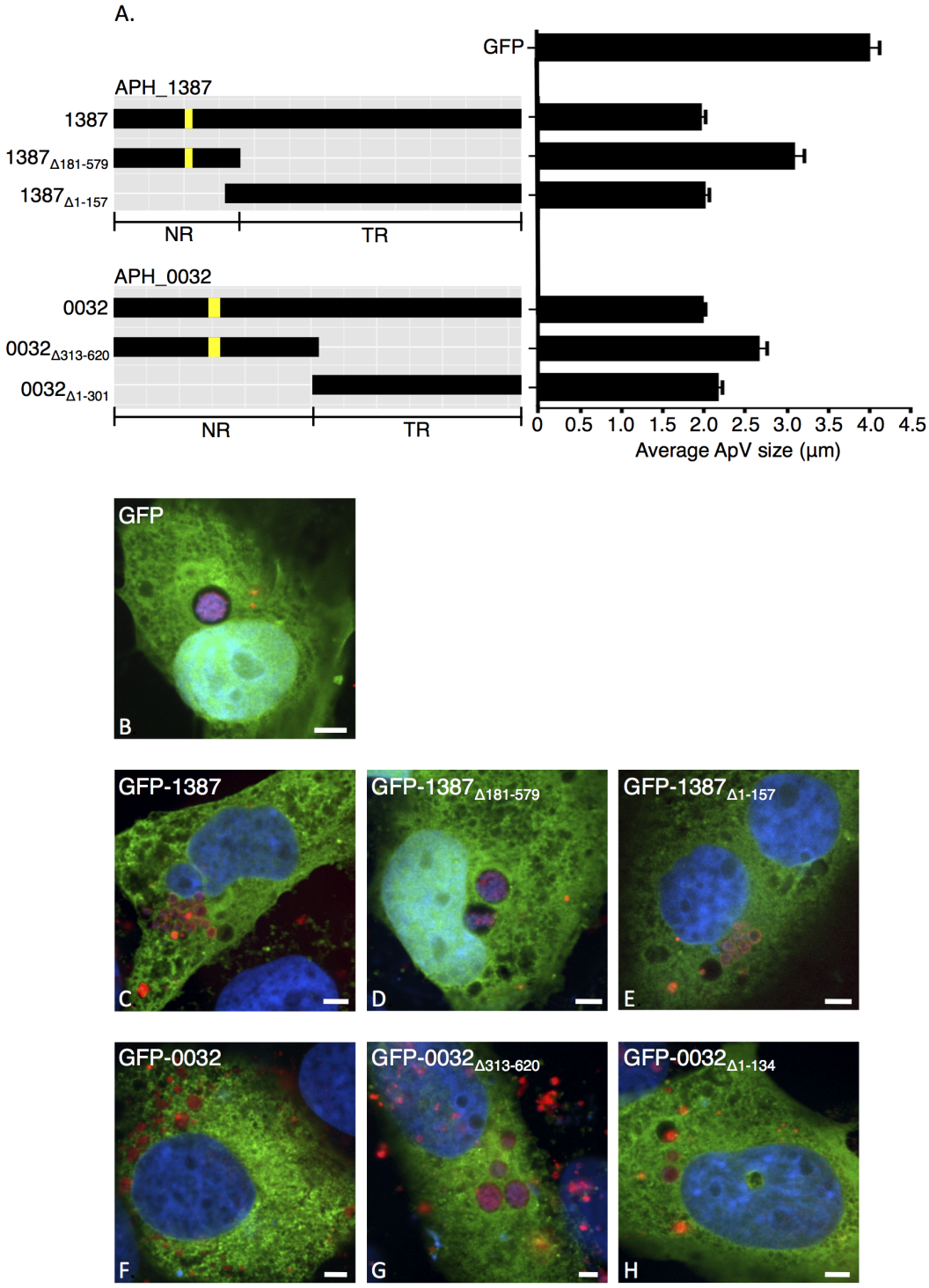
A.
GFP
APH_1387
1387
1387Δ181-579
1387Δ1-157
NR
TR
APH_0032
0032
0032Δ313-620
0032Δ1-301
NR
TR
0 0.5 1.0 1.5 2.0 2.5 3.0 3.5 4.0 4.5
Average ApV size (µm)
GFP
B
GFP-1387
C
GFP-1387Δ181-579
D
GFP-1387Δ1-157
E
GFP-0032
F
GFP-0032Δ313-620
G
GFP-0032Δ1-134
H

Figure 31

6.3 Discussion

To date, three *A. phagocytophilum* AVM proteins, APH_1387, APH_0032 and AptA (*A. phagocytophilum* toxin A), have been identified (86, 87, 192). The study of these proteins is hindered by the overall lack of sequence identity with proteins of known function. In addition, the obligate intracellular nature of *Anaplasma* limits the ability to perform targeted gene deletion or site directed mutagenesis for functional analyses. In this study, we extend our understanding of APH_1387 and APH_0032 to show they are present on the cytoplasmic face of the AVM and contribute to the proper maturation of the ApV. Similar approaches have been used to investigate secreted vacuolar membrane proteins by other pathogens (15, 42, 166).

Upon translocation from the bacteria, APH_1387 and APH_0032 localize to the AVM. It is unlikely that APH_0032 and APH_1387 are T4SS substrates. Indeed, the C-termini of both proteins are negatively charged, which is in conflict with T4SS substrates having positively charged C-termini (201). Also, most intravacuolar *A. phagocytophilum* organisms are not intimately associated with the inner face of the AVM, which goes against the fact that type IV secretion is contact dependent (7, 201). Lastly, the *L. pneumophila* Dot/Icm system failed to translocate CyaA-tagged versions of APH_0032 and APH_1387. One could argue that this is attributable to the Dot/Icm system being unable to secrete heterologous VirB/D effectors. However, Dot/Icm-mediated delivery of other VirB/D substrates has been reported (46). Moreover, *L. pneumophila* could translocate CyaA-AnkA, which is the first demonstration that the Dot/Icm system can secrete a heterologous *A. phagocytophilum* VirB/D effector. These results warrant cautiously accepting the hypothesis that APH_0032 and APH_1387 are not T4SS effectors.

We speculate that *A. phagocytophilum* delivers APH_0032 and APH_1387 to the intravacuolar space via type I, or ATP-binding cassette-dependent secretion and that the

substrates subsequently localize to the AVM. T1SSs recognize a C-terminal uncleaved secretion signal that is rich in certain amino acids (LDAVTSIF) and poor in others (KHPMWC) (48). 72.7% of the APH_0032 C-terminal amino acids (APSTGVEIRFMDRDS DDDVLAL) are found in type I secretion signals. 71.4% of the APH_1387 C-terminal amino acids (LVDVPTALPLKDPDDEDVLSY) are found in type I secretion signals. T1SS effectors are acidic (pI $\sim$4) and contain very few or no cysteines (48). Only 5 of the 619 and 4 of the 578 amino acids that compose APH_0032 and APH_1387, respectively, are cysteines. Accordingly, we propose that APH_0032 and APH_1387 are delivered to the intravacuolar space via type I secretion and subsequently localize to/integrate into the AVM.

We identified the regions of APH_1387 and APH_0032 necessary for host cell membrane association. GFP-tagged APH_0032 deletion constructs revealed that APH_0032 requires a N-terminal TMPred predicted transmembrane domain for associating with host cell membranes. GFP-APH_0032 fusion proteins that lacked the transmembrane domain were poorly retained following digitonin permeabilization, indicating they were not specifically interacting with the host cell membrane. Moreover, in non permeabilized cells, the same constructs exhibited a diffuse cytoplasmic distribution similar to that observed for GFP alone. However, amino acids flanking the transmembrane domain are likely important for host membrane association since retention was only partially restored when GFP-APH_0032$_{\Delta 1-134}$ and GFP-APH_0032$_{\Delta 175-620}$ were expressed. It is possible that other *A. phagocytophilum* proteins are involved in APH_0032 insertion into the membrane. Alternatively, APH_0032 may require additional amino acids flanking the transmembrane domain for proper membrane association. APH_1387 does not have a predicted transmembrane domain. However, analysis of GFP-APH_1387 deletion constructs identified a stretch of amino acids in the N-terminal region that encode a hydrophobic beta pleated sheet necessary for membrane association. Similar to APH_1387 and APH_0032, it has been reported that AptA also requires an N-terminal domain for subcellular localization (139). As such, all *A. phagocytophilum*

AVM proteins identified to date require discrete hydrophobic N-terminal domains for host cell membrane association. Continued identification of AVM proteins may help to reveal common secondary structures or primary sequence identity that will aid in the identification of additional candidate *A. phagocytophilum* vacuolar membrane proteins. This approach has been used to identify a unique bilobed hydrophobic secondary structural for chlamydial Inc proteins and the subsequent identification of over 40 Inc orthologs (14, 167).

The topology of a vacuolar membrane protein dictates its accessibility to interacting partners and provides functional clues. The results from the differential permeabilization studies with digitonin and saponin indicate that APH_1387 and APH_0032 are present on the cytoplasmic face of the AVM. Cells permeabilized with digitonin and incubated with anti-APH_1387 or anti-APH_0032 antibodies specifically labeled the periphery of the AVM, but did not label intravacuolar bacteria. For APH_1387 we hypothesize the C-terminal domain is projected into the host cell cytosol. Support for this premise is the immunoblots of lysates from HeLa cells expressing GFP fusions to full-length, non-repeat and tandem repeat regions of APH_1387. When the immunoblot was probed with an antibody against APH_1387 only the full length and C-terminal tandem repeat region were detectable (**Figure 25B**). However, when the blot was stripped and re-probed with an antibody against GFP a prominent band was detected for all three constructs, including the non-repeat region of APH_1387 (**Figure 25C**). This indicates the antibody against APH_1387 is immunoreactive against the C-terminal portion of the protein. Thus, positive detection of APH_1387 on the AVM suggests the C-terminal portion is exposed to the host cytosol. It has been shown that the C-terminal portions of inclusion membrane proteins from *C. trachomatis* and *C. psittaci* are exposed to the host cytosol, presumably to allow interaction with host cytoplasmic proteins (42, 166). Specifically the C-terminal of the *C. pneumoniae* Inc protein, Cpn0585, faces the cytosol and interacts with multiple Rab GTPases (42).

Vesicular trafficking is mediated by protein-protein interaction at the surfaces of transport

vesicles and target membranes. The presence of APH_1387 and APH_0032 on the cytoplasmic face of the AVM makes them likely candidates for interacting with host proteins. Here, we expressed GFP fusion of APH_1387 and APH_0032 in *A. phagocytophilum* infected RF/6A cells and examined the resulting phenotypes by confocal microscopy. There was no observable reduction in the number of ApVs when the cells were transfected prior to infection, suggesting that neither APH_1387 nor APH_0032 are essential for *A. phagocytophilum* replication. However, we found that ectopic expression of APH_1387 competitively inhibits proper *A. phagocytophilum* development and yields atypical ApVs at 24 h. Similar experiments have shown that ectopic expression of the *C. pneumoniae* Inc protein Cpn0585 results in atypical inclusions that are smaller in size and contain larger reticulate bodies (RBs), the metabolically active chlamydial form (42). The exact mechanism for the chlamydial developmental block is unknown. Cpn0585 recruits multiple Rabs – Rab1, Rab10 and Rab11 – to the *C. pneumoniae* inclusion (42); therefore, it is possible that overexpression of GFP-Cpn0585 may compete with endogenous Cpn0585 for Rabs and consequently disrupt development. Indeed, since APH_1387 is expressed early in infection (87), ectopic expression of GFP-APH_1387 may also compete with endogenous APH_1387 for a specific host protein that is important for ApV maturation. As a result, by 24 h *A. phagocytophilum* development is blocked and atypical ApVs are formed. On the other hand, APH_0032 is not expressed in high abundance until 24 h post infection. The expression kinetics is consistent with the detection of atypical ApVs at 48 h post infection in cells expressing GFP-APH_0032, and explains why the ApVs appeared normal at 24 h. Further analyses revealed the C-terminal repeat regions of APH_1387 and APH_0032 are responsible for the aberrant development of ApVs. The mechanism by which ectopic expression of APH_1387 and APH_0032 blocks *A. phagocytophilum* development is unclear. We hypothesize that the transfected fusion protein acts as a competitive inhibitor for host proteins that are important for *A. phagocytophilum* development. Therefore, future studies to identify the interacting

partners of APH_1387 and APH_0032 will be critical to understanding their functional roles in ApV intracellular development and survival.

Monoubiquitinated proteins decorate the *A. phagocytophilum*-occupied vacuolar membrane (AVM)

7.1 Introduction

Post-translational modification by ubiquitin is a highly conserved eukaryotic cell-specific process. Ubiquitin is a 76 amino acid protein that is covalently attached to lysine residues of target proteins. Attachment of ubiquitin to a protein substrate occurs in three successive steps that are mediated by the activating enzyme E1, the conjugating enzyme E2, and the ubiquitin ligase E3. Protein modification by ubiquitin can be classified as poly- or monoubiquitination (62, 155). Polyubiquitination occurs when a chain of four or more covalently linked ubiquitin moieties is added to a single lysine of a target protein. In monoubiquitination, a single ubiquitin molecule is conjugated to one or several (multi-monoubiquitination) lysines (79, 116). Poly- and monoubiquitination differentially dictate the localization and/or activity of the modified protein. Polyubiquitination has long been known to destine proteins for 26S proteasome-mediated destruction, but can also direct proteins to lysosomes for degradation, activate protein kinases, and contribute to DNA repair (36, 197). Monoubiquitination does not target proteins for degradation, but rather occurs after ligand binding to a variety of cell surface receptors and can act as an internalization signal, thereby directing plasma membrane-associated proteins to endosomes (40, 84, 151). Monoubiquitination of the peroxisome membrane targets the organelle for autophagosome-mediated destruction (101). Additionally, monoubiquitination is involved in transcriptional regulation and DNA repair

(84, 117). Lastly, ubiquitination of a variety of human pathogens in the host cell cytosol targets them to autophagosomes (37, 40). While this process is emerging as an infection control against intracellular pathogens, evidence also hints that intracellular bacteria can subvert it, as *S.* Typhimurium, after being mono- and polyubiquitinated in the cytosol, survives to occupy a damaged membranous compartment (19).

Given the importance of ubiquitination in modulating numerous eukaryotic cell processes, it is not surprising that many vacuole-adapted pathogens have evolved mechanisms to exploit the ubiquitin conjugation pathway. For example, the *L. pneumophila*-containing vacuole (LCV) recruits polyubiquitinated proteins by virtue of the actions of translocated bacterial effector proteins (51, 106, 154). *S.* Typhimurium manipulates the ubiquitin pathway to ensure proper trafficking of its effector, SopB to the SCV (104, 151). Given that *A. phagocytophilum* hijacks an array of intracellular trafficking pathways, we set out to test the hypothesis that the ApV co-opts ubiquitin. In this chapter, we demonstrate that ubiquitinated proteins accumulate on the AVM during infection of mammalian myeloid and endothelial cells and, to a lesser extent, tick cells. The AVM becomes ubiquitinated early following entry of HL-60 cells and continues to do so throughout infection. Notably, the AVM is decorated by mono-, not polyubiquitinated proteins in an *A. phagocytophilum* protein synthesis-dependent manner. Collectively, these data identify a novel means by which the AVM is remodeled during the course of infection and provide the first evidence of a Rickettsiales pathogen co-opting ubiquitin during intracellular residence. Monoubiquitinating the AVM is presumably part of the multifaceted approach by which *A. phagocytophilum* ensures its survival within eukaryotic host cells.

7.2 Results

7.2.1 Ubiquitinated proteins accumulate on the AVM.

To assess whether ubiquitinated proteins decorate the AVM, we screened *A. phagocytophilum* infected HL-60 cells with mAb FK2, which recognizes mono- and polyubiquitinated conjugates (61), in conjunction with antisera against APH_1387 or APH_0032, both of which are *A. phagocytophilum* effectors that are associated with the bacterial surface and localize to the AVM (86, 87). The cells were visualized by confocal microscopy. Anti-APH_1387 (**Figure 32B and H**) and anti-APH_0032 (**Figure 32E**) detected *A. phagocytophilum* organisms within the ApV and the target antigens on the AVM. FK2 staining exhibited punctate distribution throughout infected and uninfected control cells (**Figure 32A, D and J**). FK2 also yielded intense ring-like staining patterns that surrounded intravacuolar *A. phagocytophilum* bacteria and colocalized with APH_1387 or APH_0032 signal on the AVM (**Figure 32C and F**). FK2 labeled the AVMs of 51.0 $\pm$ 2.0% ApVs in infected HL-60 cells (**Figure 33G**).

In addition to human promyelocytic HL-60 cells, *A. phagocytophilum* also infects and resides in ApVs in the monkey choroidal endothelial cell line RF/6A and the *I. scapularis* embryonic cell line ISE6 (82, 132, 133). To determine if the AVM is ubiquitinated in each of these cell lines, *A. phagocytophilum* infected RF/6A and ISE6 cells were screened with FK2 in conjunction with antibody against Msp2 (P44), which is the most abundant *A. phagocytophilum* surface protein (163), and examined by confocal microscopy. Comparable to observations of infected HL-60 cells, 61.0 $\pm$ 6.2% AVMs in RF/6A cells were FK2-positive (**Figure 33A-C and G**). Notably fewer AVMs exhibited detectable ubiquitination in ISE6 cells, as only 13.8 $\pm$ 0.4% were FK2-positive (**Figure 33D-G**).

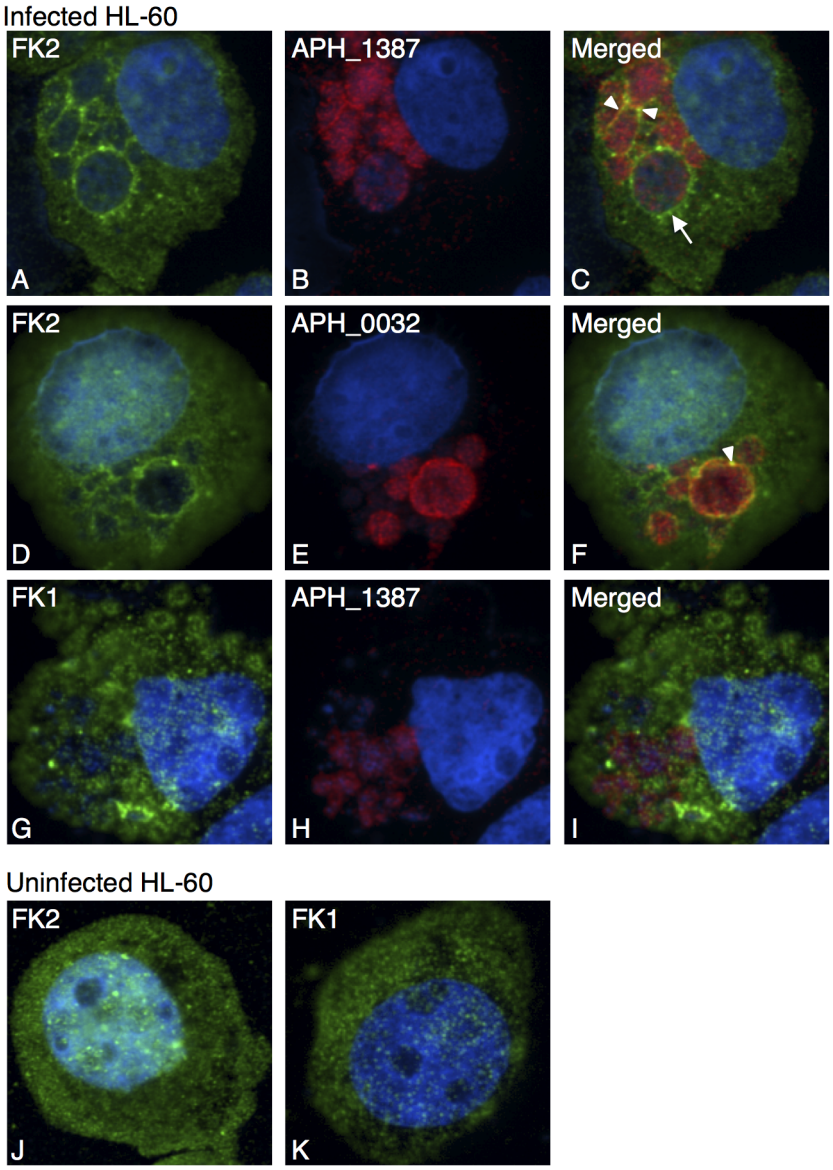

Figure 32. Monoubiquitinated proteins decorate the AVM in HL-60 cells.
A. phagocytophilum infected (**A–I**) or uninfected (**J–K**) HL-60 cells were fixed, screened with mAb FK2 (**A, D,** and **J**), which recognizes poly- and monoubiquitinated proteins, or mAb FK1 (**G** and **K**), which recognizes only polyubiquitinated conjugates, in conjunction with antisera against *A. phagocytophilum*-derived APH_1387 (**B** and **H**) or APH_0032 (**E**), both of which present at the bacterial surface and on the AVM. Merged fluorescent images are shown in panels **C, F,** and **I**. DAPI stained host and bacterial nuclei are blue and are present in all panels. In panel **C**, an arrow denotes intense FK2 staining that surrounds intravacuolar *A. phagocytophilum* organisms. In panels **C** and **F**, arrowheads denote examples of colocalization of FK2 and APH_1387 (**C**) or APH_0032 (**F**) signals at the AVM. Images are representative of at least three separate experiments.

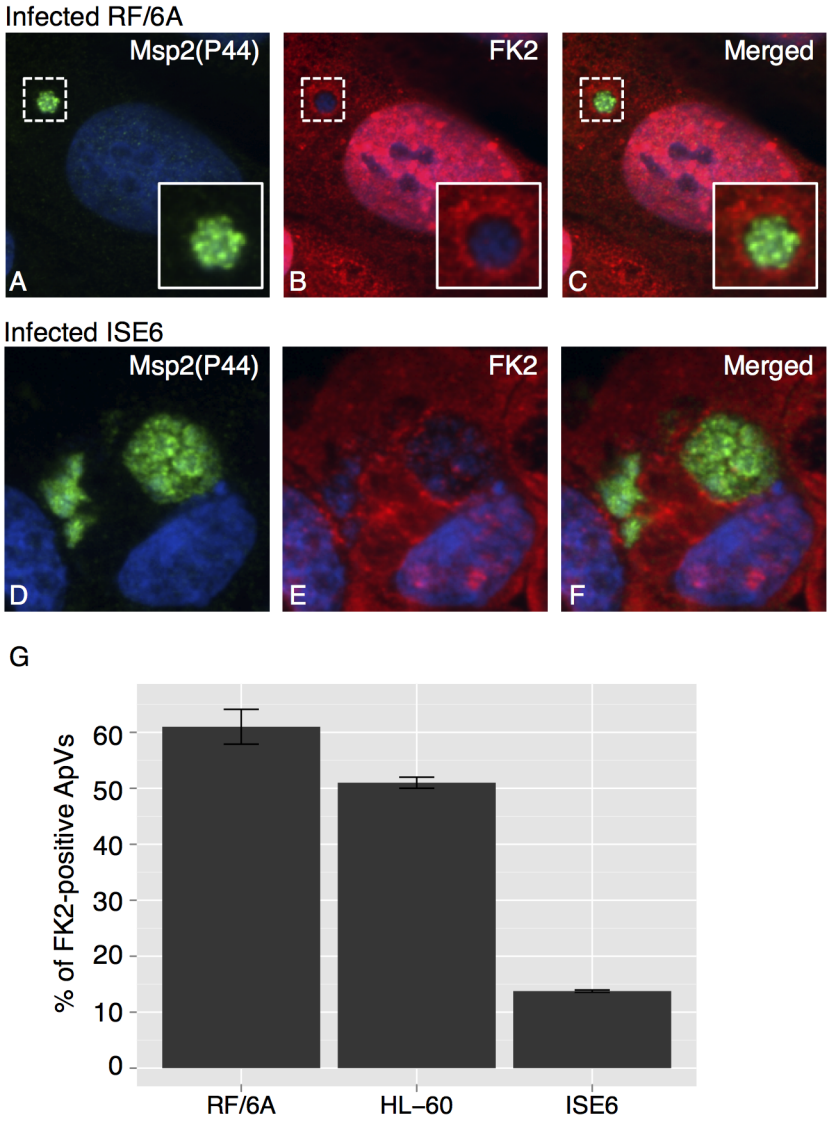

Figure 33. Ubiquitinated proteins localize to the AVM in infected host cells.
(**A–F**) *A. phagocytophilum* infected RF/6A (**A–C**) or ISE6 cells (**D–F**) were fixed and viewed by confocal microscopy to determine immunoreactivity with antibodies against Msp2 (P44) (**A** and **D**) and FK2 (**B** and **E**). Merged fluorescent images are shown in panels **C** and **F**. The insets demarcated by a solid box in the lower right corners of panels **A, B,** and **C** are magnified versions of the regions in the respective panels denoted by hatched boxes, each of which demarcate an AVM that is intensely labeled with FK2 and that surrounds Msp2 (P44)-positive bacteria. DAPI stained host and bacterial nuclei are blue and are present in all panels. (**G**) Percentages of FK2-positive ApVs [based on the presence of Msp2 (P44)-positive *A. phagocytophilum* bacteria] in infected HL-60, RF/6A, and ISE6 cells. Results are the means (±SD) for two or three separate experiments in which a minimum of 700 bacterial inclusions was examined.

7.2.2 The AVM accumulates ubiquitinated proteins over the course of *A. phagocytophilum* infection in HL-60 cells.

After binding to the HL-60 cell surface, most *A. phagocytophilum* organisms enter to reside in ApVs within 4 h (20, 28, 96), after which they replicate by binary fission for approximately 24 h and subsequently exit the host cell (199). Reinfection occurs between 24 and 36 h following a synchronous infection (199). To assess the temporal association of ubiquitinated conjugates with the AVM over the course of infection, *A. phagocytophilum* organisms were added to HL-60 cells and allowed to bind for 40 min followed by the removal of unbound bacteria. At various post infection time points over a 48 h period, aliquots were screened with FK2 and anti-Msp2 (P44) and examined by confocal microscopy (**Figure 34**). At 4 and 6 h, a time period during which nascent ApVs form, ubiquitin association with 22.1 $\pm$ 0.8% and 27.1 $\pm$ 0.4% AVMs was detected as aggregative and/or punctate staining patterns surrounding intravacuolar *A. phagocytophilum* organisms (**Figure 34A-F** and **Figure 35**). AVM ubiquitination consistently increased over the next 12 h, as 35.2 $\pm$ 6.7%, 41.3 $\pm$ 5.7%, and 52.6 $\pm$ 4.2% exhibited FK2 staining at 8, 12, and 18 h (**Figure 35**). The aggregative FK2 staining pattern on most of the AVMs continually increased over infection (**Figure 34**). By and after 12 h, many AVMs were decorated such that a ring-like staining pattern surrounding the bacteria resulted (**Figure 34J-d**). By 24 h, AVM ubiquitination began to decline, as 46.2 $\pm$ 5.0% and 38.9 $\pm$ 10.1% of AVMs were FK2 positive at 24 and 30 h (**Figure 35**). Beginning at 36 h, the percentages of ubiquitinated AVMs began to increase once again. At 30 and 36 h, in addition to large ApVs full of *A. phagocytophilum* bacteria, many HL-60 cells also harbored small ApVs that contained one to a few organisms (**Figure 34S-X**). The small ApVs exhibited punctate FK2 staining reminiscent of the staining patterns observed at 4 and 6 h (**Figure 34A-F**), thereby indicating that reinfection had occurred between 24 h and 36 h and that the infection had become asynchronous.

Figure 34. Ubiquitinated proteins are detectable on the AVM following *A. phagocytophilum* entry into nascent vacuoles and continue to accumulate on the AVM throughout infection.

HL-60 cells were synchronously infected with *A. phagocytophilum*. At 4 h (**A-C**), 6 h (**D-F**), 8 h (**G-I**), 12 h (**J-L**), 18 h (**M-O**), 24 h (**P-R**), 30 h (**S-U**), 36 h (**V-X**), 42 h (**Y-a**) and 48 h (**b-d**) post infection, the cells were stained with antibodies against Msp2 (P44) (**A, D, G, J, M, P, S, V, Y,** and **b**) and FK2 (**B, E, H, K, N, Q, T, W, Z,** and **c**) and viewed by confocal microscopy. Merged fluorescent images are presented in panels **C, F, I, L, O, R, U, X, a** and **d**. DAPI stained host and bacterial nuclei are blue and are present in all panels. In panels **C** and **F**, arrows indicate portions of AVMs that exhibit intense punctate and/or ring-like FK2 staining surrounding intravacuolar *A. phagocytophilum* bacteria. The images are representative of results from three separate experiments.

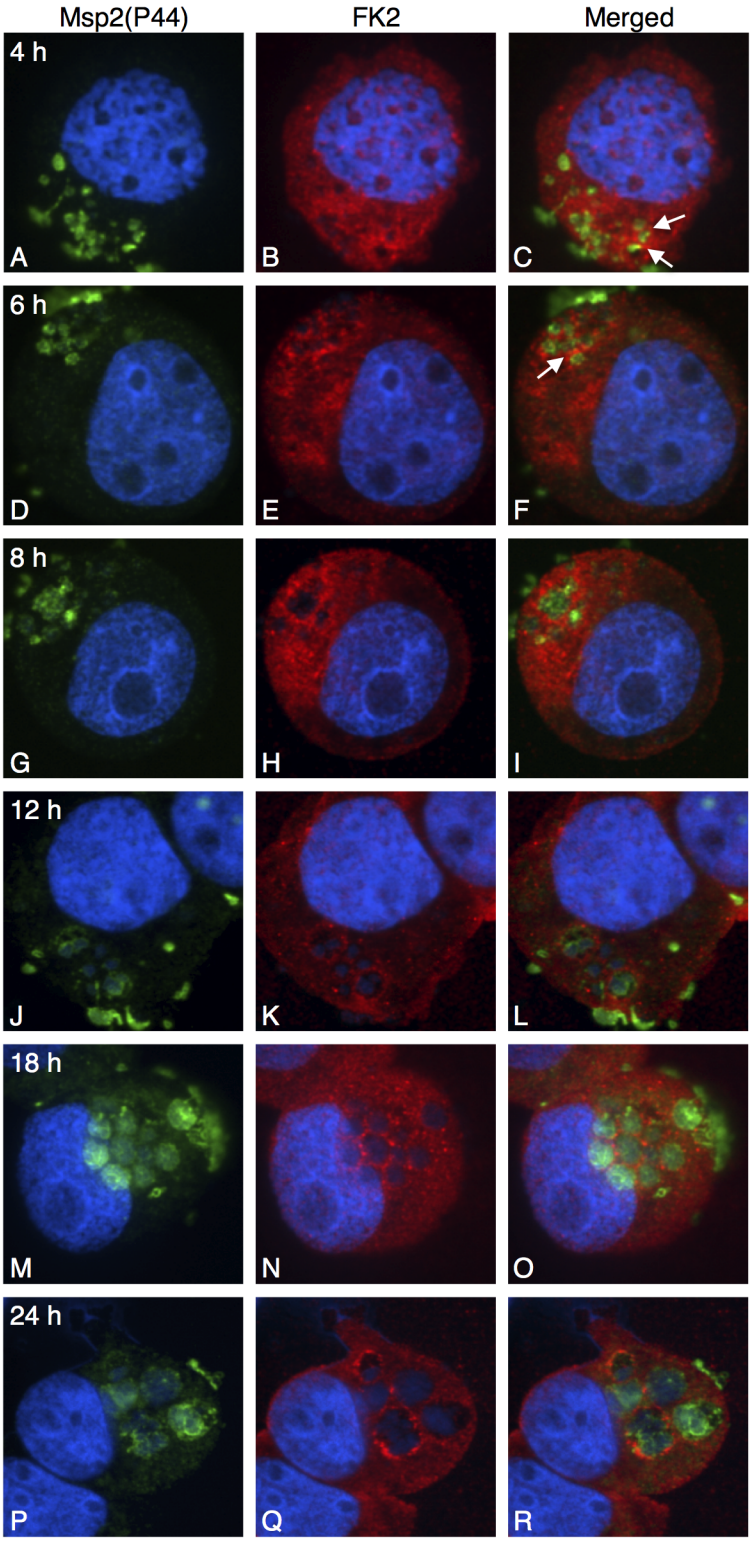

Figure 34

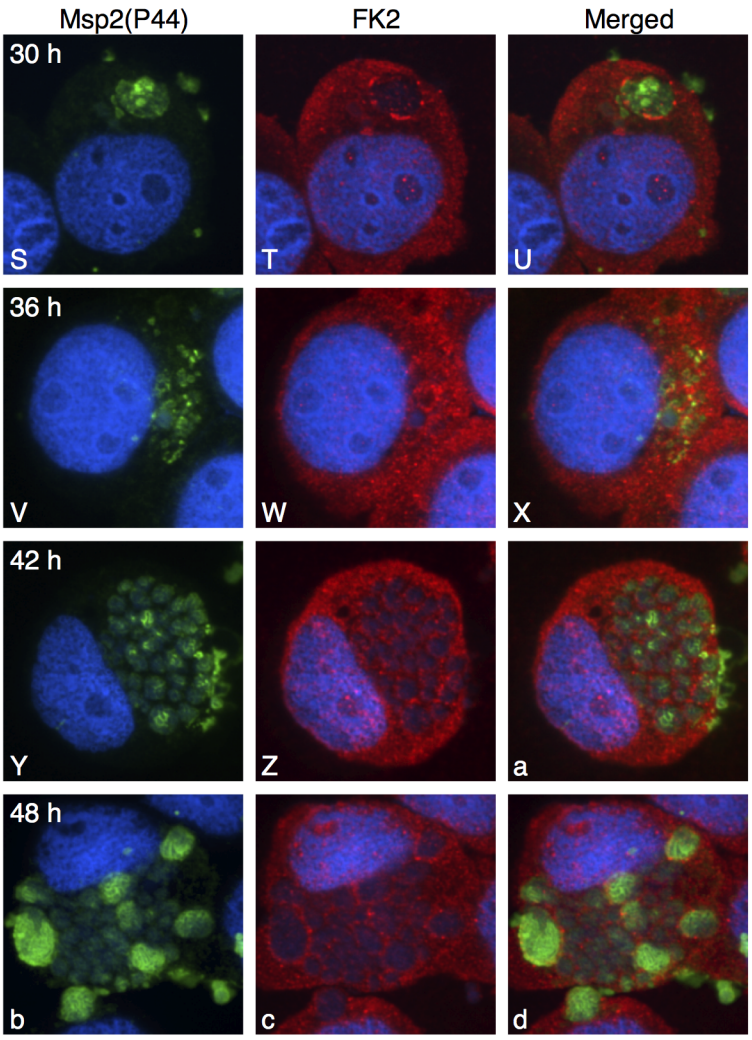

Figure 34

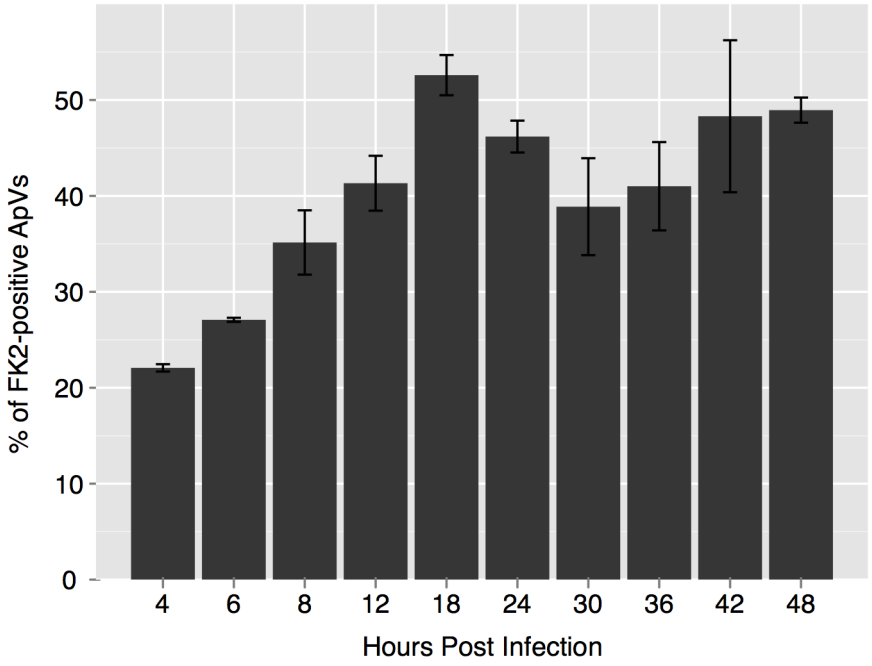

Figure 35. Percentages of AVMs exhibiting ubiquitinated protein association over the course of *A. phagocytophilum* infection of HL-60 cells.
ApVs, as demarcated by anti-Msp2 (P44) staining of intravacuolar bacteria, were scored for FK2 staining of the AVM. The number of FK2-positive ApVs was divided by the total number of ApVs, which was multiplied by 100 to determine the percentage of FK2-positive ApVs. Data are the mean percentages (±SD) of ApVs exhibiting FK2 staining and are derived from three separate experiments. A minimum of 600 ApVs was examined per time point per experiment.

7.2.3 The AVM is monoubiquitinated.

Because mono- and polyubiquitination differentially dictate the subcellular trafficking of downstream processes in which protein substrates participate (36, 50, 156), we next determined whether mono- or polyubiquitinated proteins accumulate on the AVM. Accordingly, we stained *A. phagocytophilum* infected HL-60 cells with mAb FK1, which detects only polyubiquitinated proteins and does not detect monoubiquitinated substrates or free ubiquitin (61) in conjunction with anti-APH_1387 and examined the cells using confocal microscopy. By comparing the staining patterns obtained with FK1 and FK2, we can infer whether the AVM is mono- or polyubiquitinated (41, 80, 93). AVM staining by both FK2 and FK1 would indicate that the AVM is polyubiquitinated or poly- and monoubiquitinated, whereas staining with FK2 but not FK1 would suggest that the AVM is only monoubiquitinated. FK1 staining yielded punctate patterns throughout infected and uninfected control cells (**Figure 32G and K**) similar to those obtained using FK2 (**Figure 32A, D and J**). However, in contrast to that observed for FK2, neither an intense ring-like nor an aggregate FK1 staining pattern surrounding APH_1387- or APH_0032-positive *A. phagocytophilum* organisms was observed (**Figure 32I** and data not shown). Moreover, FK1 staining did not colocalize with AVM-associated APH_1387 or APH_0032 signal. Similar results were obtained for *A. phagocytophilum* infected RF/6A cells (data not shown).

7.2.4 *de novo* bacterial protein synthesis is important for continued association of ubiquitinated proteins at the AVM.

Because tetracycline treatment of *A. phagocytophilum* infected host cells results in dissociation of Rab GTPases from the AVM and delivery of the bacterium to lysosomes (70, 85), we rationalized that bacterial protein synthesis is critical for the AVM to accumulate ubiquitinated conjugates. To test our hypothesis, we treated *A. phagocytophilum* infected HL-60

cells with tetracycline or vehicle control for 1 h. The cells were screened with anti-Msp2 (P44) and FK2 and analyzed by confocal microscopy. Whereas 39.9 $\pm$ 9.4% of AVMs in control cells were FK2-positive, tetracycline treated cells exhibited a significant reduction in ubiquitination, as only 16.0 $\pm$ 3.7% of AVMs were stained with FK2 (**Figure 36**). This effect was reversible, as removed of the antibiotic restored AVM ubiquitination by 4 h. Thus, *de novo* bacterial protein synthesis is requisite for maintaining the association of ubiquitinated proteins with the AVM.

7.3 Discussion

These data demonstrate that *A. phagocytophilum* co-opts monoubiquitin conjugation machinery in a bacterial protein synthesis-dependent manner. Monoubiquitination of the AVM is important early during *A. phagocytophilum* development, as monoubiquitinated proteins rapidly associate with the ApV upon bacterial entry to produce a sparse punctate distribution pattern on the membranes of nascent ApVs. Monoubiquitination of the AVM is coincident with bacterial replication, as monoubiquitinated proteins continually accumulate on the AVM until 24 h, a time point at which we have documented that *A. phagocytophilum* begins to transition from the replicative and metabolically active RC form to the infectious DC cell form (199). Beginning at 24 h, the percentages of ubiquitin-positive AVMs declines until the second round of infection is initiated. Overall, our results hint at the importance of monoubiquitination of AVM associated proteins throughout the *A. phagocytophilum* infection cycle in promyelocytic HL-60 cells as well as endothelial cells, since a comparable degree of ubiquitination of the AVM was observed for infected RF/6A cells. Considerably fewer ApVs of infected ISE6 cells exhibited ubiquitination than infected mammalian cells. Either AVM ubiquitination does not play a prominent role in *A. phagocytophilum* infection of ISE6 cells or association of ubiquitinated proteins with the AVM may be temporally

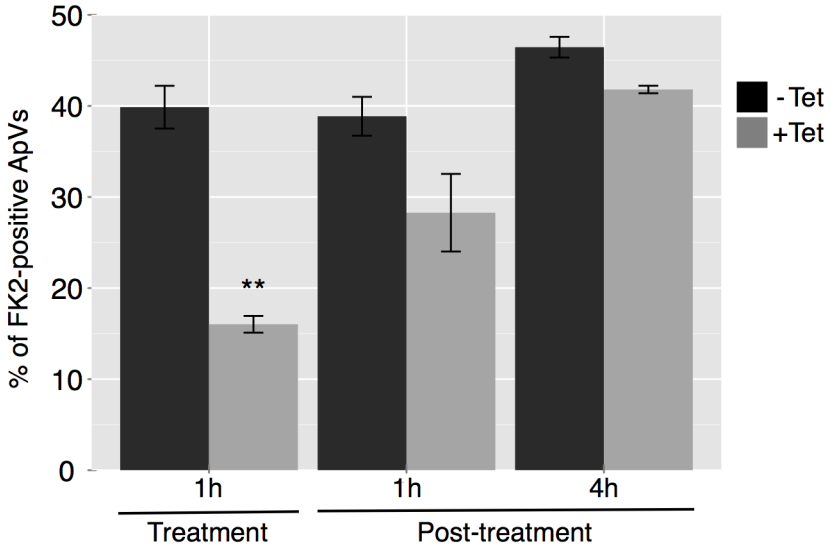

Figure 36. Ubiquitin association with the AVM is dependent on bacterial protein synthesis.

An *A. phagocytophilum* infected HL-60 cell culture was split into two cultures, one of which was incubated with tetracycline (+Tet) and the other was incubated with vehicle control (ethanol; -Tet) for 1 h (Treatment). Drug- and control-treated cells were washed with PBS and returned to cultivation conditions for 1 or 4 h (Post-treatment). At the indicated time point, the cells were fixed, screened with FK2 and anti-Msp2 (P44), and examined by confocal microscopy. ApVs were scored as being FK2-positive if an intense ring-like FK2 staining pattern was observed surrounding Msp2 (P44)-positive *A. phagocytophilum* organisms. Results are the mean ($\pm$SD) of at least two experiments in which at least 1,000 ApVs were examined per condition. Statistically significant (**P<0.01) values are indicated.

regulated during infection of ISE6 cells.

By accruing monoubiquitinated proteins that localize and direct traffic to endocytic compartments, *A. phagocytophilum* conceivably camouflages its vacuolar membrane as a means for avoiding lysosomal targeting. Support for this possibility comes from the precedent that the ApV selectively recruits Rab GTPases that are predominantly associated with recycling endosomes while concomitantly blocking recruitment of Rabs that are important for lysosomal delivery. Tetracycline treatment of infected cells culminates in the dissociation of recycling endosome-associated Rabs with the concomitant association of the lysosomal markers Rab7 and LAMP-1 (85). Confocal microscopic analysis of fixed cells reveals that no more than 52.6 $\pm$ 4.2% or 61.0 $\pm$ 6.2% ApVs in HL-60 cells or RF/6A cells, respectively, are positive for ubiquitin at any time point examined. A highly similar trend occurs when one examines the percentages of ApVs to which GFP-tagged recycling endosome-associated Rab GTPases localize (85). Ubiquitin machinery, like Rab GTPases, dynamically cycles on and off target organelle membranes (74, 177). Thus, examining fixed *A. phagocytophilum* infected cells provides a snapshot of the AVMs that are monoubiquitinated or have associated Rab GTPases at the instant at which preservative was added.

Several bacterial effectors have been shown to exploit the host cell's ubiquitination system to diversify or regulate their biological functions. Several effectors secreted by intracellular bacterial pathogens mimic the activities of E3 ubiquitin ligases to spatially or temporally regulate host or bacterial proteins (105, 106). Alternatively, the ubiquitination of other bacterial effectors regulates their activities and subcellular localization rather than serve as a signal for their proteasomal degradation (104, 122, 151). As AVM monoubiquitination is bacterial protein synthesis-dependent, it is plausible that *A. phagocytophilum* encodes one or more effectors that either may recruit monoubiquitinated host proteins to the AVM or

may be monoubiquitinated themselves.

To date, only three *A. phagocytophilum*-encoded AVM proteins – APH_1387, APH_0032 and AptA – have been identified (86, 87, 192). Whether any of these proteins are involved in recruiting ubiquitinated proteins to the AVM or are ubiquitinated themselves remains to be determined. *A. phagocytophilum* may encodes effectors that mimic the activities of endogenous ubiquitin enzymes. A challenge to elucidating whether *A. phagocytophilum* proteins are involved in monoubiquitinating the AVM is that, while some bacterial effectors share primary amino acid sequence similarity with their eukaryotic counterparts, many have evolved to functionally mimic the biochemical activities of eukaryotic proteins without obvious sequence or structural homology. For instance, members of a family of type III secretion system effector proteins functionally mimic eukaryotic HECT E3 ligase activity, but lack structural similarity to known eukaryotic or bacterial E3 ligases (181, 220).

Rickettsia conorii internalization into host cells correlates with host cell-mediated ubiquitination of the rickettsial receptor, Ku70 (125). This chapter marks the first example of a Rickettsiales member that co-opts ubiquitin during its residence within host cells. Thus, rickettsial pathogens diversely exploit ubiquitin machinery to promote infection and presumably to facilitate intracellular survival. This chapter also adds to the growing body of evidence that intercepting ubiquitination pathways is a common theme among vacuole-adapted bacterial pathogens.

Conclusions

A distinguishing feature of *A. phagocytophilum* is its unusual capacity to establish a protective niche in the hostile environment of the neutrophil. It replicates within a host cell derived vacuole that successfully avoids fusion with lysosomes and subverts antimicrobial defenses. Because *A. phagocytophilum* protein synthesis is requisite for the establishment of a protective niche, we focused on the characterization of host and bacterial factors that localize to the AVM. Based on previous work and the work presented here, it is clear that *A. phagocytophilum* has evolved the ability to exploit a broad repertoire of host processes and pathways to facilitate its survival (**Figure 37**).

Given the role of Rab GTPases in directing vesicular trafficking, it is not surprising that *A. phagocytophilum* selectively recruits a subset of Rabs to its vacuolar membrane. GFP-Rab4A, GFP-Rab10, GFP-Rab11A, GFP-Rab14, RFP-Rab22A and GFP-Rab35, which mediates endocytic recycling, and GFP-Rab1, which regulates endoplasmic reticulum to Golgi trafficking, localize to the ApV. Fluorescently tagged Rabs are recruited to the ApV upon its formation and remain associated throughout infection. Tetracycline treatment concomitantly promotes loss of recycling endosome-associated GFP-Rabs and acquisition of GFP-Rab5, GFP-Rab7, and the lysosomal marker, LAMP-1 (**Figure 37**). Thus, the selective recruitment of Rab GTPases and the altered fusogenicity of the ApV are dependent upon *A. phagocytophilum* encoded proteins. In addition, GFP-Rab10 associates with the ApV in a guanine nucleotide independent manner. This strongly suggests that *A. phagocytophilum* encode proteins that can regulate Rab10 cycling. This work highlights

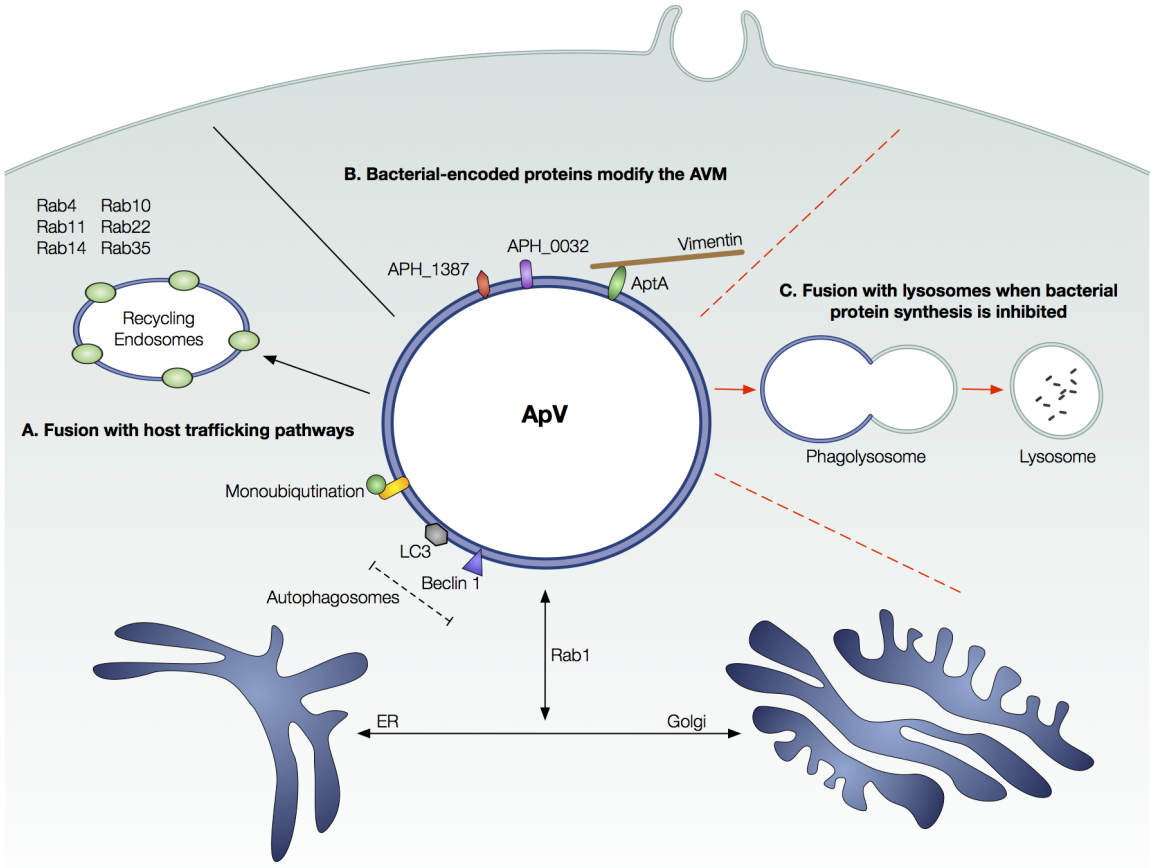

Figure 37. The *A. phagocytophilum*-occupied vacuole interacts with a broad repertoire of host pathways to facilitate its intracellular survival strategy in host cells. (**A**) The ApV associates with multiple eukaryotic pathways. During *A. phagocytophilum* inclusion biogenesis it acquires markers for: recycling endosomes (accumulates Rab GTPases that are associated with the endocytic recycline pathway), autophagosomes (LC3 and Beclin 1), and monoubiquitin pathways (accumulates monoubiquitinated proteins to the AVM). (**B**) The altered fusogenicity of the ApV is presumably due to the active modification of the vacuolar membrane by bacterial encoded proteins. To date, 3 *A. phagocytophilum* proteins have been identified: APH_1387, APH_0032 and AptA. Others have determined that AptA interacts with host vimentin, likely as a means to modulate interactions with host cytoskeleton components and maintain structural stability. (**C**) Upon inhibition of bacterial protein synthesis, the ApV no longer accumulates recycling endosome associated Rab GTPases or monoubiquitinated proteins, but instead matures along the normal endosomal pathway and fuses with lysosomes.

a key strategy by which *A. phagocytophilum* facilitates its survival within myeloid host cells. It actively controls the biogenesis of the vacuole in which it resides by selectively hijacking Rab GTPases that predominantly associate with recycling endosomes. In doing so, the ApV effectively disguises itself as a recycling endosome, which is requisite for avoiding endosomal maturation and lysosomal fusion. This strategy also likely contributes to the bacterium's acquisition of host membrane material, amino acids and cholesterol, each of which is important for bacterial growth and/or cell wall stability.

Another host pathway *A. phagocytophilum* exploits is the ubiquitin machinery. A theme emerging among vacuole-adapted bacterial pathogens is their ability to hijack the ubiquitin machinery to manipulate host processes and diversify the function of their effectors. Ubiquitination is an attractive target for pathogenic bacteria because it regulates many pathways in eukaryotic cells. Mono- and polyubiquitination differentially dictate the subcellular localization, activity, and fate of protein substrates. Monoubiquitination directs membrane traffic from the plasma membrane to the endosome and has been shown to promote autophagy. Work presented in this dissertation show that monoubiquitinated proteins are present on the AVM upon its formation and continue to accumulate throughout infection. Monoubiquitinated proteins decorate the AVM during infection of promyelocytic HL-60 cells, endothelial RF/6A cells, and to a lesser extent, embryonic tick ISE6 cells. Although it is unclear whether the ubiquitinated conjugates on the AVM are host or bacterial proteins, we speculate that ubiquitination is important for the ApV's altered fusogenicity (**Figure 37A**). Support for this premise is the loss of ubiquitinated proteins on the AVM upon tetracycline treatment. An intriguing alternative is that *A. phagocytophilum* may exploit the ubiquitin machinery to regulate the localization of it's secreted effectors. This phenomena has been reported for the *S.* Typhimurium effector, SopB, that utilizes host ubiquitin to traffic to different cellular compartments and diversify it's function (151). Association of SopB with the SCV is dependent on it being ubiquitinated when it is tethered to the plasma membrane (151). Therefore

it is possible that following secretion, APH_1387 or APH_0032 is ubiquitinated as a means to target it to the AVM. Studies to define the bacterial effectors and/or host proteins involved will be important for understanding the role of monoubiquitination to *A. phagocytophilum* survival. These results identify a novel mechanism by which *A. phagocytophilum* modifies its vacuolar membrane and present the first example of a Rickettsiales pathogen co-opting ubiquitin during intracellular survival.

PVs are composed of host-derived membranes that are modified by pathogen-encoded proteins and lipids. As a result, PVs become unique compartments that exhibit an altered fusogenicity. Therefore, we reasoned that bacterial-derived AVM proteins are central to the pathogenesis of *A. phagocytophilum* . We identified the first two *A. phagocytophilum*-derived proteins that associate with the AVM, APH_1387 and APH_0032 (**Figure 37B**). The study of these proteins is complicated by both their lack of sequence identity with proteins in the sequence databases and the absence of a system for targeted gene deletion. However, APH_1387 and APH_0032 exhibit differential expression patterns, which suggests that they have distinct pathobiological roles. Upon *A. phagocytophilum* entry into the host cell, APH_1387 is expressed early and associates with greater than 90% of ApVs by 12 h post infection. In contrast, APH_0032 is not expressed in high abundance until 24 h, at which time only about 60% of ApVs are APH_0032 positive. APH_1387 and APH_0032 are present on the cytoplasmic face of the AVM and competitively inhibit ApV development when ectopically expressed in host cells. Although we have not identified the corresponding host factors, the results presented in this dissertation strongly suggest that APH_1387 and APH_0032 mediate interactions with the host cell that are important for ApV survival.

The work here highlights the repertoire of bacterial adaptations that have evolved to hijack host pathways and secure the pathogen's survival. Further, it emphasizes the AVM as a crucial interface for deciphering host-pathogen interactions. Despite the progress made in characterizing Rab GTPases that are selectively recruited to the ApV and identifying two

bacterial encoded AVM proteins, many important questions remain unanswered. Current efforts are underway to identify *A. phagocytophilum*-encoded ligands that interact with the ApV associating Rab GTPases, specifically the bacterial protein(s) that regulate Rab10 cycling on the AVM. Further dissection of the mechanism of selective recruitment of Rab GTPases to the ApV will continue to enhance our understanding of how this unique pathogen survives within the primary effector cell of microbial killing. Of equal importance will be the identification of host proteins that interact with APH_1387 and APH_0032.

Bibliography

[1] E. W. Ades, F. J. Candal, R. A. Swerlick, V. G. George, S. Summers, D. C. Bosse, and T. J. Lawley. Hmec-1: establishment of an immortalized human microvascular endothelial cell line. *J Invest Dermatol*, 99(6):683–90, 1992. 18

[2] M. E. Aguero-Rosenfeld, L. Donnarumma, L. Zentmaier, J. Jacob, M. Frey, R. Noto, C. A. Carbonaro, and G. P. Wormser. Seroprevalence of antibodies that react with anaplasma phagocytophila, the agent of human granulocytic ehrlichiosis, in different populations in westchester county, new york. *Journal of clinical microbiology*, 40(7):2612–5, 2002. 5

[3] C. Akgul, D. A. Moulding, and S. W. Edwards. Molecular control of neutrophil apoptosis. *FEBS letters*, 487(3):318–22, 2001. 12

[4] M. Akkoyunlu and E. Fikrig. Gamma interferon dominates the murine cytokine response to the agent of human granulocytic ehrlichiosis and helps to control the degree of early rickettsemia. *Infection and immunity*, 68(4):1827–33, 2000. 13, 14

[5] M. Akkoyunlu, S. E. Malawista, J. Anguita, and E. Fikrig. Exploitation of interleukin-8-induced neutrophil chemotaxis by the agent of human granulocytic ehrlichiosis. *Infection and immunity*, 69(9):5577–88, 2001. 14

[6] P. D. Allaire, A. L. Marat, C. Dall'Armi, G. Di Paolo, P. S. McPherson, and B. Ritter. The connecdenn denn domain: a gef for rab35 mediating cargo-specific exit from early endosomes. *Molecular cell*, 37(3):370–82, 2010. 40, 64

[7] C. E. Alvarez-Martinez and P. J. Christie. Biological diversity of prokaryotic type iv secretion systems. *Microbiol Mol Biol Rev*, 73(4):775–808, 2009. 122

[8] S. Amigorena, J. R. Drake, P. Webster, and I. Mellman. Transient accumulation of new class ii mhc molecules in a novel endocytic compartment in b lymphocytes. *Nature*, 369(6476):113–20, 1994. 16, 60

[9] J. F. Anderson. The natural history of ticks. *The Medical clinics of North America*, 86(2):205–18, 2002. 2

[10] S. G. Andersson, A. Zomorodipour, J. O. Andersson, T. Sicheritz-Ponten, U. C. Alsmark, R. M. Podowski, A. K. Naslund, A. S. Eriksson, H. H. Winkler, and

C. G. Kurland. The genome sequence of rickettsia prowazekii and the origin of mitochondria. *Nature*, 396(6707):133–40, 1998. 6

[11] J. S. Bakken, J. S. Dumler, S. M. Chen, M. R. Eckman, L. L. Van Etta, and D. H. Walker. Human granulocytic ehrlichiosis in the upper midwest united states. a new species emerging? *JAMA : the journal of the American Medical Association*, 272(3):212–8, 1994. 5

[12] J. S. Bakken and S. Dumler. Human granulocytic anaplasmosis. *Infectious disease clinics of North America*, 22(3):433–48, viii, 2008. 2, 5, 6

[13] J. S. Bakken, P. Goellner, M. Van Etten, D. Z. Boyle, O. L. Swonger, S. Mattson, J. Krueth, R. L. Tilden, K. Asanovich, J. Walls, and J. S. Dumler. Seroprevalence of human granulocytic ehrlichiosis among permanent residents of northwestern wisconsin. *Clinical infectious diseases : an official publication of the Infectious Diseases Society of America*, 27(6):1491–6, 1998. 2, 5, 13

[14] J. P. Bannantine, R. S. Griffiths, W. Viratyosin, W. J. Brown, and D. D. Rockey. A secondary structure motif predictive of protein localization to the chlamydial inclusion membrane. *Cell Microbiol*, 2(1):35–47, 2000. 68, 86, 124

[15] J. P. Bannantine, W. E. Stamm, R. J. Suchland, and D. D. Rockey. Chlamydia trachomatis inca is localized to the inclusion membrane and is recognized by antisera from infected humans and primates. *Infection and immunity*, 66(12):6017–21, 1998. 68, 86, 122

[16] A. F. Barbet, P. F. Meeus, M. Belanger, M. V. Bowie, J. Yi, A. M. Lundgren, A. R. Alleman, S. J. Wong, F. K. Chu, U. G. Munderloh, and S. D. Jauron. Expression of multiple outer membrane protein sequence variants from a single genomic locus of anaplasma phagocytophilum. *Infection and immunity*, 71(4):1706–18, 2003. 7

[17] J. P. Bardill, J. L. Miller, and J. P. Vogel. Icms-dependent translocation of sdea into macrophages by the legionella pneumophila type iv secretion system. *Molecular microbiology*, 56(1):90–103, 2005. 34

[18] P. A. Beare, D. Howe, D. C. Cockrell, A. Omsland, B. Hansen, and R. A. Heinzen. Characterization of a coxiella burnetii ftsz mutant generated by himar1 transposon mutagenesis. *Journal of bacteriology*, 191(5):1369–81, 2009. 9

[19] C. L. Birmingham, A. C. Smith, M. A. Bakowski, T. Yoshimori, and J. H. Brumell. Autophagy controls salmonella infection in response to damage to the salmonella-containing vacuole. *The Journal of biological chemistry*, 281(16):11374–83, 2006. 128

[20] D. L. Borjesson, S. D. Kobayashi, A. R. Whitney, J. M. Voyich, C. M. Argue, and F. R. Deleo. Insights into pathogen immune evasion mechanisms: Anaplasma phagocytophilum fails to induce an apoptosis differentiation program in human neutrophils. *J Immunol*, 174(10):6364–72, 2005. 10, 13, 46, 75, 93, 132

[21] K. A. Brayton, L. S. Kappmeyer, D. R. Herndon, M. J. Dark, D. L. Tibbals, G. H. Palmer, T. C. McGuire, and Jr. Knowles, D. P. Complete genome sequencing of anaplasma marginale reveals that the surface is skewed to two superfamilies of outer membrane proteins. *Proc Natl Acad Sci U S A*, 102(3):844–9, 2005. 68

[22] F. D. Brown, A. L. Rozelle, H. L. Yin, T. Balla, and J. G. Donaldson. Phosphatidylinositol 4,5-bisphosphate and arf6-regulated membrane traffic. *J Cell Biol*, 154(5):1007–17, 2001. 38

[23] M. D. Browning, J. W. Garyu, J. S. Dumler, and D. G. Scorpio. Role of reactive nitrogen species in development of hepatic injury in a c57bl/6 mouse model of human granulocytic anaplasmosis. *Comparative medicine*, 56(1):55–62, 2006. 13

[24] J. H. Brumell and M. A. Scidmore. Manipulation of rab gtpase function by intracellular bacterial pathogens. *Microbiol Mol Biol Rev*, 71(4):636–52, 2007. 37, 40, 61, 64

[25] W. Burgdorfer, A. G. Barbour, S. F. Hayes, J. L. Benach, E. Grunwaldt, and J. P. Davis. Lyme disease-a tick-borne spirochetosis? *Science*, 216(4552):1317–9, 1982. 2

[26] W. C. Cao, Q. M. Zhao, P. H. Zhang, J. S. Dumler, X. T. Zhang, L. Q. Fang, and H. Yang. Granulocytic ehrlichiae in ixodes persulcatus ticks from an area in china where lyme disease is endemic. *Journal of clinical microbiology*, 38(11):4208–10, 2000. 2

[27] A. Capmany and M. T. Damiani. Chlamydia trachomatis intercepts golgi-derived sphingolipids through a rab14-mediated transport required for bacterial development and replication. *PloS one*, 5(11):e14084, 2010. 62

[28] J. A. Carlyon, D. Abdel-Latif, M. Pypaert, P. Lacy, and E. Fikrig. Anaplasma phagocytophilum utilizes multiple host evasion mechanisms to thwart nadph oxidase-mediated killing during neutrophil infection. *Infect Immun*, 72(8):4772–83, 2004. 10, 12, 15, 28, 35, 46, 75, 93, 132

[29] J. A. Carlyon, M. Akkoyunlu, L. Xia, T. Yago, T. Wang, R. D. Cummings, R. P. McEver, and E. Fikrig. Murine neutrophils require alpha1,3-fucosylation but not psgl-1 for productive infection with anaplasma phagocytophilum. *Blood*, 102(9):3387–95, 2003. 10, 12

[30] J. A. Carlyon, W. T. Chan, J. Galan, D. Roos, and E. Fikrig. Repression of rac2 mrna expression by anaplasma phagocytophila is essential to the inhibition of superoxide production and bacterial proliferation. *J Immunol*, 169(12):7009–18, 2002. 32

[31] J. A. Carlyon, D. Ryan, K. Archer, and E. Fikrig. Effects of anaplasma phagocytophilum on host cell ferritin mrna and protein levels. *Infect Immun*, 73(11):7629–36, 2005. 12, 33, 78, 93, 99

[32] P. Caturegli, K. M. Asanovich, J. J. Walls, J. S. Bakken, J. E. Madigan, V. L. Popov, and J. S. Dumler. anka: an ehrlichia phagocytophila group gene encoding a cytoplasmic protein antigen with ankyrin repeats. *Infect Immun*, 68(9):5277–83, 2000. 8, 67

[33] CDC. Final 2010 reports of nationally notifiable infectious diseases. *Morbidity and Mortality Weekly Report*, 60(32):1088–1101, 2011. 5

[34] C. Checroun, T. D. Wehrly, E. R. Fischer, S. F. Hayes, and J. Celli. Autophagy-mediated reentry of francisella tularensis into the endocytic compartment after cytoplasmic replication. *Proceedings of the National Academy of Sciences of the United States of America*, 103(39):14578–83, 2006. 114

[35] S. M. Chen, J. S. Dumler, J. S. Bakken, and D. H. Walker. Identification of a granulocytotropic ehrlichia species as the etiologic agent of human disease. *J Clin Microbiol*, 32(3):589–95, 1994. 1, 2, 5

[36] Z. J. Chen and L. J. Sun. Nonproteolytic functions of ubiquitin in cell signaling. *Molecular cell*, 33(3):275–86, 2009. 127, 137

[37] M. J. Clague and S. Urbe. Ubiquitin: same molecule, different degradation pathways. *Cell*, 143(5):682–5, 2010. 128

[38] D. R. Clifton, K. A. Fields, S. S. Grieshaber, C. A. Dooley, E. R. Fischer, D. J. Mead, R. A. Carabeo, and T. Hackstadt. A chlamydial type iii translocated protein is tyrosine-phosphorylated at the site of entry and associated with recruitment of actin. *Proc Natl Acad Sci U S A*, 101(27):10166–71, 2004. 81

[39] M. S. Cohen. Molecular events in the activation of human neutrophils for microbial killing. *Clinical infectious diseases : an official publication of the Infectious Diseases Society of America*, 18 Suppl 2:S170–9, 1994. 12

[40] C. A. Collins and E. J. Brown. Cytosol as battleground: ubiquitin as a weapon for both host and pathogen. *Trends in cell biology*, 20(4):205–13, 2010. 127, 128

[41] C. A. Collins, A. De Maziere, S. van Dijk, F. Carlsson, J. Klumperman, and E. J. Brown. Atg5-independent sequestration of ubiquitinated mycobacteria. *PLoS pathogens*, 5(5):e1000430, 2009. 137

[42] C. Cortes, K. A. Rzomp, A. Tvinnereim, M. A. Scidmore, and B. Wizel. Chlamydia pneumoniae inclusion membrane protein cpn0585 interacts with multiple rab gtpases. *Infect Immun*, 75(12):5586–96, 2007. 40, 62, 65, 122, 124, 125

[43] F. S. Dahlgren, E. J. Mandel, J. W. Krebs, R. F. Massung, and J. H. McQuiston. Increasing incidence of ehrlichia chaffeensis and anaplasma phagocytophilum in the united states, 2000-2007. *The American journal of tropical medicine and hygiene*, 85(1):124–31, 2011. 5

[44] M. J. Dark, D. R. Herndon, L. S. Kappmeyer, M. P. Gonzales, E. Nordeen, G. H. Palmer, Jr. Knowles, D. P., and K. A. Brayton. Conservation in the face of diversity: multistrain analysis of an intracellular bacterium. *BMC Genomics*, 10:16, 2009. 68

[45] R. S. Davies, J. E. Madigan, E. Hodzic, D. L. Borjesson, and J. S. Dumler. Dexamethasone-induced cytokine changes associated with diminished disease severity in horses infected with anaplasma phagocytophilum. *Clinical and vaccine immunology : CVI*, 2011. 14

[46] M. F. de Jong, Y. H. Sun, A. B. den Hartigh, J. M. van Dijl, and R. M. Tsolis. Identification of vcea and vcec, two members of the vjbr regulon that are translocated into macrophages by the brucella type iv secretion system. *Molecular microbiology*, 70(6):1378–96, 2008. 106, 122

[47] J. de la Fuente, J. C. Garcia-Garcia, A. F. Barbet, E. F. Blouin, and K. M. Kocan. Adhesion of outer membrane proteins containing tandem repeats of anaplasma and ehrlichia species (rickettsiales: Anaplasmataceae) to tick cells. *Veterinary microbiology*, 98(3-4):313–22, 2004. 83, 86, 100

[48] P. Delepelaire. Type i secretion in gram-negative bacteria. *Biochimica et biophysica acta*, 1694(1-3):149–61, 2004. 123

[49] I. Derre and R. R. Isberg. Legionella pneumophila replication vacuole formation involves rapid recruitment of proteins of the early secretory system. *Infect Immun*, 72(5):3048–53, 2004. 40

[50] I. Dikic and V. Dotsch. Ubiquitin linkages make a difference. *Nature structural molecular biology*, 16(12):1209–10, 2009. 137

[51] M. S. Dorer, D. Kirton, J. S. Bader, and R. R. Isberg. Rna interference analysis of legionella in drosophila cells: exploitation of early secretory apparatus dynamics. *PLoS pathogens*, 2(4):e34, 2006. 128

[52] J. S. Dumler, N. C. Barat, C. E. Barat, and J. S. Bakken. Human granulocytic anaplasmosis and macrophage activation. *Clinical infectious diseases : an official publication of the Infectious Diseases Society of America*, 45(2):199–204, 2007. 13

[53] J. S. Dumler, A. F. Barbet, C. P. Bekker, G. A. Dasch, G. H. Palmer, S. C. Ray, Y. Rikihisa, and F. R. Rurangirwa. Reorganization of genera in the families rickettsiaceae and anaplasmataceae in the order rickettsiales: unification of some species of ehrlichia with anaplasma, cowdria with ehrlichia and ehrlichia with neorickettsia, descriptions of six new species combinations and designation of ehrlichia equi and 'hge agent' as subjective synonyms of ehrlichia phagocytophila. *International journal of systematic and evolutionary microbiology*, 51(Pt 6):2145–65, 2001. 1

[54] J. S. Dumler, K. S. Choi, J. C. Garcia-Garcia, N. S. Barat, D. G. Scorpio, J. W. Garyu, D. J. Grab, and J. S. Bakken. Human granulocytic anaplasmosis and anaplasma phagocytophilum. *Emerging infectious diseases*, 11(12):1828–34, 2005. 13

[55] J. S. Dumler, J. E. Madigan, N. Pusterla, and J. S. Bakken. Ehrlichioses in humans: epidemiology, clinical presentation, diagnosis, and treatment. *Clinical infectious diseases : an official publication of the Infectious Diseases Society of America*, 45 Suppl 1:S45–51, 2007. 5, 6

[56] J. S. Dumler, E. R. Trigiani, J. S. Bakken, M. E. Aguero-Rosenfeld, and G. P. Wormser. Serum cytokine responses during acute human granulocytic ehrlichiosis. *Clinical and diagnostic laboratory immunology*, 7(1):6–8, 2000. 13, 14

[57] J. C. Dunning Hotopp, M. Lin, R. Madupu, J. Crabtree, S. V. Angiuoli, J. A. Eisen, R. Seshadri, Q. Ren, M. Wu, T. R. Utterback, S. Smith, M. Lewis, H. Khouri, C. Zhang, H. Niu, Q. Lin, N. Ohashi, N. Zhi, W. Nelson, L. M. Brinkac, R. J. Dodson, M. J. Rosovitz, J. Sundaram, S. C. Daugherty, T. Davidsen, A. S. Durkin, M. Gwinn, D. H. Haft, J. D. Selengut, S. A. Sullivan, N. Zafar, L. Zhou, F. Benahmed, H. Forberger, R. Halpin, S. Mulligan, J. Robinson, O. White, Y. Rikihisa, and H. Tettelin. Comparative genomics of emerging human ehrlichiosis agents. *PLoS Genet*, 2(2):e21, 2006. 6, 7, 8, 58, 65, 68, 87

[58] C. A. Eyster, J. D. Higginson, R. Huebner, N. Porat-Shliom, R. Weigert, W. W. Wu, R. F. Shen, and J. G. Donaldson. Discovery of new cargo proteins that enter cells through clathrin-independent endocytosis. *Traffic*, 10(5):590–9, 2009. 38, 58

[59] S. Felek, 3rd Telford, S., R. C. Falco, and Y. Rikihisa. Sequence analysis of p44 homologs expressed by anaplasma phagocytophilum in infected ticks feeding on naive hosts and in mice infected by tick attachment. *Infection and immunity*, 72(2):659–66, 2004. 7

[60] R. F. Felsheim, M. J. Herron, C. M. Nelson, N. Y. Burkhardt, A. F. Barbet, T. J. Kurtti, and U. G. Munderloh. Transformation of anaplasma phagocytophilum. *BMC biotechnology*, 6:42, 2006. 9

[61] M. Fujimuro, H. Sawada, and H. Yokosawa. Production and characterization of monoclonal antibodies specific to multi-ubiquitin chains of polyubiquitinated proteins. *FEBS letters*, 349(2):173–80, 1994. 129, 137

[62] N. Fujita and T. Yoshimori. Ubiquitination-mediated autophagy against invading bacteria. *Current opinion in cell biology*, 23(4):492–7, 2011. 127

[63] J. E. Futse, K. A. Brayton, S. D. Nydam, and G. H. Palmer. Generation of antigenic variants via gene conversion: Evidence for recombination fitness selection at the locus level in anaplasma marginale. *Infect Immun*, 77(8):3181–7, 2009. 32, 81

[64] J. E. Galan. Common themes in the design and function of bacterial effectors. *Cell Host Microbe*, 5(6):571–9, 2009. 65

[65] J. C. Garcia-Garcia, N. C. Barat, S. J. Trembley, and J. S. Dumler. Epigenetic silencing of host cell defense genes enhances intracellular survival of the rickettsial pathogen anaplasma phagocytophilum. *PLoS Pathog*, 5(6):e1000488, 2009. 75

[66] J. C. Garcia-Garcia, K. E. Rennoll-Bankert, S. Pelly, A. M. Milstone, and J. S. Dumler. Silencing of host cell cybb gene expression by the nuclear effector anka of the intracellular pathogen anaplasma phagocytophilum. *Infection and immunity*, 77(6):2385–91, 2009. 8

[67] Y. Ge and Y. Rikihisa. Anaplasma phagocytophilum delays spontaneous human neutrophil apoptosis by modulation of multiple apoptotic pathways. *Cellular microbiology*, 8(9):1406–16, 2006. 12, 13

[68] Y. Ge, K. Yoshiie, F. Kuribayashi, M. Lin, and Y. Rikihisa. Anaplasma phagocytophilum inhibits human neutrophil apoptosis via upregulation of bfl-1, maintenance of mitochondrial membrane potential and prevention of caspase 3 activation. *Cellular microbiology*, 7(1):29–38, 2005. 12

[69] H. J. Geuze, W. Stoorvogel, G. J. Strous, J. W. Slot, J. E. Bleekemolen, and I. Mellman. Sorting of mannose 6-phosphate receptors and lysosomal membrane proteins in endocytic vesicles. *J Cell Biol*, 107(6 Pt 2):2491–501, 1988. 16

[70] H. I. Gokce, G. Ross, and Z. Woldehiwet. Inhibition of phagosome-lysosome fusion in ovine polymorphonuclear leucocytes by ehrlichia (cytoecetes) phagocytophila. *J Comp Pathol*, 120(4):369–81, 1999. 16, 55, 58, 137

[71] J. L. Goodman. *Human granylocytic anaplasmosis*, pages 218–238. ASM Press, Washington, DC, 2005. 72, 88

[72] J. L. Goodman, C. Nelson, B. Vitale, J. E. Madigan, J. S. Dumler, T. J. Kurtti, and U. G. Munderloh. Direct cultivation of the causative agent of human granulocytic ehrlichiosis. *The New England journal of medicine*, 334(4):209–15, 1996. 2, 9

[73] J. L. Goodman, C. M. Nelson, M. B. Klein, S. F. Hayes, and B. W. Weston. Leukocyte infection by the granulocytic ehrlichiosis agent is linked to expression of a selectin ligand. *The Journal of clinical investigation*, 103(3):407–12, 1999. 9

[74] C. Grabbe, K. Husnjak, and I. Dikic. The spatial and temporal organization of ubiquitin networks. *Nature reviews. Molecular cell biology*, 12(5):295–307, 2011. 140

[75] Jennifer L Granick, Dexter V Reneer, Jason A Carlyon, and Dori L Borjesson. Anaplasma phagocytophilum infects cells of the megakaryocytic lineage through sialylated ligands but fails to alter platelet production. *J Med Microbiol*, 57(Pt 4):416–23, Apr 2008. 2

[76] B. D. Grant and J. G. Donaldson. Pathways and mechanisms of endocytic recycling. *Nat Rev Mol Cell Biol*, 10(9):597–608, 2009. 38, 40, 45, 49, 59

[77] M. G. Gutierrez, D. B. Munafo, W. Beron, and M. I. Colombo. Rab7 is required for the normal progression of the autophagic pathway in mammalian cells. *J Cell Sci*, 117(Pt 13):2687–97, 2004. 40

[78] M. G. Gutierrez, C. L. Vazquez, D. B. Munafo, F. C. Zoppino, W. Beron, M. Rabinovitch, and M. I. Colombo. Autophagy induction favours the generation and maturation of the coxiella-replicative vacuoles. *Cell Microbiol*, 7(7):981–93, 2005. 40

[79] K. Haglund and I. Dikic. Ubiquitylation and cell signaling. *The EMBO journal*, 24(19):3353–9, 2005. 127

[80] K. Haglund, S. Sigismund, S. Polo, I. Szymkiewicz, P. P. Di Fiore, and I. Dikic. Multiple monoubiquitination of rtks is sufficient for their endocytosis and degradation. *Nature cell biology*, 5(5):461–6, 2003. 137

[81] W. D. Heo, T. Inoue, W. S. Park, M. L. Kim, B. O. Park, T. J. Wandless, and T. Meyer. Pi(3,4,5)p3 and pi(4,5)p2 lipids target proteins with polybasic clusters to the plasma membrane. *Science*, 314(5804):1458–61, 2006. 64

[82] M. J. Herron, M. E. Ericson, T. J. Kurtti, and U. G. Munderloh. The interactions of anaplasma phagocytophilum, endothelial cells, and human neutrophils. *Annals of the New York Academy of Sciences*, 1063:374–82, 2005. 2, 75, 129

[83] D. Heuer, A. Rejman Lipinski, N. Machuy, A. Karlas, A. Wehrens, F. Siedler, V. Brinkmann, and T. F. Meyer. Chlamydia causes fragmentation of the golgi compartment to ensure reproduction. *Nature*, 457(7230):731–5, 2009. 62

[84] L. Hicke and R. Dunn. Regulation of membrane protein transport by ubiquitin and ubiquitin-binding proteins. *Annual review of cell and developmental biology*, 19:141–72, 2003. 127, 128

[85] B. Huang, A. Hubber, J. A. McDonough, C. R. Roy, M. A. Scidmore, and J. A. Carlyon. The anaplasma phagocytophilum-occupied vacuole selectively recruits rab-gtpases that are predominantly associated with recycling endosomes. *Cell Microbiol*, 12(9):1292–307, 2010. 59, 137, 140

[86] B. Huang, M. J. Troese, D. Howe, S. Ye, J. T. Sims, R. A. Heinzen, D. L. Borjesson, and J. A. Carlyon. Anaplasma phagocytophilum aph_0032 is expressed late during infection and localizes to the pathogen-occupied vacuolar membrane. *Microb Pathog*, 49(5):273–84, 2010. 102, 106, 114, 122, 129, 141

[87] B. Huang, M. J. Troese, S. Ye, J. T. Sims, N. L. Galloway, D. L. Borjesson, and J. A. Carlyon. Anaplasma phagocytophilum aph_1387 is expressed throughout bacterial intracellular development and localizes to the pathogen-occupied vacuolar membrane. *Infect Immun*, 78(5):1864–73, 2010. 27, 99, 101, 102, 106, 114, 122, 125, 129, 141

[88] H. Huang, X. Wang, T. Kikuchi, Y. Kumagai, and Y. Rikihisa. Porin activity of anaplasma phagocytophilum outer membrane fraction and purified p44. *Journal of bacteriology*, 189(5):1998–2006, 2007. 7

[89] H. L. Huang, L. W. Fang, S. P. Lu, C. K. Chou, T. Y. Luh, and M. Z. Lai. Dna-damaging reagents induce apoptosis through reactive oxygen species-dependent fas aggregation. *Oncogene*, 22(50):8168–77, 2003. 12

[90] M. Hussain, A. Haggar, G. Peters, G. S. Chhatwal, M. Herrmann, J. I. Flock, and B. Sinha. More than one tandem repeat domain of the extracellular adherence protein of staphylococcus aureus is required for aggregation, adherence, and host cell invasion but not for leukocyte activation. *Infect Immun*, 76(12):5615–23, 2008. 81

[91] J. W. Ijdo, W. Sun, Y. Zhang, L. A. Magnarelli, and E. Fikrig. Cloning of the gene encoding the 44-kilodalton antigen of the agent of human granulocytic ehrlichiosis and characterization of the humoral response. *Infect Immun*, 66(7):3264–9, 1998. 41

[92] A. Ingmundson, A. Delprato, D. G. Lambright, and C. R. Roy. Legionella pneumophila proteins that regulate rab1 membrane cycling. *Nature*, 450(7168):365–9, 2007. 64, 65

[93] S. S. Ivanov and C. R. Roy. Modulation of ubiquitin dynamics and suppression of dalis formation by the legionella pneumophila dot/icm system. *Cellular microbiology*, 11(2):261–78, 2009. 137

[94] J. R. Junutula, A. M. De Maziere, A. A. Peden, K. E. Ervin, R. J. Advani, S. M. van Dijk, J. Klumperman, and R. H. Scheller. Rab14 is involved in membrane trafficking between the golgi complex and endosomes. *Mol Biol Cell*, 15(5):2218–29, 2004. 49

[95] I. Jdo JW, A. C. Carlson, and E. L. Kennedy. Anaplasma phagocytophilum anka is tyrosine-phosphorylated at epiya motifs and recruits shp-1 during early infection. *Cell Microbiol*, 9(5):1284–96, 2007. 8, 67, 81

[96] I. Jdo JW and A. C. Mueller. Neutrophil nadph oxidase is reduced at the anaplasma phagocytophilum phagosome. *Infect Immun*, 72(9):5392–401, 2004. 10, 12, 15, 24, 46, 75, 93, 132

[97] J. C. Kagan, M. P. Stein, M. Pypaert, and C. R. Roy. Legionella subvert the functions of rab1 and sec22b to create a replicative organelle. *J Exp Med*, 199(9):1201–11, 2004. 40

[98] V. A. Kelley and J. S. Schorey. Mycobacterium's arrest of phagosome maturation in macrophages requires rab5 activity and accessibility to iron. *Mol Biol Cell*, 14(8):3366–77, 2003. 40, 61

[99] E. E. Kelly, C. P. Horgan, C. Adams, T. M. Patzer, D. M. Ni Shuilleabhain, J. C. Norman, and M. W. McCaffrey. Class i rab11-family interacting proteins are binding targets for the rab14 gtpase. *Biol Cell*, 102(1):51–62, 2010. 40, 46, 49

[100] H. Y. Kim and Y. Rikihisa. Expression of interleukin-1beta, tumor necrosis factor alpha, and interleukin-6 in human peripheral blood leukocytes exposed to human granulocytic ehrlichiosis agent or recombinant major surface protein p44. *Infect Immun*, 68(6):3394–402, 2000. 14

[101] P. K. Kim, D. W. Hailey, R. T. Mullen, and J. Lippincott-Schwartz. Ubiquitin signals autophagic degradation of cytosolic proteins and peroxisomes. *Proceedings of the National Academy of Sciences of the United States of America*, 105(52):20567–74, 2008. 127

[102] B. Kleba, T. R. Clark, E. I. Lutter, D. W. Ellison, and T. Hackstadt. Disruption of the rickettsia rickettsii sca2 autotransporter inhibits actin-based motility. *Infection and immunity*, 78(5):2240–7, 2010. 9

[103] M. B. Klein, S. Hu, C. C. Chao, and J. L. Goodman. The agent of human granulocytic ehrlichiosis induces the production of myelosuppressing chemokines without induction of proinflammatory cytokines. *The Journal of infectious diseases*, 182(1):200–5, 2000. 14

[104] L. A. Knodler, S. Winfree, D. Drecktrah, R. Ireland, and O. Steele-Mortimer. Ubiquitination of the bacterial inositol phosphatase, sopb, regulates its biological activity at the plasma membrane. *Cellular microbiology*, 11(11):1652–70, 2009. 128, 140

[105] T. Kubori and J. E. Galan. Temporal regulation of salmonella virulence effector function by proteasome-dependent protein degradation. *Cell*, 115(3):333–42, 2003. 140

[106] T. Kubori, N. Shinzawa, H. Kanuka, and H. Nagai. Legionella metaeffector exploits host proteasome to temporally regulate cognate effector. *PLoS pathogens*, 6(12):e1001216, 2010. 128, 140

[107] Y. Kumar and R. H. Valdivia. Leading a sheltered life: intracellular pathogens and maintenance of vacuolar compartments. *Cell Host Microbe*, 5(6):593–601, 2009. 61

[108] G. B. Kyei, I. Vergne, J. Chua, E. Roberts, J. Harris, J. R. Junutula, and V. Deretic. Rab14 is critical for maintenance of mycobacterium tuberculosis phagosome maturation arrest. *EMBO J*, 25(22):5250–9, 2006. 40, 61

[109] H. C. Lee and J. L. Goodman. Anaplasma phagocytophilum causes global induction of antiapoptosis in human neutrophils. *Genomics*, 88(4):496–503, 2006. 13

[110] K. N. Lee, I. Padmalayam, B. Baumstark, S. L. Baker, and R. F. Massung. Characterization of the ftsz gene from ehrlichia chaffeensis, anaplasma phagocytophilum, and rickettsia rickettsii, and use as a differential pcr target. *DNA and cell biology*, 22(3):179–86, 2003. 10

[111] M. Lin, A. den Dulk-Ras, P. J. Hooykaas, and Y. Rikihisa. Anaplasma phagocytophilum anka secreted by type iv secretion system is tyrosine phosphorylated by abl-1 to facilitate infection. *Cell Microbiol*, 9(11):2644–57, 2007. 8, 67, 81, 106

[112] M. Lin and Y. Rikihisa. Ehrlichia chaffeensis and anaplasma phagocytophilum lack genes for lipid a biosynthesis and incorporate cholesterol for their survival. *Infect Immun*, 71(9):5324–31, 2003. 6, 7, 10, 16, 58

[113] Q. Lin, C. Zhang, and Y. Rikihisa. Analysis of involvement of the recf pathway in p44 recombination in anaplasma phagocytophilum and in escherichia coli by using a plasmid carrying the p44 expression and p44 donor loci. *Infection and immunity*, 74(4):2052–62, 2006. 7

[114] Q. Lin, N. Zhi, N. Ohashi, H. W. Horowitz, M. E. Aguero-Rosenfeld, J. Raffalli, G. P. Wormser, and Y. Rikihisa. Analysis of sequences and loci of p44 homologs expressed by anaplasma phagocytophila in acutely infected patients. *Journal of clinical microbiology*, 40(8):2981–8, 2002. 7

[115] L. Liscum and N. J. Munn. Intracellular cholesterol transport. *Biochimica et biophysica acta*, 1438(1):19–37, 1999. 108

[116] F. Liu and K. J. Walters. Multitasking with ubiquitin through multivalent interactions. *Trends in biochemical sciences*, 35(6):352–60, 2010. 127

[117] Y. C. Liu. Ubiquitin ligases and the immune response. *Annual review of immunology*, 22:81–127, 2004. 128

[118] Z. M. Liu, A. M. Tucker, L. O. Driskell, and D. O. Wood. Mariner-based transposon mutagenesis of rickettsia prowazekii. *Applied and environmental microbiology*, 73(20):6644–9, 2007. 9

[119] T. Luo, J. A. Kuriakose, B. Zhu, A. Wakeel, and J. W. McBride. Ehrlichia chaffeensis trp120 interacts with a diverse array of eukaryotic proteins involved in transcription, signaling, and cytoskeleton organization. *Infection and immunity*, 79(11):4382–91, 2011. 83, 100

[120] M. P. Machner and R. R. Isberg. Targeting of host rab gtpase function by the intravacuolar pathogen legionella pneumophila. *Dev Cell*, 11(1):47–56, 2006. 40, 64, 65

[121] L. A. Magnarelli, 3rd Stafford, K. C., T. N. Mather, M. T. Yeh, K. D. Horn, and J. S. Dumler. Hemocytic rickettsia-like organisms in ticks: serologic reactivity with antisera to ehrlichiae and detection of dna of agent of human granulocytic ehrlichiosis by pcr. *Journal of clinical microbiology*, 33(10):2710–4, 1995. 2

[122] S. L. Marcus, L. A. Knodler, and B. B. Finlay. Salmonella enterica serovar typhimurium effector sigd/sopb is membrane-associated and ubiquitinated inside host cells. *Cellular microbiology*, 4(7):435–46, 2002. 140

[123] M. E. Martin, J. E. Bunnell, and J. S. Dumler. Pathology, immunohistology, and cytokine responses in early phases of human granulocytic ehrlichiosis in a murine model. *The Journal of infectious diseases*, 181(1):374–8, 2000. 13

[124] M. E. Martin, K. Caspersen, and J. S. Dumler. Immunopathology and ehrlichial propagation are regulated by interferon-gamma and interleukin-10 in a murine model of human granulocytic ehrlichiosis. *The American journal of pathology*, 158(5):1881–8, 2001. 13

[125] J. J. Martinez, S. Seveau, E. Veiga, S. Matsuyama, and P. Cossart. Ku70, a component of dna-dependent protein kinase, is a mammalian receptor for rickettsia conorii. *Cell*, 123(6):1013–23, 2005. 141

[126] S. Mayor and R. E. Pagano. Pathways of clathrin-independent endocytosis. *Nat Rev Mol Cell Biol*, 8(8):603–12, 2007. 38, 58

[127] J. W. McBride, X. Zhang, A. Wakeel, and J. A. Kuriakose. Tyrosine-phosphorylated ehrlichia chaffeensis and ehrlichia canis tandem repeat orthologs contain a major continuous cross-reactive antibody epitope in lysine-rich repeats. *Infection and immunity*, 79(8):3178–87, 2011. 83

[128] A. R. Moorhead, K. A. Rzomp, and M. A. Scidmore. The rab6 effector bicaudal d1 associates with chlamydia trachomatis inclusions in a biovar-specific manner. *Infect Immun*, 75(2):781–91, 2007. 40

[129] J. Mott, R. E. Barnewall, and Y. Rikihisa. Human granulocytic ehrlichiosis agent and ehrlichia chaffeensis reside in different cytoplasmic compartments in hl-60 cells. *Infect Immun*, 67(3):1368–78, 1999. 15, 16, 45, 60, 61, 62

[130] J. Mott, Y. Rikihisa, and S. Tsunawaki. Effects of anaplasma phagocytophila on nadph oxidase components in human neutrophils and hl-60 cells. *Infect Immun*, 70(3):1359–66, 2002. 12, 15

[131] K. Mukherjee, S. Parashuraman, M. Raje, and A. Mukhopadhyay. Sope acts as an rab5-specific nucleotide exchange factor and recruits non-prenylated rab5 on salmonella-containing phagosomes to promote fusion with early endosomes. *J Biol Chem*, 276(26):23607–15, 2001. 40

[132] U. G. Munderloh, S. D. Jauron, V. Fingerle, L. Leitritz, S. F. Hayes, J. M. Hautman, C. M. Nelson, B. W. Huberty, T. J. Kurtti, G. G. Ahlstrand, B. Greig, M. A. Mellencamp, and J. L. Goodman. Invasion and intracellular development of the human granulocytic ehrlichiosis agent in tick cell culture. *Journal of clinical microbiology*, 37(8):2518–24, 1999. 10, 18, 19, 129

[133] U. G. Munderloh, M. J. Lynch, M. J. Herron, A. T. Palmer, T. J. Kurtti, R. D. Nelson, and J. L. Goodman. Infection of endothelial cells with anaplasma marginale and a. phagocytophilum. *Vet Microbiol*, 101(1):53–64, 2004. 2, 10, 75, 129

[134] T. Murata, A. Delprato, A. Ingmundson, D. K. Toomre, D. G. Lambright, and C. R. Roy. The legionella pneumophila effector protein drra is a rab1 guanine nucleotide-exchange factor. *Nat Cell Biol*, 8(9):971–7, 2006. 40, 64, 65

[135] H. Nagai, J. C. Kagan, X. Zhu, R. A. Kahn, and C. R. Roy. A bacterial guanine nucleotide exchange factor activates arf on legionella phagosomes. *Science*, 295(5555):679–82, 2002. 34

[136] J. J. Neefjes, V. Stollorz, P. J. Peters, H. J. Geuze, and H. L. Ploegh. The biosynthetic pathway of mhc class ii but not class i molecules intersects the endocytic route. *Cell*, 61(1):171–83, 1990. 16, 60

[137] C. M. Nelson, M. J. Herron, R. F. Felsheim, B. R. Schloeder, S. M. Grindle, A. O. Chavez, T. J. Kurtti, and U. G. Munderloh. Whole genome transcription profiling of anaplasma phagocytophilum in human and tick host cells by tiling array analysis. *BMC Genomics*, 9:364, 2008. 81, 99

[138] S. Ninio, J. Celli, and C. R. Roy. A legionella pneumophila effector protein encoded in a region of genomic plasticity binds to dot/icm-modified vacuoles. *PLoS pathogens*, 5(1):e1000278, 2009. 119

[139] H. Niu, V. Kozjak-Pavlovic, T. Rudel, and Y. Rikihisa. Anaplasma phagocytophilum ats-1 is imported into host cell mitochondria and interferes with apoptosis induction. *PLoS pathogens*, 6(2):e1000774, 2010. 8, 13, 123

[140] H. Niu, Y. Rikihisa, M. Yamaguchi, and N. Ohashi. Differential expression of virb9 and virb6 during the life cycle of anaplasma phagocytophilum in human leucocytes is associated with differential binding and avoidance of lysosome pathway. *Cellular microbiology*, 8(3):523–34, 2006. 8, 106

[141] H. Niu, M. Yamaguchi, and Y. Rikihisa. Subversion of cellular autophagy by anaplasma phagocytophilum. *Cellular microbiology*, 10(3):593–605, 2008. 16

[142] N. Ohashi, N. Zhi, Q. Lin, and Y. Rikihisa. Characterization and transcriptional analysis of gene clusters for a type iv secretion machinery in human granulocytic and monocytic ehrlichiosis agents. *Infect Immun*, 70(4):2128–38, 2002. 8

[143] N. Ojogun, B. Barnstein, B. Huang, C. A. Oskeritzian, J. W. Homeister, D. Miller, J. J. Ryan, and J. A. Carlyon. Anaplasma phagocytophilum infects mast cells via alpha1,3-fucosylated but not sialylated glycans and inhibits ige-mediated cytokine production and histamine release. *Infection and immunity*, 79(7):2717–26, 2011. 2, 14

[144] A. Omsland, P. A. Beare, J. Hill, D. C. Cockrell, D. Howe, B. Hansen, J. E. Samuel, and R. A. Heinzen. Isolation from animal tissue and genetic transformation of coxiella burnetii are facilitated by an improved axenic growth medium. *Applied and environmental microbiology*, 77(11):3720–5, 2011. 9

[145] A. Omsland, D. C. Cockrell, D. Howe, E. R. Fischer, K. Virtaneva, D. E. Sturdevant, S. F. Porcella, and R. A. Heinzen. Host cell-free growth of the q fever bacterium coxiella burnetii. *Proceedings of the National Academy of Sciences of the United States of America*, 106(11):4430–4, 2009. 9

[146] J. A. Oteo, J. R. Blanco, V. Martinez de Artola, and V. Ibarra. First report of human granulocytic ehrlichiosis from southern europe (spain). *Emerging infectious diseases*, 6(4):430–2, 2000. 2

[147] P. Pancholi, C. P. Kolbert, P. D. Mitchell, Jr. Reed, K. D., J. S. Dumler, J. S. Bakken, 3rd Telford, S. R., and D. H. Persing. Ixodes dammini as a potential vector of human granulocytic ehrlichiosis. *The Journal of infectious diseases*, 172(4):1007–12, 1995. 2

[148] E. Papanikou, S. Karamanou, and A. Economou. Bacterial protein secretion through the translocase nanomachine. *Nature reviews. Microbiology*, 5(11):839–51, 2007. 7

[149] J. Park, K. S. Choi, and J. S. Dumler. Major surface protein 2 of anaplasma phagocytophilum facilitates adherence to granulocytes. *Infect Immun*, 71(7):4018–25, 2003. 72, 90

[150] J. Park, K. J. Kim, K. S. Choi, D. J. Grab, and J. S. Dumler. Anaplasma phagocytophilum anka binds to granulocyte dna and nuclear proteins. *Cellular microbiology*, 6(8):743–51, 2004. 8

[151] J. C. Patel, K. Hueffer, T. T. Lam, and J. E. Galan. Diversification of a salmonella virulence protein function by ubiquitin-dependent differential localization. *Cell*, 137(2):283–94, 2009. 127, 128, 140, 144

[152] G. A. Petsko and D. Ringe. *From sequence to structure. Protein structure and function*. New Science Press, London, United Kingdom, 2004. 102

[153] H. Plutner, A. D. Cox, S. Pind, R. Khosravi-Far, J. R. Bourne, R. Schwaninger, C. J. Der, and W. E. Balch. Rab1b regulates vesicular transport between the endoplasmic reticulum and successive golgi compartments. *J Cell Biol*, 115(1):31–43, 1991. 62

[154] C. T. Price, S. Al-Khodor, T. Al-Quadan, M. Santic, F. Habyarimana, A. Kalia, and Y. A. Kwaik. Molecular mimicry by an f-box effector of legionella pneumophila hijacks a conserved polyubiquitination machinery within macrophages and protozoa. *PLoS pathogens*, 5(12):e1000704, 2009. 128

[155] C. T. Price and Y. A. Kwaik. Exploitation of host polyubiquitination machinery through molecular mimicry by eukaryotic-like bacterial f-box effectors. *Frontiers in microbiology*, 1:122, 2010. 127

[156] S. Raasi, R. Varadan, D. Fushman, and C. M. Pickart. Diverse polyubiquitin interaction properties of ubiquitin-associated domains. *Nature structural molecular biology*, 12(8):708–14, 2005. 137

[157] H. Radhakrishna and J. G. Donaldson. Adp-ribosylation factor 6 regulates a novel plasma membrane recycling pathway. *J Cell Biol*, 139(1):49–61, 1997. 38

[158] Emer P Reeves, Hui Lu, Hugues Lortat Jacobs, Carlo G M Messina, Steve Bolsover, Giorgio Gabella, Eric O Potma, Alice Warley, Jürgen Roes, and Anthony W Segal. Killing activity of neutrophils is mediated through activation of proteases by k+ flux. *Nature*, 416(6878):291–7, Mar 2002. 12

[159] A. Rejman Lipinski, J. Heymann, C. Meissner, A. Karlas, V. Brinkmann, T. F. Meyer, and D. Heuer. Rab6 and rab11 regulate chlamydia trachomatis development and golgin-84-dependent golgi fragmentation. *PLoS Pathog*, 5(10):e1000615, 2009. 62

[160] D. V. Reneer, S. A. Kearns, T. Yago, J. Sims, R. D. Cummings, R. P. McEver, and J. A. Carlyon. Characterization of a sialic acid- and p-selectin glycoprotein ligand-1-independent adhesin activity in the granulocytotropic bacterium anaplasma phagocytophilum. *Cellular microbiology*, 8(12):1972–84, 2006. 9

[161] D. V. Reneer, M. J. Troese, B. Huang, S. A. Kearns, and J. A. Carlyon. Anaplasma phagocytophilum psgl-1-independent infection does not require syk and leads to less efficient anka delivery. *Cell Microbiol*, 10(9):1827–38, 2008. 8, 9, 67

[162] Y. Rikihisa. The tribe ehrlichieae and ehrlichial diseases. *Clinical microbiology reviews*, 4(3):286–308, 1991. 1

[163] Y. Rikihisa. Anaplasma phagocytophilum and ehrlichia chaffeensis: subversive manipulators of host cells. *Nature reviews. Microbiology*, 8(5):328–39, 2010. 129

[164] Y. Rikihisa. Mechanisms of obligatory intracellular infection with anaplasma phagocytophilum. *Clinical microbiology reviews*, 24(3):469–89, 2011. 5

[165] E. A. Roberts, J. Chua, G. B. Kyei, and V. Deretic. Higher order rab programming in phagolysosome biogenesis. *J Cell Biol*, 174(7):923–9, 2006. 61

[166] D. D. Rockey, D. Grosenbach, D. E. Hruby, M. G. Peacock, R. A. Heinzen, and T. Hackstadt. Chlamydia psittaci inca is phosphorylated by the host cell and is exposed on the cytoplasmic face of the developing inclusion. *Molecular microbiology*, 24(1):217–28, 1997. 122, 124

[167] D.D. Rockey and D.T. Alzhanov. *Proteins in the chlamydial inclusion membrane*, pages 235–254. Horizon Scientific Press, Norfolk, United Kingdom, 2006. 68, 70, 85, 124

[168] P. S. Romano, M. G. Gutierrez, W. Beron, M. Rabinovitch, and M. I. Colombo. The autophagic pathway is actively modulated by phase ii coxiella burnetii to efficiently replicate in the host cell. *Cell Microbiol*, 9(4):891–909, 2007. 40

[169] Dirk Roos, Robin van Bruggen, and Christof Meischl. Oxidative killing of microbes by neutrophils. *Microbes Infect*, 5(14):1307–15, Nov 2003. 12

[170] K. A. Rzomp, A. R. Moorhead, and M. A. Scidmore. The gtpase rab4 interacts with chlamydia trachomatis inclusion membrane protein ct229. *Infect Immun*, 74(9):5362–73, 2006. 21, 26, 40, 52, 62, 65

[171] K. A. Rzomp, L. D. Scholtes, B. J. Briggs, G. R. Whittaker, and M. A. Scidmore. Rab gtpases are recruited to chlamydial inclusions in both a species-dependent and species-independent manner. *Infect Immun*, 71(10):5855–70, 2003. 19, 40, 41, 61, 62, 63

[172] K. Sandvig, M. L. Torgersen, H. A. Raa, and B. van Deurs. Clathrin-independent endocytosis: from nonexisting to an extreme degree of complexity. *Histochem Cell Biol*, 129(3):267–76, 2008. 38, 58

[173] M. Sarkar, D. V. Reneer, and J. A. Carlyon. Sialyl-lewis x-independent infection of human myeloid cells by anaplasma phagocytophilum strains hz and hge1. *Infection and immunity*, 75(12):5720–5, 2007. 9

[174] D. Scheel-Toellner, K. Wang, R. Craddock, P. R. Webb, H. M. McGettrick, L. K. Assi, N. Parkes, L. E. Clough, E. Gulbins, M. Salmon, and J. M. Lord. Reactive oxygen species limit neutrophil life span by activating death receptor signaling. *Blood*, 104(8):2557–64, 2004. 12

[175] M. C. Schlumberger and W. D. Hardt. Triggered phagocytosis by salmonella: bacterial molecular mimicry of rhogtpase activation/deactivation. *Curr Top Microbiol Immunol*, 291:29–42, 2005. 65

[176] D. G. Scorpio, K. Caspersen, H. Ogata, J. Park, and J. S. Dumler. Restricted changes in major surface protein-2 (msp2) transcription after prolonged in vitro passage of anaplasma phagocytophilum. *BMC Microbiol*, 4:1, 2004. 72, 90

[177] N. Segev. Coordination of intracellular transport steps by gtpases. *Seminars in cell developmental biology*, 22(1):33–8, 2011. 140

[178] R. Seshadri and J. Samuel. Genome analysis of coxiella burnetii species: insights into pathogenesis and evolution and implications for biodefense. *Annals of the New York Academy of Sciences*, 1063:442–50, 2005. 6

[179] N. C. Shaner, M. Z. Lin, M. R. McKeown, P. A. Steinbach, K. L. Hazelwood, M. W. Davidson, and R. Y. Tsien. Improving the photostability of bright monomeric orange and red fluorescent proteins. *Nat Methods*, 5(6):545–51, 2008. 21

[180] S. Shin and C. R. Roy. Host cell processes that influence the intracellular survival of legionella pneumophila. *Cellular microbiology*, 10(6):1209–20, 2008. 106

[181] A. U. Singer, J. R. Rohde, R. Lam, T. Skarina, O. Kagan, R. Dileo, N. Y. Chirgadze, M. E. Cuff, A. Joachimiak, M. Tyers, P. J. Sansonetti, C. Parsot, and A. Savchenko. Structure of the shigella t3ss effector ipah defines a new class of e3 ubiquitin ligases. *Nature structural molecular biology*, 15(12):1293–301, 2008. 141

[182] A. C. Smith, J. T. Cirulis, J. E. Casanova, M. A. Scidmore, and J. H. Brumell. Interaction of the salmonella-containing vacuole with the endocytic recycling system. *J Biol Chem*, 280(26):24634–41, 2005. 40, 61

[183] A. C. Smith, W. D. Heo, V. Braun, X. Jiang, C. Macrae, J. E. Casanova, M. A. Scidmore, S. Grinstein, T. Meyer, and J. H. Brumell. A network of rab gtpases controls phagosome maturation and is modulated by salmonella enterica serovar typhimurium. *J Cell Biol*, 176(3):263–8, 2007. 40, 61, 63

[184] K. R. Snapp, H. Ding, K. Atkins, R. Warnke, F. W. Luscinskas, and G. S. Kansas. A novel p-selectin glycoprotein ligand-1 monoclonal antibody recognizes an epitope within the tyrosine sulfate motif of human psgl-1 and blocks recognition of both p- and l-selectin. *Blood*, 91(1):154–64, 1998. 9

[185] A. Spielman, C. M. Clifford, J. Piesman, and M. D. Corwin. Human babesiosis on nantucket island, usa: description of the vector, ixodes (ixodes) dammini, n. sp. (acarina: Ixodidae). *Journal of medical entomology*, 15(3):218–34, 1979. 2

[186] C E Stebbins and J E Galán. Structural mimicry in bacterial virulence. *Nature*, 412(6848):701–5, Aug 2001. 103

[187] O. Steele-Mortimer, S. Meresse, J. P. Gorvel, B. H. Toh, and B. B. Finlay. Biogenesis of salmonella typhimurium-containing vacuoles in epithelial cells involves interactions with the early endocytic pathway. *Cell Microbiol*, 1(1):33–49, 1999. 40, 61

[188] H. Stenmark. Rab gtpases as coordinators of vesicle traffic. *Nature reviews. Molecular cell biology*, 10(8):513–25, 2009. 37, 40, 49, 55, 64

[189] R. S. Stephens, S. Kalman, C. Lammel, J. Fan, R. Marathe, L. Aravind, W. Mitchell, L. Olinger, R. L. Tatusov, Q. Zhao, E. V. Koonin, and R. W. Davis. Genome sequence of an obligate intracellular pathogen of humans: Chlamydia trachomatis. *Science*, 282(5389):754–9, 1998. 6

[190] J. R. Storey, L. A. Doros-Richert, C. Gingrich-Baker, K. Munroe, T. N. Mather, R. T. Coughlin, G. A. Beltz, and C. I. Murphy. Molecular cloning and sequencing of three granulocytic ehrlichia genes encoding high-molecular-weight immunoreactive proteins. *Infect Immun*, 66(4):1356–63, 1998. 8, 31, 67, 70, 81, 83, 85, 87, 88, 97, 99, 100

[191] B. Sukumaran, J. A. Carlyon, J. L. Cai, N. Berliner, and E. Fikrig. Early transcriptional response of human neutrophils to anaplasma phagocytophilum infection. *Infection and immunity*, 73(12):8089–99, 2005. 14

[192] B. Sukumaran, J. E. Mastronunzio, S. Narasimhan, S. Fankhauser, P. D. Uchil, R. Levy, M. Graham, T. M. Colpitts, C. F. Lesser, and E. Fikrig. Anaplasma phagocytophilum apta modulates erk1/2 signalling. *Cellular microbiology*, 13(1):47–61, 2011. 122, 141

[193] R Development Core Team. *R: A Language and Environment for Statistical Computing*. Vienna, Austria, 2011. 36

[194] 3rd Telford, S. R., J. E. Dawson, P. Katavolos, C. K. Warner, C. P. Kolbert, and D. H. Persing. Perpetuation of the agent of human granulocytic ehrlichiosis in a deer tick-rodent cycle. *Proceedings of the National Academy of Sciences of the United States of America*, 93(12):6209–14, 1996. 2

[195] R. J. Thomas, J. S. Dumler, and J. A. Carlyon. Current management of human granulocytic anaplasmosis, human monocytic ehrlichiosis and ehrlichia ewingii ehrlichiosis. *Expert Rev Anti Infect Ther*, 7(6):709–22, 2009. 2, 5

[196] V. Thomas and E. Fikrig. Anaplasma phagocytophilum specifically induces tyrosine phosphorylation of rock1 during infection. *Cellular microbiology*, 9(7):1730–7, 2007. 9

[197] J. S. Thrower, L. Hoffman, M. Rechsteiner, and C. M. Pickart. Recognition of the polyubiquitin proteolytic signal. *The EMBO journal*, 19(1):94–102, 2000. 127

[198] E. J. Tisdale and W. E. Balch. Rab2 is essential for the maturation of pre-golgi intermediates. *J Biol Chem*, 271(46):29372–9, 1996. 62

[199] M. J. Troese and J. A. Carlyon. Anaplasma phagocytophilum dense-cored organisms mediate cellular adherence through recognition of human p-selectin glycoprotein ligand 1. *Infect Immun*, 77(9):4018–27, 2009. 10, 31, 46, 70, 78, 88, 93, 97, 100, 132, 138

[200] S. Varde, J. Beckley, and I. Schwartz. Prevalence of tick-borne pathogens in ixodes scapularis in a rural new jersey county. *Emerging infectious diseases*, 4(1):97–9, 1998. 2

[201] A. C. Vergunst, M. C. van Lier, A. den Dulk-Ras, T. A. Stuve, A. Ouwehand, and P. J. Hooykaas. Positive charge is an important feature of the c-terminal transport signal of the virb/d4-translocated proteins of agrobacterium. *Proc Natl Acad Sci U S A*, 102(3):832–7, 2005. 8, 26, 122

[202] L. E. Via, D. Deretic, R. J. Ulmer, N. S. Hibler, L. A. Huber, and V. Deretic. Arrest of mycobacterial phagosome maturation is caused by a block in vesicle fusion between stages controlled by rab5 and rab7. *J Biol Chem*, 272(20):13326–31, 1997. 40

[203] D. E. Voth, D. Howe, P. A. Beare, J. P. Vogel, N. Unsworth, J. E. Samuel, and R. A. Heinzen. The coxiella burnetii ankyrin repeat domain-containing protein family is heterogeneous, with c-terminal truncations that influence dot/icm-mediated secretion. *Journal of bacteriology*, 191(13):4232–42, 2009. 26

[204] D. E. Voth, D. Howe, and R. A. Heinzen. Coxiella burnetii inhibits apoptosis in human thp-1 cells and monkey primary alveolar macrophages. *Infection and immunity*, 75(9):4263–71, 2007. 31, 34

[205] A. Wakeel, J. A. Kuriakose, and J. W. McBride. An ehrlichia chaffeensis tandem repeat protein interacts with multiple host targets involved in cell signaling, transcriptional regulation, and vesicle trafficking. *Infect Immun*, 77(5):1734–45, 2009. 81, 83, 100

[206] A. Wakeel, X. Zhang, and J. W. McBride. Mass spectrometric analysis of ehrlichia chaffeensis tandem repeat proteins reveals evidence of phosphorylation and absence of glycosylation. *PloS one*, 5(3):e9552, 2010. 101

[207] Tian Wang, Stephen E Malawista, Utpal Pal, Mark Grey, James Meek, Mustafa Akkoyunlu, Venetta Thomas, and Erol Fikrig. Superoxide anion production during anaplasma phagocytophila infection. *J Infect Dis*, 186(2):274–80, Jul 2002. 12

[208] X. Wang, Y. Rikihisa, T. H. Lai, Y. Kumagai, N. Zhi, and S. M. Reed. Rapid sequential changeover of expressed p44 genes during the acute phase of anaplasma phagocytophilum infection in horses. *Infection and immunity*, 72(12):6852–9, 2004. 7

[209] P. Webster, I. Jdo JW, L. M. Chicoine, and E. Fikrig. The agent of human granulocytic ehrlichiosis resides in an endosomal compartment. *J Clin Invest*, 101(9):1932–41, 1998. 15, 16, 60

[210] Hadley Wickham. *ggplot2: elegant graphics for data analysis*. Springer, New York, 2009. 36

[211] A. C. Wistedt, U. Ringdahl, W. Muller-Esterl, and U. Sjobring. Identification of a plasminogen-binding motif in pam, a bacterial surface protein. *Mol Microbiol*, 18(3):569–78, 1995. 81

[212] Z. Woldehiwet, B. K. Horrocks, H. Scaife, G. Ross, U. G. Munderloh, K. Bown, S. W. Edwards, and C. A. Hart. Cultivation of an ovine strain of ehrlichia phagocytophila in tick cell cultures. *J Comp Pathol*, 127(2-3):142–9, 2002. 75

[213] Q. Xiong, M. Lin, and Y. Rikihisa. Cholesterol-dependent anaplasma phagocytophilum exploits the low-density lipoprotein uptake pathway. *PLoS Pathog*, 5(3):e1000329, 2009. 58

[214] K. Yoshiie, H. Y. Kim, J. Mott, and Y. Rikihisa. Intracellular infection by the human granulocytic ehrlichiosis agent inhibits human neutrophil apoptosis. *Infection and immunity*, 68(3):1125–33, 2000. 12

[215] X. J. Yu, P. Crocquet-Valdes, and D. H. Walker. Cloning and sequencing of the gene for a 120-kda immunodominant protein of ehrlichia chaffeensis. *Gene*, 184(2):149–54, 1997. 81, 100

[216] N. Zhi, N. Ohashi, and Y. Rikihisa. Multiple p44 genes encoding major outer membrane proteins are expressed in the human granulocytic ehrlichiosis agent. *The Journal of biological chemistry*, 274(25):17828–36, 1999. 7

[217] N. Zhi, N. Ohashi, T. Tajima, J. Mott, R. W. Stich, D. Grover, 3rd Telford, S. R., Q. Lin, and Y. Rikihisa. Transcript heterogeneity of the p44 multigene family in a human granulocytic ehrlichiosis agent transmitted by ticks. *Infection and immunity*, 70(3):1175–84, 2002. 7

[218] B. Zhu, J. A. Kuriakose, T. Luo, E. Ballesteros, S. Gupta, Y. Fofanov, and J. W. McBride. Ehrlichia chaffeensis trp120 binds a g+c-rich motif in host cell dna and exhibits eukaryotic transcriptional activator function. *Infection and immunity*, 79(11):4370–81, 2011. 83, 100

[219] B. Zhu, K. A. Nethery, J. A. Kuriakose, A. Wakeel, X. Zhang, and J. W. McBride. Nuclear translocated ehrlichia chaffeensis ankyrin protein interacts with a specific adenine-rich motif of host promoter and intronic alu elements. *Infect Immun*, 77(10):4243–55, 2009. 81

[220] Y. Zhu, H. Li, L. Hu, J. Wang, Y. Zhou, Z. Pang, L. Liu, and F. Shao. Structure of a shigella effector reveals a new class of ubiquitin ligases. *Nature structural molecular biology*, 15(12):1302–8, 2008. 141

Copyrighted license material

Chapter 1:
Reprinted from Clinical Infectious Diseases, 45, Suppl 1:S45-52. Ehrlichioses in humans: epidemiology, clinical presentation, diagnosis, and treatment. License Number 277951137269. Portion: Figure.

Reprinted from Trends in Parasitology, Vol. 26, No. 4, The increasing recognition of rickettsial pathogens in dogs and people, Page No. 202-212, Copyright 2010, with permission from Elsevier. License Number 2779550886252. Portion: Figure.

Reprinted from Infection and Immunity, 2009, Vol. 77, No. 9, p. 4018-4027. *A. phagocytophilum* Dense-Cored Organisms Mediate Cellular Adherence through Recognition of Human P-Selectin Glycoprotein Ligand. License Number 2779540950102. Portion: Figure.

Chapter 3:
Cellular Microbiology, 2010, Vol. 12, Iss. 9, p. 1292-1307, doi: 10.1111/j.1462-5822.2010.01468. Reproduced/amended with permission from John Wiley and Sons. The *Anaplasma phagocytophilum*-occupied vacuole selectively recruits Rab-GTPases that are predominantly associated with recycling endosomes. License Number 2762080423322. Portion: Full article

Chapter 4:
Infection and Immunity, 2010, Vol. 78, No. 5, p. 1864-1873, doi: 10.1128/IAI.01418-09. Reproduced/amended with permission from American Society for Microbiology. *Anaplasma phagocytophilum* APH_1387 Is Expressed throughout Bacterial Intracellular Development and Localizes to the Pathogen-Occupied Vacuolar Membrane. License Number 2762080150204. Portion: Full article

Chapter 5:
Microbial Pathogenesis, 2010, Vol. 49, Iss. 5, p. 273-284, doi: 10.1016/j.micpath.2010.06.009. Reproduced/amended with permission from Elsevier. *Anaplasma phagocytophilum* APH_0032 is expressed late during infection and localizes to the pathogen-occupied vacuolar membrane. License Number 2762080562662. Portion: Full article

Chapter 7:
FEMS Immunology & Medical Microbiology, accepted, DOI: 10.1111/j.1574-695X.2011.00873. Reproduced/amended with permission from John Wiley and Sons. Monoubiquitinated proteins decorate the *Anaplasma phagocytophilum*-occupied vacuolar membrane. License Number 2773320586339. Portion: Full article

Vita

Bernice Huang was born on July 10, 1983 in Chapel Hill, North Carolina.She graduated with a Bachelor of Science in Business Administration in May, 2005 from the University of Richmond. A brief list of accomplishments performed during her graduate career is listed below.

Publications (In reverse chronological order):

B. Huang, N. Ojogun, S. Ragland, and J.A. Carlyon. 2011. Monoubiquitinated proteins decorate the *Anaplasma phagocytophilum*-occupied vacuolar membrane. FEMS Immunol Med Microbiol. doi: 10.1111/j.1574-695X.2011.00873.x

N.I. Ojogun, B.B. Barnstein, **B. Huang**, C.A. Ozkeritizan, J.W. Homeister, D. Miller, J.J. Ryan, and J.A. Carlyon. 2011. *Anaplasma phagocytophilum* infection of mast requires α1,3-fucosylated but not sialylated glycans and inhibits cytokine production and histamine release. Infect Immun. 79(7):2717-2726.

B. Huang, M.J. Troese, D. Howe, S. Ye, J.T. Sims, R.A. Heinzen, D.L. Borjesson, J.A. Carlyon. 2010. *Anaplasma phagocytophilum* APH_0032 is expressed late during infection and localizes to the pathogen-occupied vacuolar membrane. Microbial Pathogenesis 49(5): 273-284.

B. Huang, A. Hubber, J.A. McDonough, C.R. Roy, M.A. Scidmore, J.A. Carlyon. 2010. The *Anaplasma phagocytophilum*-occupied vacuole selectively recruits Rab-GTPases that are predominantly associated with recycling endosomes. Cellular Microbiology 1:12(9):1292-307.

B. Huang, M.J. Troese, S. Ye, J.T. Sims, N.L. Galloway, D.L. Borjesson, J.A. Carlyon. 2010. *Anaplasma phagocytophilum* APH_1387 is expressed throughout bacterial intracellular development and localizes to the pathogen-occupied vacuolar membrane. Infection and Immunity 78(5): 1864-73.

J.V. McDowell, **B. Huang**, C. Fenno, and R.T. Marconi. 2009. Analysis of a unique interaction between the complement regulatory protein factor H and the periodontal pathogen

Treponema denticola. Infection and Immunity 77(4): 1417-25.

D.V. Reneer, M.J. Troese, **B. Huang**, S.A. Kearns, and J.A. Carlyon. 2008. *A. phagocytophilum* PSGL-1-independent infection does not require Syk and leads to less-efficient AnkA delivery. Cellular Microbiology 10:1827-38.